The sub-pulmonary ventricle during exercise and impact of its absence in the Fontan circulation

Ruijsink, Jacobus Bernardus

Awarding institution:
King's College London

King's College London

DOCTORAL THESIS

The sub-pulmonary ventricle during exercise and impact of its absence in the Fontan circulation

Author:

Jacobus Bernardus (Bram) Ruijsink

Supervisors:

Prof. Reza Razavi

Dr. David Nordsletten

A thesis submitted in fulfillment of the requirements for the

degree of Doctor of Philosophy in the

Faculty of Life Sciences and Medicine

School of Biomedical Engineering & Imaging Sciences

March, 2018

"That's not right, that's not even wrong."

Wolfgang Pauli

To my parents.
I can't be more proud of all the things you taught me.

Acknowledgements

This thesis is the result of a not insignificant amount of hard work, persistence, even frustration, and devotion. But besides all of this especially the satisfaction and great joy of making something happen. This would have never been possible without the continuous support of friends, family and great academics at the department.

Foremost, I would like to express my deepest gratitude to Reza. You were an inspiring supervisor. Your devotion, sharp analytics, enthusiasm and desire to achieve the most challenging and ambitious goals have been a great support over the years. Thank you for igniting my enthusiasm, setting a great example and making me achieve 150%.
I am also very thankful to David. Your guidance, mentorship and commitment have helped me a lot during my work. You taught me about biomechanics and I have very much enjoyed the plentiful academic and personal discussions I have had with you.
I also want to very much thank Radek. Your help, guidance and commitment to our modelling projects was, and still is, 'grandiose'. I very much enjoy working with you. I much appreciate your endless enthusiasm and passion, both academically and personally, and hope we will continue our close collaboration in the future.
Also my clinical supervisors, Kuberan and Alessandra, thank you for all your academic, clinical and also personal input and mentorship. You make GSTT a great place to work and learn.
Over the years in this department, I have worked with a lot of great colleagues from different backgrounds who have taught me a lot about MRI physics, image-processing and mathematical modelling, but who have also become great friends. Thank you Usman and Josh for your input in the project. Simone, Lauren, Eoin, Des, Carolina, Fernandez, Mari, Phuoc, Milou, Marlies, Ana, Nick, Jorge, Matt, Dan, Myria, Liya thanks for all the fun at work and in the wild. Esther, you were an invaluable help in getting my project done. You taught me a lot. Not only programming but also how not to moan. I very much enjoyed working together, and even more value the friendship that we've build. Thomas, over the years you became a really good friend (I know, Ana you're jealous of the bromance ;)). I enjoyed our, very occasional – I admit –, gym sessions;). Wherever we'll roam off to; let's keep track buddy.
I also want to take this occasion to the many great friends from outside work, both in London

and at home. Steven, Emma, Vedrana, Jason, Ruth, James, Dan, Ilze, Bastien, Sanja and all of the ‘Croydon crew’; thanks for making London such a great home.
Eric, Martijn, Michiel we have build a very deep friendship. I appreciate all of you very much. Emergency hotel, holiday fun and good talks; thanks a lot for all them. The great lives we live, I hope they stay intertwined until we’re old.
Louise, you are a great friend: a heart of gold and wit. I am pleased that I finally managed to graduate from something before you did ;)
Auke and Ed, you both have been around for nearly decade(s). Thanks for all the joy we had growing up and the bond we still share up till today.
Barbara, thanks for hopping on the express and adding a lot of joy to my life.
Jeroen, Bastiaan, Bart, Nadine, Carlijn, Petra, Rosina, Wies, Rick, Judith, Esther, Manouk, Tessa and Leonie you have all been a large part of what got me here. Thank you. Ofcourse I will have forgotten someone – you all know me – don’t feel less appreciated!
But most of it all, I have to thank my family.
Lieve Pap, Mam, Aafke, Daan, Tom, Melis en kids. Jullie zijn er altijd voor me geweest. Door dik en soms heel dun. Dat betekent ontzettend veel voor me. Onze werelden kunnen soms mijlen ver uit elkaar liggen, letterlijk en figuurlijk, maar waar ik ook ben, jullie zijn altijd onlosmakelijk dichtbij. Ik ben trots op jullie. Op de mooie mensen die jullie zijn, op de mooie levens die jullie bouwen. En dankbaar voor jullie liefde voor deze vreemde, verstrooide eend! Pap en Mam; jullie hebben me meer geleerd dan welke studie ooit zal kunnen. Daar ben ik ongelofelijk trots op en dat is wat me hier heeft gebracht.

Bram Ruijsink, March 2018

Abstract

Assessment of the cardiac response during exercise remains challenging. So far, no ready-to-use, accurate methods for assessment of biventricular function have been available. However, such a method could greatly improve assessment of cardiac physiology, early detection and prognostic stratification of heart diseases. In this PhD a new technique for quantification of cardiac function during exercise with cardiac magnetic resonance imaging (exercise CMR) was developed. Subsequently, this method was utilized to answer the core questions of this PhD project: 1) *What is the role of the sub-pulmonary ventricle in cardiac function during exercise?* and 2) *What is the impact of its absence in patients with Fontan circulation?* In this thesis, the process of development and validation of exercise CMR was presented. This showed that exercise CMR is a valid tool for assessing cardiac volumes during exercise. Next, exercise CMR was used to investigate the fundamental physiological mechanism of biventricular cooperativity during exercise in the healthy heart. These experiments demonstrated that the RV plays a key role in biventricular synergy and is vital in optimization of cardiac performance during exercise. Subsequently, exercise CMR was used to investigate the impact of the absence of the RV on exercise haemodynamics in patients with Fontan circulation. These results showed that the absence of a sub-pulmonary ventricle significantly impairs cardiac performance during exercise in patients with Fontan circulation and that the physiological heart rate response to exercise is inappropriate in the single-ventricle circulation. Selective heart rate inhibition improves acute exercise haemodynamics in this small group of patients and might be a potential new treatment target for optimization the Fontan circulation. Finally, the potential added value of computational modelling for the diagnostic interpretation of stress / exercise exams was evaluated. It was demonstrated that computational models can help improve diagnostic assessment of stress examinations in patient with Fontan circulation. This thesis present the results of a cross-disciplinary, translational research project that involved the fields of MRI physics, image processing, mathematical modelling and medicine. It demonstrates the value of such cross-disciplinary work for clinical medicine.

Publications

1. **Ruijsink B**, Puyol-Anton E, Duong P, Usman M, Van Amerom J, Frigiola A, Pusparajah K King A, Nordsletten D, Razavi R Semi-automatic respiratory and cardiac gated cine MRI for cardiac assessment during exercise. *LNCS Artificial Intelligence* 2017;10555:86-95.

2. **Ruijsink B*,** Grotenhuis HB*, Chetan D, Dragulescu A, Friedberg MK, Kotani Y, Caldarone C, Honjo O, Mertens L Impact of Norwood versus hybrid palliation on cardiac size and function in hypoplastic left heart syndrome. *Heart* 2016;102(12):966-74.*authors contributed equally.

3. Puyol-Anton E, **Ruijsink B**, Langer H, De Craene M, Schnabel JA, Piro P, King AP, Sinclar M. Fully automated myocardial strain estimation form cine MRI using convolutional neural networks. *IEEE Explore* 2017:1139-1143.

4. Usman M, **Ruijsink B**, Nazir M, Cruz G, Prieto *C* Free breathing whole-heart 3D CINE MRI with self-gated Cartesian trajectory. *Mag Res Im* 2017:38:129-37.

5. Peresutti D, Sinclair M, **Ruijsink B**, Rueckert D, King A et al. A framework for combining a motion atlas with non-motion information to learn clinically useful biomarkers: application to cardiac resynchronization therapy response prediction. *Med Image Anal.* 2017;35:669-84.

6. Oksuz I, **Ruijsink B**, Puyol-Anton E, Sinclair M, Rueckert D, Schnabel JA, King AP. Automatic left ventricular outflow tract classification for accurate cardiac MRI planning. Accepted. *IEEE Explore* 2018:462-465.

7. Dillon-Murphy D, Larsson D, **Ruijsink B**, Qureshi A, Chubb H, O'Neill M, Nordsletten D, Aslanidi O, de Vecchi A. Changes in left atrial flow distribution between atrial fibrillation and sinus rhythm in humans. Submitted. *Frontiers in Physiol.* 2018.

8. Velasco Forte, M, Pusparajah K, Schaeffter T, Valverde I, Rhode K, **Ruijsink B**, Alhrishy M, Chiribiri A, Ismail T, Hussain T, Razavi R, Roujol S. Improved passive catheter tracking with positive contrast for MR-guided cardiac catheteriszation using partial saturation (pSAT) *J Cardiovasc Magn Reson* 2017 Aug 15;19(1):60

9. Wong J, Pushparajah K, de Vecchi A, **Ruijsink B**, Greil GF, Hussain T, Razavi R. Pressure-volume loop derived cardiac indices during dobutamine stress: a step towards understanding limitations in cardiac output in children with hypoplastic left heart syndrome. *Int J Cardiol* 2017:230:439-46.

10. Velasco Forte MN, Nassar N, Byrne N, Vieira MS, Perez IV, **Ruijsink B**, Simpson J, Hussain T. Morphological three-dimensional analysis of papillary muscles in borderline left ventricles. *Cardiol Young* 2017:1-8.

11. Veel E, Westera L, van Gent R, Bont L, Otto S, **Ruijsink B**, Rabouw HH, Mudrikova T, Wensing A, Hoepelman AIM, Borghans JAM, Tesselaar K Impact of Aging, Cytomegalovirus Infection, and Long-Term Treatment for Human Immunodeficiency Virus on CD8+ T-Cell Subsets. *Front Immunol.* 2018:9:572.

Currently submitted publications:

12. **Ruijsink B**, Moireau P, Pusparajah K, Wong J, Hussain T, Razavi R, Chapelle D, Chabinoik R et al. Biomechanical modeling of the dobutamine stress response in exercise induced failure of the Fontan circulation. Submitted for publication 2018.

Contents

List of Figures

List of Tables

Abbreviations

CO	Cardiac Output
HR	Heart Rate
EDV	End-systolic Volume
ESV	End-diastolic Volume
SV	Stroke Volume
EF	Ejection Fraction
RA	Right Atrium
RV	Right Ventricle
MPA	Main Pulmonary Artery
Ppa	Pulmonary Artery Pressure
PVR	Pulmonary Vascular Resistance
PVD	Pulmonary vasodilation
LA	Left Atrium
LV	Left Ventricle
EDV	End-diastolic Volume
SVR	Systemic Vascular Resistance
MSFP	Mean systemic Filling Pressure
MRI	Magnetic Resonance Imaging
CMR	Cardiac Magnetic Resonance
XMR	Combined cardiac catheter and magnetic resonance imaging

CPET	Cardio-Pulmonary Exercise Testing
TCPC	Total Cavo-Pulmonary Connaction
ms	milliseconds
Hz	Herz

Chapter 1 Introduction

1.1 Motivation

In the recent decades, quantitative assessment of cardiac function using non-invasive imaging has become routine in clinical cardiology practice. This development has improved prognostic stratification and therapy planning and reduced the need for invasive assessment in patients with heart diseases [1]. However, current state of the art imaging techniques only allow high quality imaging at rest. This means that diagnostic and prognostic assessment of heart disease is limited to detection of abnormalities that occur in the heart at its most relaxed state. Therefore, some pathological abnormalities can be missed or only be detected in a very late stage of disease.

In essence, the heart is a mechanical pump. In order to maintain adequate supply of oxygen during stress, the heart has a large reserve capacity, the so-called cardiac reserve. It can increase cardiac output up to 6x its resting values by increasing ejection of blood (contraction) and frequency of pumping (heart rate) [2]. This response significantly increases the amount of work for the heart. During exercise, cardiac oxygen consumption per minute increases up to nearly 500-600% resting values [3].

Investigating the functional reserve of the heart has great potential value for clinical cardiology and research. It can improve early detection and prognostic stratification of cardiac disease, but also allows for investigation of key (patho-)physiological mechanism that involve not only the heart but also the circulation [4]. The latter is especially important in patients with complex congenital heart diseases in whom a mix of cardiac and circulatory abnormalities often play a significant role.

The value of assessing cardiac function during exercise is widely recognized. However, all currently available exercise examinations have limitations that impede assessment of biventricular function. Cardiopulmonary exercise testing (CPET) allows identification of an abnormal exercise response of the heart, but the lack of imaging data means the mechanism underlying the abnormal response can often not be identified. Exercise echocardiography and exercise radio-nucleotide ventriculography provide images of the heart. However the quality

of imaging during exercise is suboptimal, resulting in inaccuracies in measurements of cardiac function [5]. Furthermore, both techniques only allow accurate quantification of left ventricular (LV) function, hereby ignoring the right ventricular response.

Cardiac magnetic resonance imaging (CMR) is the current gold standard for non-invasive assessment of cardiac function and allows measurements of both left and right ventricular function and quantification of blood flow [1]. Conventional CMR requires ECG gating and breath-held acquisitions that collect image data over multiple heartbeats. This prohibits any bodily movement and therefore imaging can only be performed at rest. In recent years, several CMR research group have developed highly accelerated 'real-time' non-ECG gated, free breathing CMR sequences that allow imaging during or directly after physiological exercise [4, 6–8]. These techniques have shown promising results for quantification of biventricular function during exercise, however through-plane motion of the heart during heavy breathing significantly impacts accuracy of the cardiac volume measurements [9]. Manual processing of the images, by selecting target images for volume classification on each slice in a predefined breathing state, overcomes these inaccuracies but is very time-consuming and therefore also not desirable for frequent use in clinical studies [4].

As no good techniques currently exist, comprehensive imaging studies of the heart during exercise are scarce. As a result, fundamental mechanisms of cardiac function during exercise have remained unknown. One of the largest gaps in current knowledge is what the exact role of the RV is in the biventricular heart. The RV has often been viewed as a weak, supportive pump. However, recent evidence of the importance of RV function in exercise performance [10] and its impact on the course of cardiac diseases typically linked to the LV [11, 12] seems to suggest that the RV plays a key role in overall cardiac function, especially during exercise and other forms of stress. The RV and LV are very different in structure, function and loading conditions. This suggests distinct roles for the two ventricles in the operation of the biventricular heart. It therefore seems logical that the two ventricles work highly cooperatively to optimize total cardiac performance. However, too date such a mechanism remains unidentified and the two ventricles are still generally viewed as individual entities [13].

Stroke volume (SV) is the ultimate functional output of cardiac contraction. During exercise, the heart maintains SV despite a striking decrease in ejection and, especially, filling times as a consequence of the increase in heart rate (HR) [14–16]. This means that the heart must use its functional reserve during exercise to maintain ejection and filling. If there is a fundamental synergy between RV and LV function in the heart, it is likely that this

mechanism plays a central role in the heart's ability to maintain SV during exercise. Therefore, investigation of SV preservation during exercise is likely to allow identification of the mechanism of biventricular cooperation.

Establishing the role of the RV in cardiac function is relevant for understanding cardiac physiology in general. However, for patients with a Fontan circulation this understanding is pivotal. The Fontan circulation is a surgically established single-ventricular circulation [17]. It is a palliative treatment option for patients in whom one of the two ventricles in functionally unable to support the circulation. As a consequence, the Fontan circulation lacks a sub-pulmonary pump. While lifesaving, patients with Fontan circulation experience a burden of morbidity and profound exercise intolerance [18]. In particular, a constant and progressive decline in cardiac performance is observed in nearly all Fontan patients with age, resulting in premature failure of the circulation and a decreased life expectancy. The cause and pathway of this seemingly inevitable decline to failure of the Fontan circulation is unclear [19]. As a result, no current therapy has been recognized that successfully halts or slows down the decline in function in Fontan patients. It seems obvious that the absence of a sub-pulmonary ventricle plays a crucial role in development of failure. This makes understanding of the biventricular synergy in the heart, in particular the role of the RV in this synergy, key to the understanding of the general principles of Fontan haemodynamics.

Besides understanding the general principles of Fontan haemodynamics, patient-specific investigation of mechanisms of heart failure in patients with Fontan circulation also remains challenging. Due to the complexity and unusual physiology of the Fontan circulation, conventional non-invasive imaging parameters and invasive pressure measurements often fail to identify clear causes of failure. Therefore, several specialized centres, including our Guys' and St Thomas Hospital and Evelina Children's Hospital, utilize detailed, combined diagnostic cardiac catheter and CMR exams (XMR) during dobutamine stress to provide better diagnostic assessment of patients developing failure of the Fontan circulation [20]. These exams provide a wealth of information in the form of simultaneous measurements of invasive pressures and CMR derived blood flow and cardiac volumes. Unfortunately, interpretation of these results remains challenging. All the obtained measurements are interrelated and the complexity of the circulation makes it hard to interpret all this data in an integrated, comprehensive way.

Computational modelling methods could potentially improve the ability to identify causes of failure in patients with Fontan circulation. Over recent years, highly detailed multi-scale biomechanical models of the heart and circulation have been developed. These models have shown their efficacy in predictions of cardiac physiology in both acquired and congenital heart diseases [21–23]. Cardiovascular computational modelling frameworks are build based on experimentally derived physical principles from the macro-structural level down to the

level of the sarcomere [24]. By integrating multiple measurements of cardiac and vascular function into such a modelling framework, a comprehensive overview of the state of the cardiovascular system can be obtained. This patient-specific, calibrated model then allows to determine the impact of key factors of the cardiovascular system (such as contractility and stiffness of the heart, vascular resistance, venous return propagation and heart rate) in the development of heart failure in individual patients. Therefore, such models are potentially well suited to enhance the diagnostic assessment of stress / exercise investigations in patients with Fontan circulation whom develop heart failure.

In summary, there is currently a lack of accurate, comprehensive non-invasive imaging for assessment of biventricular function during exercise / stress. This has restricted the investigation of the role of the sub-pulmonary ventricle (RV) in fundamental cardiac physiology. In turn, this limits our understanding of the impact of absence of the sub-pulmonary ventricle in patients with Fontan circulation, and the potential implications for treatment of these patients. Improved techniques for cardiac imaging during exercise and better use of quantitative methods to integrate data of diagnostic stress and exercise exams have the potential to enhance the understanding of physiological mechanisms in the heart in health and disease, both on population level as well as in individual patients.

This thesis aimed to: 1) address the shortcomings of imaging during exercise by developing a new method for CMR during exercise (Exercise CMR) and 2) utilize the developed Exercise CMR method to investigate the role of the RV in cardiac function and the impact of its absence in the Fontan circulation. To achieve this goal, cross-disciplinary translational imaging and image analysis methods needed to be developed involving the fields of MRI physics, image-processing, mathematical modelling and clinical medicine. In this thesis the results of this process are presented. First, the Exercise CMR method was developed and validated. This method was subsequently used to investigate the biventricular cooperation in SV preservation and augmentation during exercise in healthy individuals. After this, the impact of absence of the RV on exercise haemodynamics in Fontan patients was investigated and a potential new treatment target for optimization of cardiac function in Fontan patients was identified. Finally, the potential role of a computational modelling framework in aiding patient-specific diagnostic assessment of patients with Fontan circulation undergoing an XMR dobutamine stress exam was evaluated. An overview of the original contributions and the outline of this thesis are provided in the sections below.

1.2 Contributions

The original contribution of this thesis in the field of exercise imaging and clinical cardiology can be summarized as follows:

Developed an accurate, fast Exercise CMR imaging and processing framework. Accurate quantitative assessment of biventricular cardiac function during exercise has remained challenging. Real-time CMR imaging has shown promising results, but bodily motion currently still complicates accurate assessment. In this thesis, a new method for CMR during exercise is presented to overcome the current limitations. The developed framework for image acquisition and image processing allows imaging during physiological exercise while automatically correcting breathing and exercise motion. Using a pipeline for retrospective respiratory and cardiac gating, real-time images where converted to conventional cine stacks. This method enhanced usability of Exercise CMR and experimental evaluation showed improved accuracy of quantification of volumes over other techniques.

Defined the role of the RV in the healthy heart during exercise. The two ventricles of the heart are very different in structure, function and loading conditions. This suggests that they have distinct roles in cardiac function and cooperate to optimize total cardiac performance. Whereas clinical observations have shown that the RV must have a significant impact of LV function, the mechanism underlying this cooperation, and the importance of the RV in this mechanism, remains largely unknown. In this thesis the experiments that were designed to investigate this cooperative mechanism between RV and LV function are presented. These Exercise CMR experiments demonstrated a fundamental synergy between RV and LV function in the biventricular heart that optimizes efficiency of SV delivery during exercise. RV systolic function has a pivotal role in this synergetic mechanism. By regulating LV filling it optimizes efficiency of LV SV augmentation. This work illustrates the pivotal interdependency of the two ventricles in optimizing cardiac function. This is a significant contribution to the current understanding of cardiac physiology.

Demonstrated the impact of absence of a sub-pulmonary ventricle in the Fontan circulation during exercise and showed the benefit of acute HR reduction therapy on ventricular function and cardiac output in patients with Fontan circulation. The mechanism behind development of exercise intolerance and heart failure in patients with Fontan circulation has not been well understood. Inefficient haemodynamics potentially contribute to the constantly progressive decline in cardiac performance in these patients. Using Exercise CMR, exercise haemodynamics were investigated in patients with a Fontan circulation (type: total cavo-pulmonary connection). This work showed that the absence of a sub-pulmonary ventricle significantly deteriorates cardiac function during exercise, as ventricular filling cannot be maintained with increasing

HR, resulting in a drop in SV and CO. Acute selective heart rate inhibition significantly improved exercise haemodynamics in our group of Fontan, resulting in an improved cardiac output and a higher energetic efficiency of the single ventricle during exercise. These experiments illustrate the key role of HR in Fontan physiology, hereby improving understanding of the Fontan haemodynamics. This might imply a potential beneficial role of for selective heart rate modulation in optimization of cardiac function in patients with Fontan circulation. Whether this benefit remains beyond this acute study in larger trails and for patients with other variants of Fontan circulation, needs to be further investigated.

Evaluated the use of a computational modelling framework to aid patient-specific CMR assessment of exercise intolerance in patients with Fontan circulation. Causes of exercise intolerance and failure of Fontan circulation are often hard to assess even when highly detailed examinations are used, such as combined cardiac catheterisation and CMR (XMR) during dobutamine stress. In this thesis, the potential value of computational modelling in improving diagnostic capacity of the XMR dobutamine stress exam was evaluated. A framework was developed to utilize the data obtained during the XMR exam to inform and calibrate patient-specific biomechanical models of the single ventricle coupled with the circulation. It was shown that the proposed modelling framework allows identification of patient-specific pathophysiological mechanisms underlying the exercise intolerance, thereby improving the diagnostic value of the XMR exam.

1.3 Outline

The thesis is organised in 6 further Chapters. Chapter 2 provides a background to the topics fundamental to this thesis. Chapters 2, 3, 4, 5 and 6 will describe the original contributions of the PhD. Chapter 7 provides a summary of the contributions and focuses on future directions.

Chapter 2 Background

In this Chapter, a review of the literature and background relevant to the studies performed during the PhD is given. In the first section, an overview of cardiovascular exercise dynamics is given. After this, the Fontan circulation is discussed, including Fontan haemodynamics at rest and during exercise. Finally, Section 2.3 will provide a background of cardiac magnetic resonance imaging.

2.1 Healthy Heart during Exercise

Together, the two ventricles of the heart generate stroke volume (SV) and consequentially provide cardiac output (CO) to the body. One of the main topics of this thesis is the investigation of the mechanism underlying SV preservation and augmentation during exercise. In this chapter a basic introduction is given to cardiac physiology including the cardiac response during exercise to put the original contributions of this thesis in context. Most information is inspired by textbooks of medical physiology and cardiology [2, 25].

2.1.1 Basic concepts of biventricular cardiac function

In the healthy heart, the right and left ventricles (RV and LV, respectively) are connected in series with the pulmonary circulation and systemic circulation. As a consequence, both ventricles are forced to generate a similar SV. However, the two ventricles have very distinct geometrical, structural and functional differences. These differences originate from early development. The two ventricles have a separate embryological origin; the LV develops from the primary heart field, while the RV originates from the secondary heart field [26].

2.1.2 Anatomy of LV and RV

This fundamental difference in development is reflected in the macro- and micro-anatomical structure of RV and LV. The RV is thin walled, highly trabeculated and has a triangular and crescent shape. On the other hand, the LV has a thick muscular wall, which is mostly smooth and has a bullet-like, ellipsoid shape. The myofibre architecture is also different between the two ventricles. In the RV, the superficial outer myofibres are oriented circumferentially, parallel to the atrio-ventricular valve plane, and point obliquely towards the apex. The deeper

RV myofibres are arranged longitudinally. The LV, the superficial (inner and outer) myofibre structure are obliquely and helically oriented, with a fibre angle of ~60°, while in the middle layer the fibres are oriented circumferentially. These macro- and micro-anatomical differences between the two ventricles are reflected in their contraction patterns. The RV contraction is peristaltic, starting at the inlet and propagating towards the outlet, with a mostly longitudinal motion. While in the LV, contraction of the muscle is predominantly circumferential and radial, with additionally a prominent contribution of twisting motion. Compared to the LV, the RV has a larger myocardium-blood surface to volume ratio. Therefore, a smaller inward motion of the ventricular wall is needed to eject a similar SV [27].

The two ventricles are supplied by three main coronary arteries: the left anterior descending (LAD), the left circumflex (LCx) and the right coronary artery (RCA). In general, the LV anterior wall and anterior parts of the septum are supplied by the LAD, while the lateral wall is supplied by the LCx and the inferior wall and inferior septum by the RCx. In a right dominant coronary system (~80% of the population) the RCA supplies most of the RV, with the branches of the LAD supplying the anterior wall and the antero-septal region. The infundibulum is supplied by the conal artery, which in ~30% of the population has a separate ostial origin.

2.1.2.1 Myocardial perfusion

In the LV, coronary blood flow largely occurs during diastole, with complete to near cessation of flow during systole (due to the high pressure in the LV muscle). However in the healthy RV, coronary blood flow occurs both in systole and diastole. Interestingly, while having a lower oxygen demand, the RV has a more extensive system for collateral perfusion than the LV, which has almost none. This is mostly due to the presence of the moderator band artery, a branch of one of the septal perforator arteries originating for the LAD. Coronary artery flow consists of approximately 5% of total cardiac output. The LV oxygen extraction is large, even at rest it extracts ~75-80% of all the supplied oxygen. Therefore, increasing oxygen supply to the LV is dependent on increasing perfusion. The RV, typically only extracts 50% of oxygen [28]. This reflects its lower work but also means that the RV has a significant myocardial perfusion reserve. Indeed, during exercise, the RV can first increases its oxygen extraction, before having to rely on vasodilation, whereas the LV is purely dependent vasodilation from the start [29]. Altogether, this suggests that the RV has a much larger reserve capacity to increase myocardial perfusion than the LV. While at rest, this might seem contradictory, during exercise this reserve is utilized by the RV. While LV afterload

only rises by a factor 1.5, RV afterload can rise significantly more (100-150%), resulting in a disproportionate increase of RV systolic wall stress [10].

2.1.2.2 Sarcomere Contraction

The heart contracts due to shortening of the muscle cells. The sarcomeres, contained within myofibrils, deliver the actual shortening of the muscle cell that allows the heart (and other muscles) to contract with force, see Figure 2.1. This shortening is based on an interaction between the thick and thin myofilaments of the sarcomere. Actin fibres combined with regulatory proteins such as tropomyosin and troponin form the thin myofilaments. The thick myofilaments consist of a myosin protein. Repeated cycles of cross-bridge formation between the myosin heads and the binding sites of actin causes a sliding motion of the myosin myofilament along the actin fibrils, leading to shortening.

Under resting conditions, the binding sites on the actin fibres are blocked by troponin-tropomyosin complexes. However, the presence of Calcium ions (Ca^{2+}) causes a change in conformation of the troponin-tropomyosin complexes, which uncovers the actin binding sites. ATP-activated (elongated) myosin heads bind with high affinity to the actin myofilaments and forms a cross-bridge under tension. Formation of the cross bridge is then followed by a passive re-conformation of the myosin head into a non-elongated state. This shifts the myosin myofilament along the actin myofilament. Renewed binding of ATP to the myosin head activates it again, causing it to release the binding site and elongate. It will then form a new cross bridge with the next available binding site on the actin myofilament and the cycle of cross bridge formation and sliding is repeated. This process of passive myosin-actin binding and active myosin elongation is repeated as long as the actin binding sites are uncovered (i.e. as long as the Ca^{2+} concentration is high). In order to relax, Ca^{2+} must be actively removed from the cytosol.

Muscle cells have well developed sarcoplasmatic reticulum (SR). SR stores Ca^{2+} and transporter channels on its surface regulate the influx and active removal Ca^{2+} from the cytosol. After generation of the membrane action potential, electrically activated slow reacting Ca^{2+} channels, so called dihydropyridine receptors (L-Ca^{2+} channel), that are located in the T-tubules, release Ca^{2+} into the cell. After an initial 10-20% increase in Ca^{2+} concentration via these cells, a second Ca^{2+} channel (called the ryanodine receptor) is activated. This channel rapidly releases a large amount of Ca^{2+} ions from the SR into the cytosol. Ca^{2+} re-uptake is an active process in which several active transporter channels are involved, such as the Na^{+} / Ca^{2+} channel and an ATP consuming calcium pump.

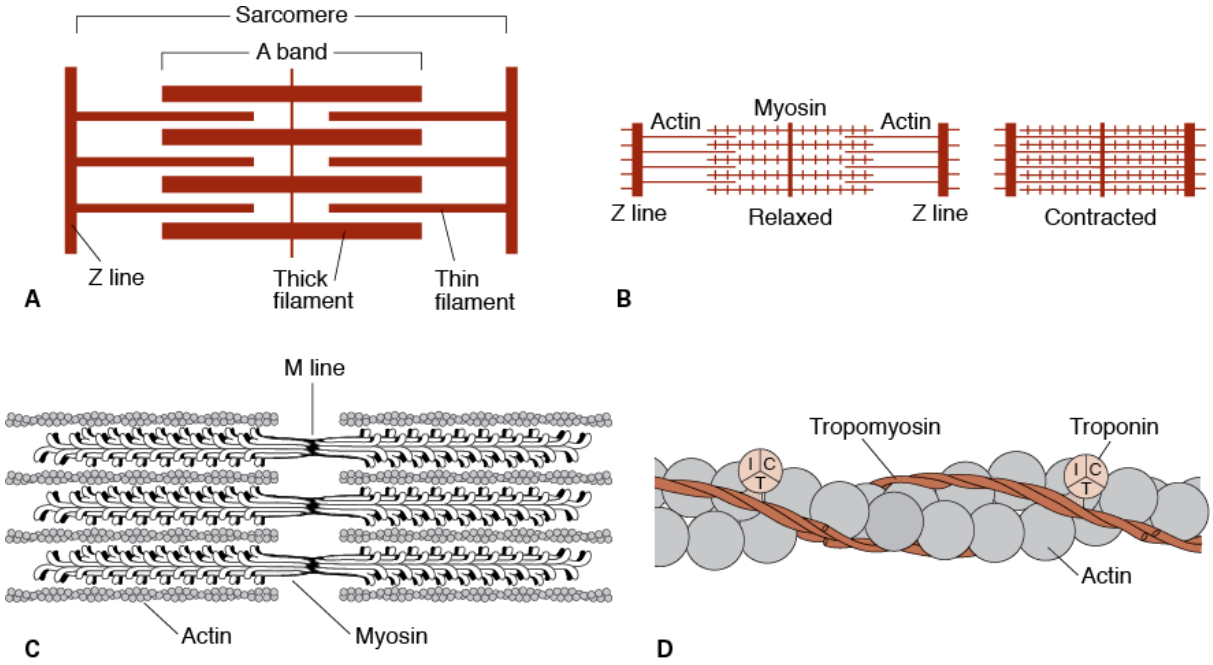

Figure 2.1 Sarcomere and its components. A) Schematic representation of the sarcomere, B) sarcomere in relaxed and fully contracted state, C) actin and myosin filaments, interactions in the sarcomere and D) actin myofilament with the troponin-tropomyosin complexes. From [25].

2.1.2.3 Ventricular Function and Loading conditions

The individual anatomical and functional features of the LV and RV seem to fit their individual loading conditions. At rest, the RV operates with a relative low preload, while it ejects against a highly complaint, low-pressure pulmonary circulation. Filling of the RV is mostly dependent on systemic venous return flow, which in turn is dependent on cardiac output, systemic venous tone and propagation of flow through, for example active muscle contractions. The thin wall, large volume-surface area and relative high compliance of the ventricle support is beneficial in this environment, as it minimizes the resistance to filling of the ventricle [30]. However, due to the low afterload, wall stress remains relatively low. A second benefit of the low RV afterload is that iso-volumetric contraction and relaxation times are relatively short in the RV. Therefore, duration of filling is longer [31]. This compensates for the lower filling velocities in the RV compared to the LV.

In the LV, systemic afterload is ~5-6 times higher than the RV. Therefore, the LV needs to generate a significantly larger stroke work to eject blood, see Figure 2.2. As a result, oxygen consumption of the LV at rest is nearly 5 imes as much as that of the RV at rest. The LV

geometry supports its task of overcoming the high afterload; the LV has a thick muscular wall and an ellipsoid shape that keeps its volume-surface ratio low. This minimizes wall stress. Furthermore, its radial and circumferential contraction pattern optimally utilizes the generated wall stress to rapidly increase intra-ventricular pressure.

The distinct different contractions in the ventricles can be well observed using pressure-volume (PV) loops; while the LV has a squared shape PV-loop (fast pressure generation to overcome afterload) the RV has a more trapezoid shaped pressure volume loop, in which pressure is still build up during ejection and increases while the ventricle is still ejecting, see Figure 2.2. While aiding ejection, the structure of the LV makes it less compliant compared to filling than the RV. In order to maintain similar filling, the LV thus needs a higher preload. Indeed, left atrial pressures are significantly larger than right atrial pressures (LA pressure: 6-12 mmHg, RA pressure: 3-8 mmHg). As a result, the LV is less influenced by factors such as filling time and heart rate compared to the RV, despite having a lower compliance [32].

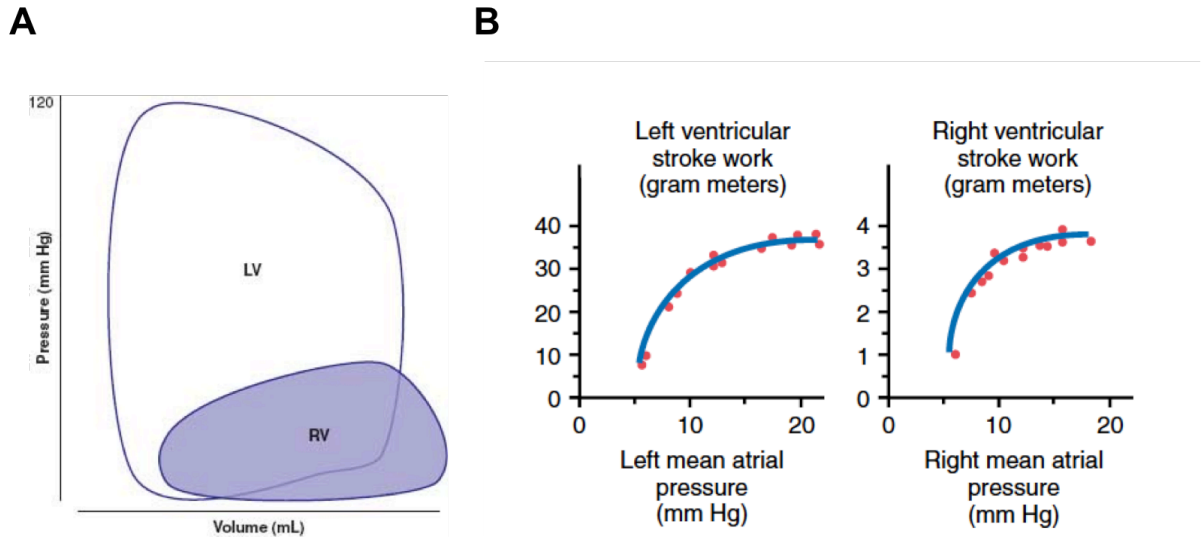

Figure 2.2 Right and left ventricular function and work. A) Pressure-volume (PV) loops of RV and LV. Note the trapezoid shape of RV compared to LV, with minimal isovolumetric contraction. Also note the larger RV size. B) Left and right ventricular stroke work (= area within the PV loop in A) function plot shows significant larger work in LV compared to RV throughout a range of atrial pressures. See Section 3.2.2 for explanation of function plot. A adapted from [33], B from [25].

2.1.3 The healthy heart during exercise

The hearts' behaviour during exercise has been of interest of researchers since more than a decennium. However, the inevitable body motion and exertion that accompany exercise have made detailed assessment of the heart difficult; see Chapter 2.3.4 for more details. Imaging

studies of the heart have so far been limited and sometimes resulted in variable results due to inaccuracies in methods of measurement. In this section, the most consistent findings are presented to give an overview of the cardiac behaviour during exercise. Most exercise studies so far have only analysed LV behaviour. Therefore, most of this section will cover the behaviour of the LV, with a more cautious description of RV dynamics during exercise, as evidence of RV behaviour during exercise is scarce.

2.1.3.1 Regulation of cardiac function during exercise

Cardiac output is the product of the frequency of cardiac contraction, heart rate (HR) and the volume ejected per beat, stroke volume (SV): CO = HR times SV. At rest, cardiac output in healthy adults is ~5-6 L/min, but this can increase 5- to 6-fold during exercise. Cardiac output in the body is tightly regulated by oxygen demand of the peripheral tissues. Higher metabolic needs in the tissue causes a direct effect of increased perfusion thanks to auto-regulation mechanisms within the tissues themselves. The response of the heart to the increased metabolic demand of the body is regulated through a direct heterotropic regulation based on the Frank-Starling mechanism and indirect regulation of inotropy (contractility), chronotropy (heart rate), dromotropy (increase in conductivity in the conducting system of the heart) and lusitropy (an increased rate of relaxation), mostly, but not exclusively, through sympathetic activation. All these factors contribute to acute regulation of CO. In the longer term (months-years), the heart's ability to increase CO can be regulated further by growth of the ventricles (myocardial hypertrophy and ventricular dilatation) combined with down-regulation of resting heart rate.

2.1.3.1.1 Heterotropic regulation (Frank-Starling Law)

In the end of the 19th and beginning of 20th century, Otto Frank and Ernst Starling described a phenomenon of a 'spontaneous' increase in stroke volume of the left ventricle after increasing end-diastolic volume [34]. This effect was found independent of inotropic, chronotropic and lusitropic regulations and has become known as the Frank-Starling law. It describes the relationship between end-diastolic myocardial fibre length and its force of contraction, see Figure 2.3A. Initially, the effect of increased force with length was explained by a better overlap between actin and myosin molecules when the myocardial fibre is stretched, which would result in a higher number of cross-bridge formations. Nowadays, an increased Ca^{2+} sensitivity due to stretch and passive tension of the sarcomeres is believed to be the major component increasing contractile force [35].

Stretch of the ventricle (e.g. end-diastolic fibre length) is determined by end-diastolic volume. End-diastolic volume in turn is dependent on end-diastolic pressure. For an individual muscle fibre, preload is defined as the passive force that establishes muscle fibre length before contraction. In the heart, preload can therefore be best defined as end-diastolic pressure, as this determines maximal volume of the ventricle and therefore is the main determinant of end-diastolic fibre length. Most physiological experiments demonstrating the Frank-starling mechanism have been performed in ex-vivo isolated heart-lung preparates. In these preparates, the pericardium is often not present allowing for an unlimited, regulated increase end-diastolic pressure. Figure 2.3B shows typical cardiac output curves (so called Starling or ventricular function curves). As illustrated in this figure, CO can markedly increase just by stretch alone (up to 12-13 L/min). In vivo, such effects are less pronounced, as the heart is constrained by the pericardium and thoracic cage, but this illustrates the important potential contribution of the Frank Starling mechanism in CO generation. The Frank Starling mechanism is believed to be especially important in maintaining equilibrium between right and left ventricular output. As the circulation is a closed-loop in which the two ventricles are coupled in series, a mismatch in ventricular output would lead to a shift of blood to one of the two circulations. Due to the presence of the Frank-Starling mechanism, an unequal increase in output of one ventricle, resulting in a larger preload of the other, would automatically increase in adaption of output of the second through increased stretch and vice-versa. As previously discussed, the RV operates under lower preloads than the LV. This is reflected in the Frank-Starling curves of the two ventricles, in which the RV curve is shifted to the right compared to the LV curve, see Figure 2.3B.

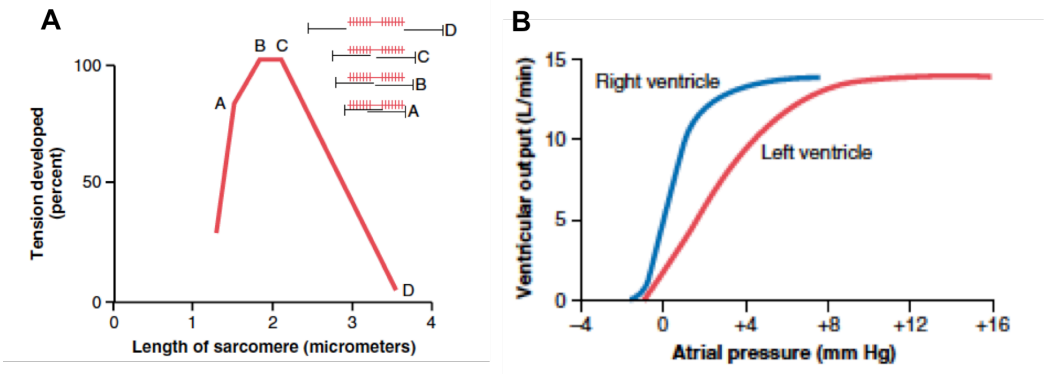

Figure 2.3 A) Force-tension relationship in the sarcomere. Note the increase in tension during stretch of the sarcomere (A, B) up to a maximal distance (C) before overstretching results in a decrease in tension (D). B) Frank-Starling curves of LV and RV show the relationship between atrial pressure and LV and RV ventricular output respectively. Note the different sensitivity for preload in RV and LV. From [25].

2.1.3.2 Heart Rate Response during Exercise

Heart rate is often regarded as the main mechanism contributing to the acute increase in CO during exercise or other causes of increased metabolic demand of the body. However, it is noteworthy that this HR response is only effective when SV can be preserved. When HR increases cause a drop in SV due to impaired filling, these HR increases become less efficient.

At initiation of exercise, a coordinated autonomic response is triggered in the medulla that withdrawals parasympathetic activation to the heart. This withdrawal of vagal function contributes to the initial 15-20% of HR increase. Following with the parasympathetic withdrawal, sympathetic activation starts, resulting in a further stimulus of the sinusnode to increase frequency. Muscle motion and metabolism than further stimulate the sympathetic system local chemo- and mechanoreceptors that identify muscle contractions. Additionally to this direct sympathetic effect, catecholamine's are released from the adrenal medulla resulting in a further reinforce the increasing HR. Altogether, these mechanisms can increase HR from resting values of 60-80 beats per minute (bpm) up to as high as ~200 bpm. The increase in HR results in a significant change in systolic and, especially, diastolic time-intervals (reference time intervals). Systolic time reduces mildly due to fast ejection by approximately 30% (from ~320 millisecond to 230 milliseconds). Changes in diastolic time, however, are significantly larger. Diastole falls more than 50-60% (from ~500-600 milliseconds to ~200-220 milliseconds) [36].

2.1.3.3 Inotropic and lusitropic regulation

The force of contraction is not only regulated by fibre length, but also by frequency of contraction (force-frequency relationship) and the sympathetic nerve activity. These stimuli increase alter the contractile properties of the myocardium, e.g. the strength of the contractions after activation. This is defined as an increase in inotropy. Inotropic stimulation increases contractility by several mechanisms, such as increased sensitivity of the ryanodine receptors, resulting in a larger concentration of Ca^{2+} in the cytosol, increased myosin ATPase activity or direct increase of the rate of cross-bridge formation. Lusitropy (the force of relaxation) is enhanced by an increased re-uptake rate of Ca^{2+} ions from the cytosol into the SR. Both inotropy and lusitropy are controlled by sympathetic activation. As shown by

Janssen et al. the kinetics of relaxation and contraction in the heart muscle are tightly linked and do not vary independently [37].

The sympathetic nerve system is central in regulation of chronotropy, inotropy, lusitropy and dromotropy of the heart. It additionally plays an important role in regulation of the peripheral vascular responses. See Figure 2.4 for a schematic of the sympathetic nerve system's influence on stress haemodynamics.

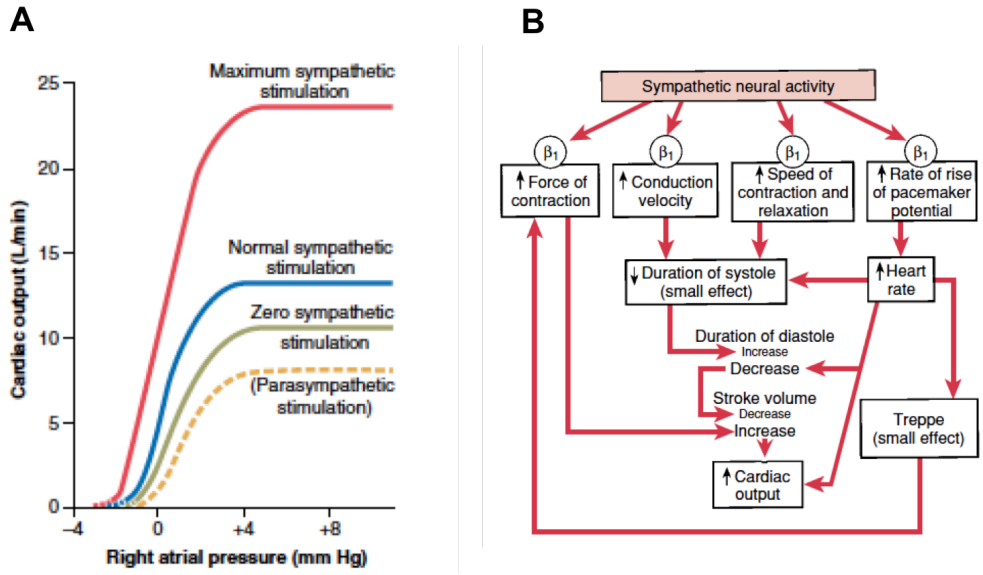

Figure 2.4 Impact of sympathetic activation on cardiac output curve (A) and function (B). From [25].

2.1.3.4 RV during exercise

As noted before, only few studies have investigated the RV response to exercise due to the challenges in imaging the RV during exercise using the currently available methods. Invasive studies are available, however imaging studies are scarce lacking. Even if available, data needs to be reviewed cautiously as the complex shape of the RV is likely to make quantitative assessment challenging. Recently, some research groups have used dobutamine stress as a pharmacological surrogate to exercise to investigate RV behaviour using CMR. Pharmacological stress does not mimic all the complex physiological responses during exercise. However, the findings of these studies give some idea about the behaviour of the RV during exercise.

Based on previous invasive studies, it is clear that RV preload does not significantly increase up to near maximal levels of exercise [38, 39]. In the human cardiovascular system, RV preload is governed by systemic venous return, which in turn is determined by factors outside the heart (the muscle pump, venous capacitance and venous return). This implies that RV

filling is only mildly augmented during exercise, despite a significant reduction in diastolic filling time. This is in keeping with the observation in dobutamine stress CMR studies that RV end-diastolic volume (EDV) falls with increasing HR's [40–42]. Although the muscle pump is not active during dobutamine stress, the only available physiological exercise CMR investigations, from La Gerche et al., shows a similar fall in RV EDV [9].

The fall in EDV in the RV with increasing HR seems to imply that during exercise RV SV is maintained by a constant increase in contractility, in order to lower ESV. However, this is currently not well established.

2.1.3.5 Pulmonary Circulation during Exercise

The pulmonary circulation is a highly distensible high flow, low-pressure circulation. Whereas the relative volume of the pulmonary vascular bed is small, it accommodates total CO. Especially during exercise, this means that blood flow through the lungs increases up to 5 times its resting values. At rest, pulmonary vascular resistance is low (1-2 Woods units•m^2) and the vasculature is close to maximally dilated. Only in hypoxic conditions or lung diseases, PVR is increased. As a result, PVR decreases only minimally during exercise at sea level in healthy individuals. Pulmonary vasodilation (PVD) has shown to not impact pulmonary blood flow at sea level in healthy individuals, even during exercise.

Main pulmonary arterial pressure (Ppa) is low at rest (< 20 mmHg mean pressure) resulting in a low RV afterload. However, as PVR decreases only minimally during exercise, augmentation of CO leads to a nearly linear increase in Ppa [43, 44]. Therefore, during exercise Ppa pressures increase significantly, resulting in a large increase in afterload and myocardial wall stress in the RV [45]. Based on invasive measurements during supine exercise in 63 healthy subjects (including 21 women) regression models showed an average increase of 1±0.91 mmHg mean Ppa for each liter increase in Q in healthy young adults [46]. However, it must be noted that there was a large individual variety in linear regression slopes (SD of 0.91 mmHg) making individual estimates based on these regression lines not feasible.

The size of the pulmonary circulation is small. Therefore, pressure generated by the RV is propagated through the pulmonary circulation towards the left atrium (LA). As a result LA pressures increase significantly during exercise [15, 45, 47]. The relationship between LA pressure and Ppa relates nearly linearly during exercise, suggesting that preload of the LV is significantly increased with increasing HR [44].

2.1.3.6 LV during exercise

2D echocardiographic exercise studies and cardiopulmonary exercise tests in healthy trained and untrained volunteers suggests that LV SV, after an initially increase of 15-30% at onset, remains constant during all stages of exercise [48–50]. This preservation of SV is vital for CO augmentation; it allows the heart to linearly increase CO with increasing HR (as CO = SV x HR).

Both echocardiographic [51, 52] and CMR [53, 54] exercise studies have reported that LV EDV is maintained during exercise. This is keeping with the previous discussed enhancement of LV preload, which supports LV filling during the increase in HR. The initial increase in SV during exercise is caused by a fall in LV ESV. This fall seems to be the consequence of a decrease is systemic vascular resistance (SVR) and an increased contractility [55, 56]. After a heart rate of 130-135, ESV does not change any further. From that moment, SV is maintained [14, 57], likely as a result of the preload enhancement in the LV. This preservation of EDV in the face of the striking decreased diastolic filling rate implies that filling needs to be augmented to 4 to 5 times the resting values during peak exercise. In trained athletes, LV EDV even seems to increase during exercise [58–60]. This is in keeping with reports that show that endurance trained athletes increase pulmonary artery pressures to a larger extend during all levels of exercise than non-athletic controls [45, 61].

2.1.3.7 Systemic Circulation during Exercise

During exercise, the systemic circulation undergoes a range of changes to accommodate the increased CO of the heart and transport it to the metabolically active tissues. In order to distribute the blood effectively to the exercising muscles, a complex neural, hormonal and mechanical response mechanism affects the systemic circulation. Blood is redistributed to the specific vascular beds (exercising muscles, skin), while blood flow to other regions (e.g. the visceral organs) is decreased. A review of all of these mechanisms is beyond the scope of this thesis. While the sympathetic drive during exercise initially leads to general in arterial vasoconstriction, this drives is locally suppressed in metabolic active tissues and muscles, resulting in hyperemia. This mechanism allows the body to distribute blood to the most metabolic active regions, while non-active regions do not experience overperfusion. This way, the peripheral vasodilation, and the resulting drop in systemic vascular resistance (SVR), is proportional to the amount of muscles used and their activity.

SVR is significantly larger than PVR (25-30 Woods units•m^2). Due to the extensive vasodilation during exercise, SVR can drop up to 50-60%. However, even after the more pronounced fall in SVR during exercise, SVR remains significantly higher than PVR.

2.1.3.8 Atrial function during exercise

The atria contribute to filling by being a reservoir for blood during ventricular systole and a conduit for venous blood during diastole. Towards the end of ventricular diastole, the atria contract actively, hereby supporting filling. In the healthy heart, this atrial contraction attributes to about 15% of ventricular filling. Studies on atrial function during exercise in healthy individuals are scarce. Using echocardiography, it was shown that left atrial strain is significantly increased during [62] and directly after cessation of exercise [63]. Schnell et al. recently published the only available study on atrial volume and ejection during exercise [64]. This study showed that both right and left atrial function increases during exercise. Their work also showed that maximal right atrial size decreases with exercise, while maximal left atrial size does not. This is in keeping with the changes in RV vs. LV preload during exercise and suggests that the LA is (and thus LV) filling is better maintained during exercise than RA and RV filling.

In athletes, atrial function is not significantly different from healthy during exercise [62, 64]. Atrial volumes at rest are larger compared to sedentary healthy volunteers, but the changes during exercise are similar in the two groups. This suggests that the larger atria especially function as reservoir for early ventricular filling.

2.1.4 Ventricular interdependence in the biventricular heart

Based on [30, 31]

Due to their inherent structural connection and shared ventricular septum, the two ventricles impact each-others behaviour. This interdependence is called mechanical ventriculo-ventricular interaction. In-vivo and ex-vivo animal experiments have shown that approximately 20-40% of RV ejection is dependent on contraction of the LV (including the septum). On the other hand, pressure or volume loading of the RV can result in inward bulging of the septum towards the LV (septal shift) that impairs LV inflow or can result in decreased LV elastance. As RV pressure is lower than LV pressure, the shared septum implies that the RV can utilize the firm contracted LV as a wall to contract towards. This decreases its contractile costs and makes RV function less to RV myocardial scarring or damage, as long as the LV function remains intact.

Researching ventricular interdependence in this thesis

The clear differences in structure, loading and contraction between the RV and LV suggest that the two ventricles are likely to have distinct functional roles in the process of CO generation. The heart is a single organ with two pumping chambers and it seems likely that these chambers both play an individual role to optimize the total function of the heart. This notion is supported by the observation that the RV seems to have an important impact on prognosis and treatment efficacy of typical LV diseases [11, 12]. Also, the fact that the single-ventricle circulation is burdened by progressive decline of cardiac function, see 2.2, seems to point towards an interdependency between the two ventricles. Understanding of this mechanism of ventricular interdependency can provide a fundamental physiological understanding of cardiac function and might help to better understand the impact of absence of the RV on cardiac function in patients Fontan circulation. Therefore, one of the main focuses of this PhD was to investigate this mechanism.

2.2 The Fontan Circulation

The Fontan circulation is a surgically established palliation for complex congenital heart diseases in which one of the ventricles is functionally unable to support the circulation, a group also commonly referred to as 'univentricular hearts'. Although exact figures are unknown, the incidence of univentricular hearts is estimated at 3/10,000 live births [18]. Every year, over 200 of these patients undergo Fontan completion in the UK [65]. This surgery can be regarded as a major success in the treatment of this otherwise lethal disease. However, the unusual circulation in these patients results in a high incidence of morbidity and progressive deterioration of cardiac performance over the years, leading to a significantly reduced life expectancy. The mechanisms behind this deterioration are poorly understood. As a result, treatment options remain scarce and prognostic parameters are largely absent in this disease.

2.2.1 The Fontan Procedure

The Fontan procedure was originally developed by Dr. Fontan and Dr. Baudet as a palliation strategy for tricuspid atresia [17]. During the initial procedure, the right atrium was connected to the main pulmonary artery to allow blood flow to the lungs, while bypassing the ventricle. The Fontan operation was soon extended to the treatment of other forms of univentricular hearts and in 1987 Leval et al. proposed to functionally bypass the right heart completely by anastomosing the superior vena cava (SVC) directly to the right pulmonary artery (RPA) and creating an intra-atrial tunnel from the inferior vena cava (IVC) to the RPA [66]. An extra-atrial variant of this so-called total cavopulmonary connection (TCPC) followed soon and connected the IVC to the RPA via an extra cardiac tunnel, anatomically bypassing the heart completely. The intra- and extra-atrial TCPC have become standard treatment options for univentricular hearts over the years, and the original Fontan procedure is largely abandoned.

To minimize volume loading and acute changes in ventricular mass / volume ratio in these patients, Fontan palliation nowadays typically consists of three staged surgeries, of which the TCPC is the last one [18]. During the first stage, systemic blood flow from the single ventricle is secured and a temporary systemic-pulmonary shunt is constructed to allow blood-supply to the lungs (see

Figure 2.55). The second stage surgery unloads the heart partially by redirecting SVC flow towards the pulmonary arteries [67]. The third procedure, the Fontan procedure, finally completes the Fontan circulation by connecting the IVC to the RPA. Surgical mortality rates of the Fontan procedure has decreased markedly over the last decades; from 39% before 1982 to <2% between 2000-2010 [18, 68]. The overall mortality from birth to Fontan completion

remains high, with reported mortality rates ranging from 25-40% depending on the institution [69, 70], illustrating the complexity of construction of the Fontan circulation.

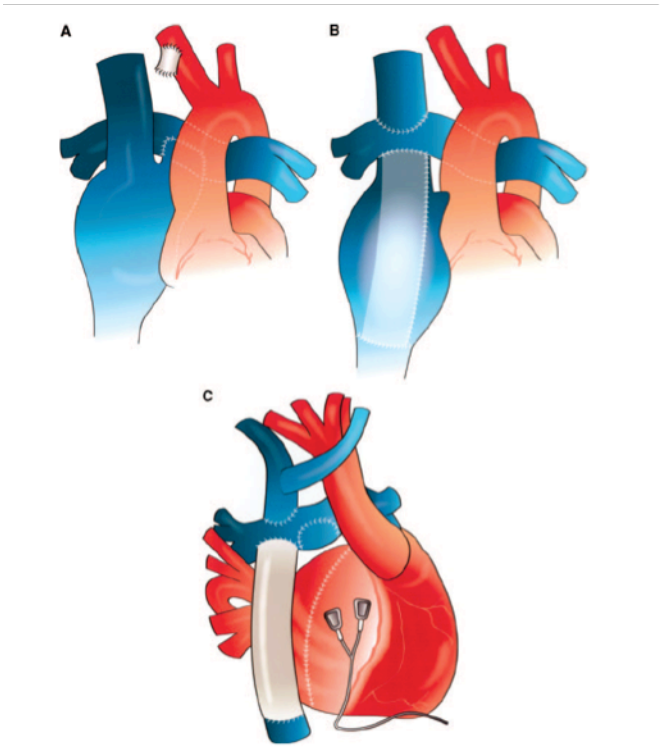

Figure 2.5 Variations of Fontan surgery. A the 'classic' Fontan, in which the RA is anastomosed to the pulmonary artery. B: total cavopulmonary connection (TCPC); intra-cardiac lateral tunnel with the IVC anastomosed to the RPA. C: extra-cardiac TCPC. Note the Blalock Taussig-shunt in A (original blood supply to the lung) that is taken down and over sewn. Note in C epicardial pacemaker leads. From [18]

2.2.2 Fontan Haemodynamics

In the Fontan circulation, systemic and pulmonary circulations are coupled in series without a ventricle supporting the pulmonary circulation. Pulmonary blood flow (PBF), and consequently preload of the heart, are therefore reliant on passive flow of systemic venous blood through the pulmonary arteries (PAs), and requires a degree of systemic venous congestion. The result is a paradoxical physiology in which caval hypertension and pulmonary vascular hypotension coexist and preload of the heart is restricted by the pulmonary vascular bed [71]. This anatomy has important implications for physiology of Fontan circulation and consequently the mechanisms behind failure of the circulation.

In Fontan patients, cardiac output (CO) at rest is typically decreased to about 70% of normal for body surface area [72]. During exercise, this difference becomes even more visible. Morphologically normal hearts can produce up to a five-fold increase in CO in response to exercise [73], whereas Fontan patients typically only achieve 50-60% of predicted exercise capacity [74]. In acquired heart diseases, ventricular dysfunction is most of the time the reason for an impaired CO response to stress. In Fontan patients, the heart seems to be less determining factor of CO.

2.2.2.1 Preload in the Fontan Circulation

Over the last two decades, it has become increasingly clear that preload of the systemic ventricle is an essential determinant of CO [19]. Already in 1982, Shachar et al. observed that CO at rest and during stress was not associated with ventricular ejection indices, but relied on unobstructed venous flow through the cavo-pulmonary connection and pulmonary arteries [75]. This observation was later supported by multiple studies that showed increases in resistance in the cavo-pulmonary connection or the pulmonary vascular system, such as small pulmonary arteries, elevated PVR and positive pressure ventilation, significantly decrease cardiac output [76–80]. The importance of preload for the Fontan heart has also clinically been recognized. Creation of a fenestration, and hereby creating a 'right to left shunt' improving preload, is now a well known intervention to increase cardiac output in Fontan patients in the early stages of accommodation after surgical completion of the Fontan circulation [81–84].

In order to maintain circulatory flow and thus preload, the Fontan circulation is critically dependent on maintaining systemic venous hypertension. Krishan et al. have shown that the vascular circulation in asymptomatic Fontan patients has adapted to facilitate this by increasing vascular resistance, reducing venous compliance and decreased microfiltration [85]. While supporting the venous pressure gradient, reducing venous pooling (and thus congestion of oedema in important venous compartments such as the splanchnic bed) and improving blood flow through the Fontan circulation, these changes have a negative impact on organ perfusion and afterload of the heart. Interestingly, the study of Krishan et al. showed that the changes in vasculature are largest in the lower extremities. This is likely the effect of the larger pressure needed to propel venous return from the legs in upright position of the body.

2.2.2.2 Cardiac function in the Fontan circulation

The Fontan circulation has become a palliative treatment option for a range of congenital heart defects in which one of the two ventricles is unable to support the circulation [18]. As a result, there is a wide variety of morphological and geometrical differences between single

ventricles. Some single ventricles are purely of right or left ventricular origin (patients with hypoplastic left or right heart syndromes), whereas others are a mixture of the two (complex AVSD's with a hypoplastic component of the RV for example). These differences make investigation of cardiac function difficult. The origin and geometry is likely to play a significant part in the role of cardiac function in Fontan haemodynamics, in particular in chronic adaption. Patients with a single ventricle of LV origin seem, for example, to have a better long-term preservation of cardiac function and exercise capacity than patients with a ventricle of RV origin [86]. Ideally, cardiac morphology is taken into account when investigating ventricular function. However, due to the relative rarity of the disease and therefore small patient numbers, this is not always possible.

Conventionally, systolic and diastolic function of the heart is measured using global ventricular parameters, especially cardiac volumes and ejection fraction (EF), that are easy estimated or directly measured from widely available diagnostic examinations at rest such as echocardiography and cardiac MRI. However, such measures are load dependent. Loading conditions of the Fontan circulation are severely abnormal. Furthermore, univentricular hearts are often severely dilated. These factors decrease the sensitivity of conventional markers of cardiac function for myocardial status and can lead to erroneous conclusions. Diastolic dysfunction has, for example, been reported in over 70% of all Fontan patients of the paediatric heart network cohort based on echocardiographic measures [87]. However, Senzaki et al. elegantly showed that the clues of diastolic dysfunction seen on echocardiography are consequence of loading conditions of the Fontan circulation, and that during invasive assessment such diastolic dysfunction was not present [88]. Similarly, EF is often reported as impaired or low normal. However, multiple invasive and non-invasive studies investigating load-independent parameters of systolic function have shown that in asymptomatic Fontan patients, contractile function is often normal [88–90]. Overall, this suggests that ventricular function is not the main problem in Fontan circulation. However, even asymptomatic patients experience exercise intolerance and have lower CO than healthy volunteers. This realization has over recent years led to an increasing focus on vascular factors of the circulation as the main 'problem' of CO in the Fontan circulation. As previously described, vascular adaptions to the single ventricular circulation result in a significant increase in afterload. This results in larger costs of cardiac contraction, and thus creation of CO. Indeed, in modelling, as well as clinical studies it has been shown that ventricular efficiency of the Fontan ventricle is lower than in the biventricular heart at rest [77, 91]. In addition, Saiki et al. showed that at rest HR adversely effects efficiency of the ventricular contraction more than in the healthy heart [89]. This was the result of the higher-

than-normal afterload, necessitation high contractility, and relative under filling, resulting in ventricular-arterial uncoupling. Whereas the systolic and diastolic function of the ventricle in asymptomatic Fontan patients seems to be good, the inefficiency of the circulation has a significant impact on its function and has been hypothyzed to attribute to the long-term deterioration seen in Fontan patients [19].

2.2.2.3 Exercise/stress haemodynamics of Fontan circulation.

As described in the previous section, assessment of cardiac (and vascular) function of the Fontan circulation has remained challenging using measurements at rest. In cardiology, it has widely been recognized that exercise testing is a sensitive measure of cardiovascular status, as CO, the result of total cardiovascular function, is one of the main determinants of exercise capacity. Also in Fontan patients, exercise intolerance is a sensitive predictor of morbidity and mortality [92, 93]. Therefore, investigation of cardiac (and vascular) function during exercise potentially can lead to valuable insight into the Fontan physiology and can potentially improve identification of targets for treatment in individual patients. Over the recent years, several research groups have investigated the haemodynamic response to exercise or pharmacological stress, a surrogate for physiological exercise, in Fontan patients. These studies have given some important clues regarding the physiology of the Fontan circulation.

Both cardiopulmonary exercise test (CPET) [94, 95] and dobutamine stress CMR [96, 97] studies have shown that the ability to augment CO in exercise is impaired in Fontan patients. Whereas the HR response is lower in Fontan patients than healthy volunteers, the lower CO in Fontan patients compared to healthy volunteers is largely unexplained by HR alone [72]. In their CMR study, Robbers-Vissers et al. found that, in contrast to healthy individuals, SV did not increase during low dose dobutamine stress (7.5mcg/kg/min) in adult Fontan patients, but remained constant [97]. This was the result of a fall in EDV, while HR increased. A similar report from Pushparajah et al. showed that higher doses of dobutamine stress (10mcg/kg/min and 20 mcg/kg/min) result in a further fall of EDV and consequently a decline in SV in a cohort of children with Fontan circulation. This decline in SV caused CO to plateau at moderate levels of stress, as every further increase in HR is accompanied by a similar fall in SV [98]. These results were in keeping with an exercise echocardiography study executed by Gewillig et al. [79].

Senzaki et al. [88] investigated the origin of this fall in SV during stress, using both atrial pacing and dobutamine stress in adult Fontan patients. This invasive study showed that end-diastolic pressure (EDP) fell 25% at increasing HRs in Fontan patients, whereas there was no change in healthy volunteers. Using pressure area curves, they derived that the impaired CO response was caused by a fall in EDV due to an inadequate preload reserve, while the

contractile response to dobutamine was normal. Wong et al. [99] showed a similar mechanism of reduced preload leading to a fall in SV in children with Fontan circulation during CMR dobutamine stress. These results seem to suggest a lack in preload in the Fontan circulation. However, the studies were performed using dobutamine stress or atrial pacing. The lack of active muscular contractions, which augment preload, could therefore potentially explain these results. Therefore, comprehensive assessment of the heart during physiological exercise should be performed in order to find out the exact mechanism of reduced SV during exercise.

The observed fall of SV during increasing HRs could potentially have important consequences for the efficiency of the single-ventricular heart. As described in Chapter 2, SV preservation is essential part of the HR response in healthy subjects, as it results in a linear increase in CO during HR augmentation. Fontan patients are unable to preserve SV, and reach maximum CO at moderate levels of exercise. Between moderate and high levels of stress, the increase in HR results in a significant increase in energy demand of the heart. Although the internal work (IW) increases [25, 100], it does not yield extra CO. Hence, cardiac efficiency (stroke work / total work) decreases progressively. The lower increase in HR in Fontan patients compared to healthy volunteers seen during stress / exercise might very well be a compensation mechanism of the body to prevent further deterioration of cardiac function [74]. However, as illustrated in Figure 2.6 this compensation is only partially effective compensation, as EDV still falls and results in a decrease in SV during stress.

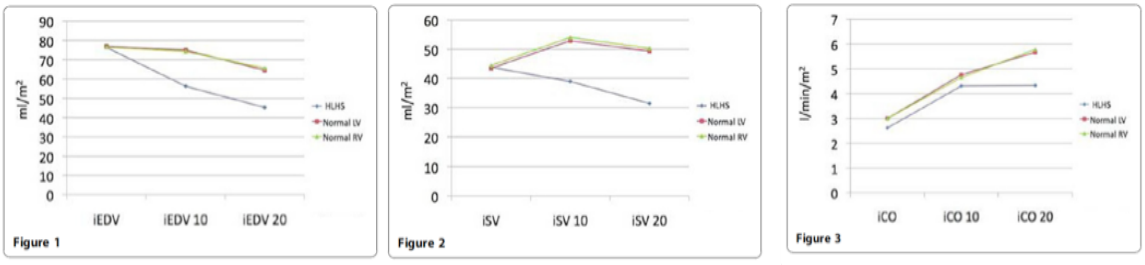

Figure 2.6 Pilot data. Changes in ventricular volumes during dobutamine stress in Fontan patients (HLHS) and healthy volunteers. Figure 1: SV decreases in Fontan patients. Figure 2: more prominent fall in ESV in Fontan patients. Figure 3: CO plateau's at moderate dobutamine (10 mcg/kg/min). With Permission *K. Pushparajah, 2014*

The above described investigations into Fontan physiology during exercise seem to suggest that the exercise and stress response in the single ventricular circulation is inherently impaired due to a fall in SV during exercise, that results a significant increase in inefficiency

of the ventricle, which already at rest was impaired. Whether these observations hold during physiological exercise remains to be seen. Therefore, investigation of this exercise response in Fontan patients, and the impact of the missing RV, is the main objective of this PhD.

2.2.2.4 Failure of the Fontan circulation

Fontan palliation is a valuable option in otherwise lethal complex congenital heart defects. However, the abnormal circulation brings a burden of hemodynamic sequelae and complications to initial survivors, resulting in a poor life expectancy [101]. Fontan patients experience a slow but constant progressive deterioration of cardiac function and exercise capacity and a high incidence heart failure, arrhythmia's and thromboembolic events [87]. This results in Fontan failure (death or transplantation) in up to 40% of the patients after 25 years of follow up [102, 103]. The mechanisms behind the decline in exercise capacity and development of heart failure are not completely understood. Complaints of exercise intolerance often occur without obvious cardiac dysfunction at examination and reliable markers that predict morbidity and mortality after Fontan palliation are currently absent.

Based on recent cohort studies, two modes of Fontan failure can be identified: failure with impaired systolic function (IVF) and failure with preserved systolic function (PVF) [104–106]. In patients with end-organ dysfunction, listed for transplantation, IVF is present in about ~40-50%, with the remainder having PVF [106].

The phenotype of IVF can be directly related to impaired systolic function, with reduced ejection fraction, a low CO and high SVR, resulting poor exercise tolerance. In these cases, medical treatment has largely focused on reducing cardiac work (beta-blockage) and reducing afterload (ACE-inhibition). Both such treatments lack scientific backing and have so far not proven to be very successful. Therefore, many patients ultimately are evaluated for transplantation.

In PVF group, the cause of failure is less obvious. Ejection fraction is normal and CO is often normal. Patients often have vascular complications such as protein losing enteropathy (PLE) or plastic bronchitis. The cause of these complications remains unclear, but both are associated with high mortality rates [104]. The pathway of PVF is often suggested to be related to high systemic venous pressures with elevated post-sinusoidal pressures in the liver. It is thought that chronic liver damage due to these high pressures results in liver mediated widespread disregulation of autonomic vascular function, with a fall in SVR. The drop in SVR subsequently leads to low perfusion pressures and shunting of blood away from non-vital organs, such as the splanchnic bed and kidney [106]. This seems to be supported by the increased resistance in the splanchnic bed observed in PLE [107]. Ozawa et al., who studied ventricular-arterial coupling in patients with PLE, suggested an increased afterload, and

resulting mismatch in VA coupling as the cause of PLE. Whereas this at first seems to contradict the previous work, a close inspection of their data shows that their interpretation of increase afterload was based on an increase in vascular elastance (Ea). Ea is measured as end-systolic blood pressure / stroke volume. Whereas in normal loading conditions this measure is mostly influenced by systemic vascular factors and contractility, filling of the ventricle also plays a role. If EDV and therefore SV decreases (as often observed in Fontan patients, see above), Ea increases. Therefore, the measured increase in Ea in the PLE patients by Ozawa et al. is potentially a reflection of lower ventricular filling, a factor previously reported in Fontan patients with PLE and PVF. Although their study does not give sufficient information to investigate whether SV was indeed decreased due to a fall in EDV, the results are not directly contradictory to the hypothesis of reduced SVR.

Treatment has remained difficult in patients with PVF. Both medical and surgical treatments have shown to be suboptimal, with only partial reduction of symptoms in most cases and rarely complete remission. For PLE, a recent suggestion of embolization of the involved lymphatic branches has shown promising short-term results, with evidence of total remission of leakage of lymph to the gut [108]. Whether such interventions also result in long-term remission, or are only a temporary solution, remains to be seen. In PVF, heart transplantation has shown good results, with even remission of vascular symptoms. However, mortality-rates of transplantation in PVF have been shown to be significantly higher than in IVF [105], although recently survival rates in this groups seems to have improved due to better post-transplantation care [109].

Whereas the results of heart transplantation improved for Fontan patients, bringing them closer to transplantation results for patients with other underlying diseases, the need for transplantation reflects the poor efficacy of alternative treatment options [110].

So far, no successful treatment regimes have been identified to prevent or even slow down the progressive functional decline in heart failure. Scientific basis for treatment is only limitedly available, and if available has yielded unsatisfying or sometimes contrasting results. ACE-inhibition, often used in acquired heart diseases to reduce afterload of the heart, has shown not to provide evident benefit and might even lead to reduced functional capacity [111]. Bearing in mind the suggestion that the increased SVR in Fontan patients is a functional adaption to provide perfusion pressure and blood flow through the circulation in the face of low CO, the use of ACE-inhibition might indeed be contra-productive [19].

Over the recent years, more attention has been given to the improvement of blood flow through the pulmonary circulation using pulmonary vasodilation (PVD). The rationale of this

treatment is based on the highly deteriorating effect of increased pulmonary vascular resistance on Fontan haemodynamics and is supported by the observation that PVR with increased age seems to increase over time due to the lack of pulsatile flow in the pulmonary arteries. Short term studies have indeed shown a beneficial short-term effect of pulmonary vasodilators (Sildenafil, Bosentan and Iloprost) on pulmonary blood flow [112, 113] and exercise capacity [114–116]. However, a 6 months follow up did not show a sustained benefit [117]. Furthermore, an exercise CMR study done by Van den Brueane et al. showed that the improved CO during exercise after Sildenafil was mainly caused by a reduction of SVR, most likely a side effect of the drug, but not by improved flow through the pulmonary circulation into the single ventricle [96]. The long-term effects of the PVD remain to be seen. Further investigation into potential treatment, PVD's, and other options, is highly needed. In particular, the mechanisms of impact of potential treatment options need to be carefully assessed, as the Fontan circulation functions so distinctively different to the normal circulation.

In this thesis, we will address the challenges in treatment of Fontan patients by aiming to better understand Fontan physiology using exercise CMR. More over, a potential new treatment target, selective HR inhibition, will be evaluated to identify its impact on Fontan haemodynamics and energetic efficiency of the circulation.

2.3 Cardiac Magnetic Resonance Imaging

In order to investigate the primary questions of this thesis, an imaging technique that allows evaluation of biventricular cardiac function during exercise needed to be developed. As discussed in Chapter 1, CMR is the most desired method for imaging during exercise. However, adaption of conventional CMR techniques in order to allow imaging during exercise is however non-trivial. Therefore, a thorough understanding of CMR techniques is needed. In this chapter, the basis of MRI physics, current standard CMR techniques and potential strategies for CMR during exercise are reviewed. Most of this information is based on a textbook for cardiovascular MRI by Plein et al. [1] and a Cardiovascular MRI course given by Dr. Gerald Greil at King's College London.

2.3.1 Introduction

Since its commercial introduction in 1980's, nuclear magnetic resonance imaging (MRI) has had a significant impact on cardiovascular imaging. It allows for imaging of cardiovascular structures without geometric restrictions, such as acoustic windows in echocardiography, and encompasses a wide array of techniques for 2 dimensional (2D) and 3-dimensional (3D) assessment of cardiac and vascular anatomy, function, blood flow and tissue characterization.

MRI manipulates the magnetic moment of protons to create a signal that can be used to generate images. Although many different elements have nuclei with magnetic resonance properties, hydrogen (H^+) nuclei are exploited during conventional MRI imaging, as their intrinsic sensitivity to magnetic resonance imaging is high and their occurrence in our body, in the form of water and fat, is abundant.

2.3.2 MRI Physics

2.3.2.1 Proton Spins and Magnetization

Hydrogen nuclei possess a positive charge and spin around their axis. Hereby, they generate their own magnetic field, also called *magnetic moment* [1]. Normally, the magnetic moments of individual hydrogen atoms are randomly orientated, but when a strong external magnetic field ($\mathbf{B}_0$) is present, the spin states of these atoms align with (parallel) or against (antiparallel) with the external field (see Figure 2.7). As aligning parallel to the magnetic field is a more favourable position for the atoms, the application of the external magnetic field results in a net-magnetization $\mathbf{M}_0$ of the tissue along the axis of $\mathbf{B}_0$. The ratio of the spins in the parallel vs. antiparallel configuration determines the size of net-magnetization and this ratio is dependent on the strength of $\mathbf{B}_0$; a stronger $\mathbf{B}_0$ results in more available signal.

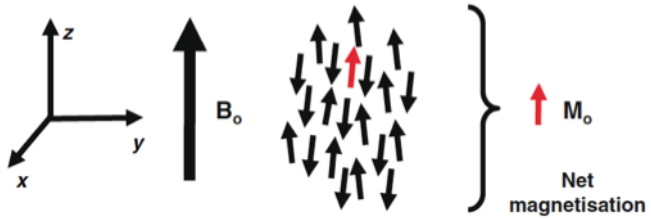

Figure 2.7 Spin alignment parallel or anti-parallel to B0. From [1]

2.3.2.2 Signal generation

Although aligned by the magnetic field, the spin axis of a proton rotates around the vertical axis. This motion is similar to the motion of a child's spinning top, that slows down and starts to spin no longer completely vertical and is called *precessional motion*. This phase of the precession motion is random and hence, the transverse component of $\mathbf{M}_0$ is zero.

The frequency of the precession motion of the spins, the *Larmour frequency* (ω_L) is given by their gyromagnetic ration γ and the strength of $\mathbf{B}_0$. When a radio-frequent (RF) pulse is given to protons at a frequency identical to their frequency of precession the system of spins is able to absorb the energy from this pulse. The absorption of energy will cause all spins to precess in phase while also flipping the parallel spins into the anti-parallel configuration. As the full spin system precesses in phase, the net magnetization will rotate around the vertical-axis, hence creating two components of $\mathbf{M}_0$; the vertical component of the net magnetization ($\mathbf{M}_z$) and the transverse component of the net magnetization of ($\mathbf{M}_{xy}$). Whereas vertical magnetization is undetectable, the rotating transverse component of the net magnetization produces an oscillating magnetic field that can be detected by a receiver coil in the MRI scanner. This receiver coil detects a sinusoid signal that slowly decreases in amplitude: due to the relaxation process that brings the net magnetization back to its original state. This slowly decaying signal is known as the *Free Induction Decay* (FID) (see Figure 2.8). The signal decay, or *relaxation*, consist of two independent relaxation processes: a recovery of the longitudinal magnetization, called *T1 relaxation,* and a decay of the transverse magnetization, with the resultant decay of the MR signal, called *T2 relaxation*. In human tissues, T2 relaxation is usually faster than T1 relaxation and therefore the signal decays away before the spin system returns to the original $\mathbf{M}_z$.

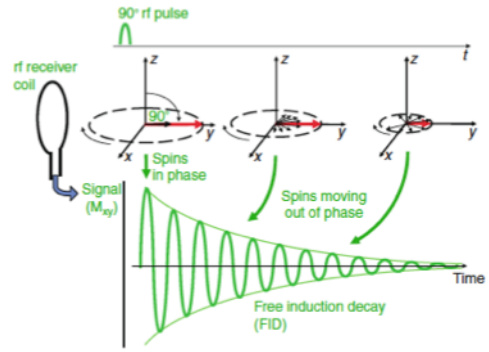

Figure 2.8 Dephasing of the spins results in a gradual decline in transverse magnetization; also called free induction decay (FID).

2.3.2.3 T1 relaxation

The recovery of the longitudinal component of the net magnetization is caused by a transfer of energy from the proton spin system to its surrounding molecular system. This recovery is an exponential process with a time constant T1 and is dependent on the size of the molecules and their motion (tumbling rate). As a result, T1 relaxation times differ for different structures: Fat has a relative fast relaxation rate, while water, which has an unfavourable tumbling rate, has a much slower relaxation rate (= longer T1 relation time).

2.3.2.4 T2 relaxation

After application of the RF pulse, all spins move in phase, resulting in transverse magnetization. However, over time the pins dephase. This dephasing has two causes: 1) interactions between neighbouring protons (*spin-spin interactions*) and 2) local inhomogeneity's in the applied magnetic field.

Spin-spin interactions represent the 'true' T2 relaxation. Due to random interactions between protons in a molecule, their individual magnetic field is slightly modified, resulting in de-phasing of their spins. This dephasing is irreversible, due to its randomness and independent of the strength of $\mathbf{B}_0$. The resulting relaxation is exponential with a time constant (T2). However, the $\mathbf{M}_{xy}$ signal decay is always faster than the true T2 relaxation rate, due to inhomogeneity's in the applied magnetic field. These small differences in the magnetic field observed by individual protons, result in additional dephasing of the spins. And therefore, the observed decay in signal $\mathbf{M}_{xy}$, the FID, is described as *T2** relaxation (see Figure 2.9).

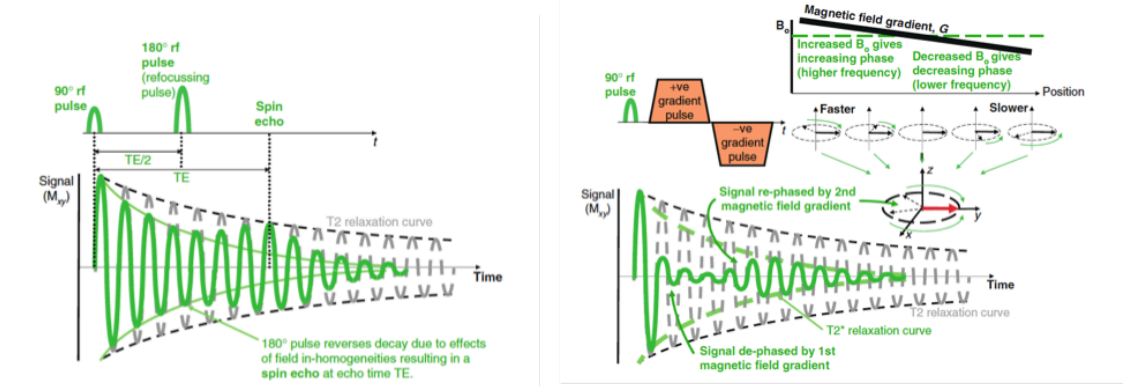

Figure 2.9 Spin echo sequence (left) and gradient echo sequence (right): the 180° refocusing pulse of the spin echo flips the spin momentum, hereby reverting the effect of field inhomogenities on the spins. The recovered signal is therefore only dependent on T2 relaxation, and results in good signal. The two opposite gradients in a gradient echo sequences (right) result in rapid dephasing and rephasing of spins. However, result in lower signal as the transverse magnetization decays with T2* relaxation. From [1]

2.3.2.5 MR echoes for signal acquisition

Although the FID could potentially be read as an MR signal, this signal is mostly ignored as it is disrupted by additional magnetic field gradients that are applied to spatially localize and encode the MRI signal. Therefore, instead of sampling the FID directly, echoes are used to be able to measure FID. The two most common types of echoes are *gradient echoes* and *spin echoes*.

2.3.2.5.1 Spin Echoes

A shown before, the FID is influenced by both T2 relaxation and local field inhomogeneity's. Whereas signal decay from T2 relaxation is irreversible due to the randomness of the spin-spin interactions, the signal decay of local field inhomogeneity's is potentially reversible, as these are constant: The degree of dephasing ('faster' or 'slower' precession) is dependent on the local magnetic field. The spin echo sequence exploits these fixed local field inhomogeneity's. After an initial 90° RF pulse, a 180° refocusing pulse is applied that the spins flip by 180°. As a result, the local field inhomogeneity's become exactly opposite to the first initial experienced local field inhomogeneity's. The precessions that initially 'slowed down' compared to average because of the local field inhomogeneity's now speed up again, whereas the 'accelerated' precessions now slow down. Hereby, the spins will come back in-phase. This pulse is therefore called the *refocusing pulse*. The signal will grow until all spins

are in phase, before decaying again. This peak signal is called the *spin echo* and as local field inhomogeneity's are cancelled out, it lies on the T2 relaxation curve. The time from the RF pulse to this echo is called Echo Time (TE). As a consequence of the 180° flip, the *refocusing pulse* is exactly at TE/2.

The use of both a 90° RF pulse and the 180° refocusing pulse gives the largest possible signal that can be obtained in MRI. Hence spin echo sequences are ideal for imaging quality imaging with reduced sensitivity to image artefacts due to magnetic field inhomogeneity's. This characteristic can be exploited, for example when imaging cardiac patients with a pacemaker: the relative low susceptibility for artefacts when using spin echo sequences will optimize the image quality obtained during CMR.

2.3.2.5.2 Gradient Echoes

Gradient magnetic fields are used to produce a linear variation of the external magnetic field $\mathbf{B}_0$. These gradient fields can be used to accelerate the normal dephasing of spins after an initial RF pulse. Switching on a gradient will diphase the spins quickly, resulting in rapid decrease of FID to zero. By subsequently applying a second gradient field along the same direction with a similar slope but opposite polarity, the spins will rephrase, causing an increase in FID, which peaks at maximal rephrasing. This peak lies on the T2* relaxation curve, as the gradient echo sequence ignores field inhomogeneity's. The peak signal is called *gradient echo*. If another pair of gradients with opposite polarities is turned on, another echo can be obtained. Gradient echo sequences use an RF pulse with a variable flip angle, which is normally less than 90°. Although this reduces the amount of transverse magnetization, and thus signal, of an individual echo, it allows for much faster repetition of the pulse sequence (repetition time; TR).

In CMR, most gradient echo sequences use a very short TR (<10 ms). The static tissue in the image slice is saturated, as there is little time for recovery of the *z*-magnetization, due to the fast repetition of RF pulses. However, as blood flows it comes into the image plain without having received any of the earlier pulses. All the spins can be fully magnetized, resulting in a relative high signal compared to the static tissue. Hence, these fast gradient echo sequences are referred to as *bright blood* sequences.

2.3.3 Cardiac Magnetic Resonance

MRI acquisitions of the heart have to take into account three important factors: motion of the heart, breathing motion and blood flow in the heart and vessels. Depending on the indication, these factors need to be compensated (for still imaging) or are part of the image that needs to be obtained. Over the last decades, a multitude of sequences have been developed for

individual imaging purposes. These range from still imaging of the heart to comprehensive assessment of three dimensional motion and blood flow.

2.3.3.1 Cine imaging

Cine imaging refers to dynamic imaging in which the motion of the heart is displayed over time and is used for the assessment of wall motion and volumetrics of the heart. '*Bright blood' cine gradient echo* sequences are used for this purpose. In the King's College London Cardiovascular Imaging Department, balanced steady state free precession sequence is most commonly used for cine imaging (see Figure 2.11 right plane)

Acceleration of image acquisition can be achieved by simply repeating the gradient echo sequence rapidly, acquiring multiple lines of *k*-space within a cardiac phase. Increasing the number of lines recorded per cardiac phase decreases the scan time, but it increases the window of acquisition per cardiac phase, thus decreasing temporal resolution of the scan. When the full *k*-space is sampled within a single cardiac phase, the sequence is called '*real time'*.

For the assessment of ventricular volumes, a complete stack of cine images is acquired that covers the whole heart (mostly commonly acquired in short axis orientation). Acquisition is mostly done during breath holds to avoid motion artefacts. Imaging without a breath hold can be achieved, but requires correction of breathing motion. Typically, 20-30 phases are acquired during cine CMR to allow assessment of cardiac motion as well as end-diastolic and end-systolic volumes.

2.3.3.2 Flow Imaging

2.3.3.2.1 2D phase contrast flow imaging

Phase contrast (PC) flow MRI was first introduced in the 1980's and since then, has gained a major role in daily clinical CMR assessment, especially in valvular and congenital heart diseases[118]. It allows for the measurement of blood flow at any location in the body and has flexible spatial and temporal resolution.

PC flow imaging makes use of the direct relationship between blood flow velocity and the phase shift observed during MRI acquisition. During a cine gradient echo pulse sequence, the application of a magnetic gradient field results in dephasing of magnetization along the gradient. By applying two gradients along the same direction with opposite signs, a so-called

bipolar gradient pulse pair, a phase shift due to movement of the spins can be measured. In static tissue, the de-phasing caused by the first gradient is reversed by the second gradient. However, as spins in the blood pool move between the two gradients, de-phasing is incomplete, leaving a phase shift in the pixels of the blood pool that is proportional to the velocity of the blood.

By measuring this phase shift, an image can be created that is depended on the phase of the transverse magnetization, a so-called phase map. This phase map, however, not only holds information on phase changes due to blood flow, but also changes due to magnetic field inhomogeneity's, eddy currents and motion along more than one gradient direction. To correct for these phase errors, two consecutive acquisitions of each phase encoding step are usually acquired (a 'reference' and a 'velocity encoded' scan). During the first acquisition, a signal s_1 is obtained, containing both static and moving spins s_s and s_m, respectively. During the second acquisition, the gradient in the flow direction is altered, hence resulting in a phase shift of the spins ($S_{m+\text{ phase shift}}$) moving in this direction. Thus,

$$S_1 = s_s + s_m$$

$$S_2 = S_s + S_{m + \text{phase shift}}$$

By subtracting the phase maps of the two scans, the phase changes due to causes other than velocity in the flow-encoded direction are removed, creating a phase contrast velocity map used for quantification of blood flow (see Figure 2.10)

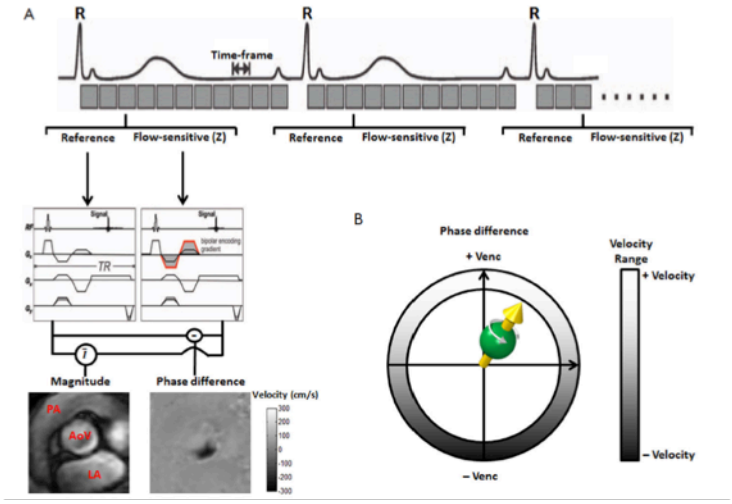

Figure 2.10 2D PC flow imaging with phase encoding in one direction. A) For every cardiac frame, a reference image and a flow-sensitive image is generated. Note the bipolar gradient applied in the flow-sensitive image From these images a phase difference map and a magnitude image are created. B) For every flow-image, an adequate velocity encoding (VENC) needs to be selected. Phase differences in an angle from +VENC (highest velocity) to –VENC (lowest velocity) are encoded as velocity. Velocities higher than the set VENC result in aliasing. From [1]

In order to obtain a strong signal from fast moving blood, turbo gradient echo sequences with a short echo-time (TE) are needed during a cine acquisition with reduced flip angle. During turbo gradient echo imaging, the gradient echo pulse is repeated several times, using different amplitudes of the phase encoding gradient. Hereby, multiple gradient echoes can be generated during one cardiac phase and hence, multiple lines of *k*-space can be acquired. The acquisition is repeated for every cardiac phase over multiple heartbeats until all lines of *k*-space are filled. Although this decreases scanning time, it increases the acquisition window for each cardiac phase and hence results in a higher temporal resolution. As for every heart beat a segment of *k*-space is acquired for each phase, turbo gradient flow imaging is also called multiple shot imaging or segmented k-space gradient echo imaging.

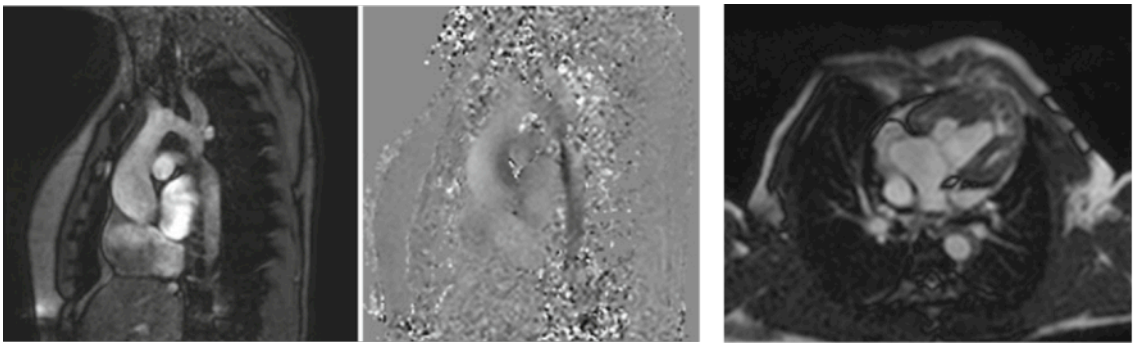

Figure 2.11 Magnitude image (left) and phase image (middle) acquired during 2D PC flow imaging of the aorta. Right: typical cine imaging (4 chamber) of a univentricular heart.

During the flow sequence, data is obtained from different heartbeats. The synchronization of data collection over the different heartbeats is achieved by either prospective or retrospective gating of the patient's electrocardiography (ECG) signal. During prospective gating, a trigger signal from the ECG starts the acquisition of the images and data is acquired over a predefined time during the heart beat, based on a pre-set duration of the heart beat. When heart rate varies from the pre-set heart rate during the scan, inaccuracies in acquisition timing arise with prospective triggering, which may lead to exclusion of late diastolic flow in the flow assessment. With retrospective gating, data collection is continuous while the ECG is recorded. As variations in heart rate during retrospective gating result in differences in the number of data points per heartbeats an average heart beat interval is calculated and the data from the different heartbeats are adapted (stretched or compressed) to fit the average heart beat interval. Hereby, an average flow data set is created that contains data from the full cardiac cycle.

2.3.3.2.2 4D phase contrast flow imaging

During the last decade time resolved three dimensional (3D) phase contrast flow imaging, also called '4D flow', has been introduced [119]. By encoding velocity in three spatial dimensions in a 3D volume, a complete picture of flow in three dimensions could be acquired in the heart and the great vessels. This enables more thorough investigation of the flow patterns inside the heart and their role in cardiac diseases.

Acquisition of this data is achieved in a similar way to 2D PC flow imaging, however instead of having a reference image for every velocity direction, three dimensional velocity information is efficiently achieved by acquiring three velocity encoded images along three orthogonal axes (x, y, z) and subtracting them from one reference image [120]. Data collection for every phase is segmented over multiple heartbeats; hence ECG gating and respiratory navigation is required to minimize breathing artifacts.

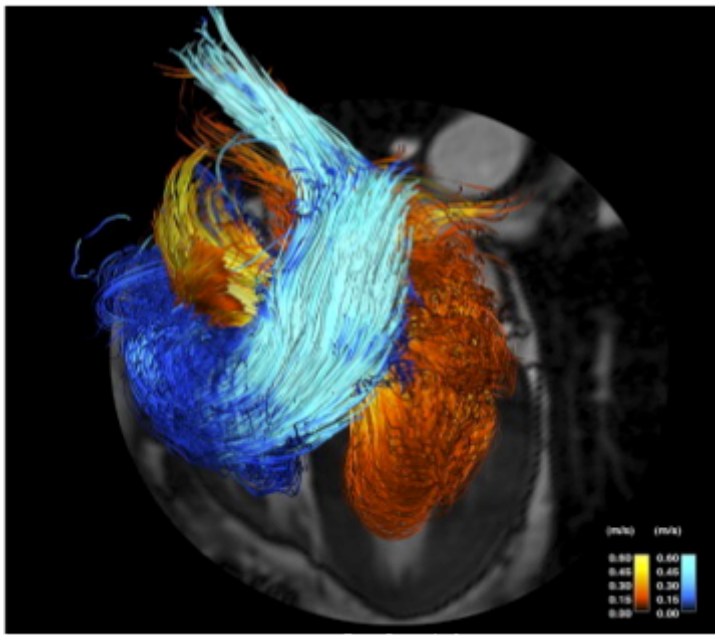

Figure 2.12 4-D flow image of a healthy heart. Time resolved path-lines are plotted over the cardiac cycle, blue is flow from the RA to the pulmonary artery, red is flow from the LA to aorta. From [121]

After reconstruction of the data, a 3D magnitude and three 3D velocity datasets are generated for an average heart beat (see Figure 2.12). Long acquisition times of a 4D flow dataset have prevented its use in daily clinical practice [122]. Therefore, speed-up techniques are essential to acquire 4D flow images within a reasonable time frame. These techniques rely on reducing the amount of data acquired for each image (e.g. under-sampling), while still being able to reconstruct an accurate image. This reconstruction can be achieved by exploiting the fact that images series contain a high degree of correlations in space and time.

Three different strategies can be used to exploit correlations between data-points [123]; correlation in *k*-space, in time and in both *k*-space and time (k-t techniques). The first technique reconstructs the image using other data-points from the same image, while the second reconstructs a missing point with data-points from images in its vicinity in time. K-t techniques use both data-points from the image itself and images closely related in time to reconstruct the missing data, hereby improving the accuracy of the reconstruction.

Using the latter strategy, Giese et al. have shown to be able to achieve a net acceleration factor of 8, using a strategy called compartment based k-t principal component analysis (k-t PCA+) [124]. Using the latter technique together with real time respiratory self gating [125], gross scan times between 10 and 15 minutes can be achieved.

2.3.4 CMR during Exercise

2.3.4.1 Cardiac assessment during Exercise

Cardiac function is a major factor influencing exercise performance. In many heart diseases, symptoms of early stages of disease are present during exercise before pathological changes occur at rest [126]. During exercise or other stress, the heart uses its reserve to improve oxygen supply to the body by augmenting cardiac output (CO). Investigation of this cardiac reserve can therefore improve the understanding of (patho-)physiological mechanisms in the heart, and potentially even improve early detection and treatment evaluation in patients with heart diseases.

Investigation of the heart during exercise is challenging as bodily motion and high heart rates complicate both non-invasive imaging techniques and invasive pressure measurements. Cardiopulmonary exercise testing (CPET) is the most used techniques to assess exercise capacity [127]. By measuring pulmonary gas-exchange, while monitoring ventilation, heart rate and electrocardiograms during ergometer or running exercise, CPET allows assessment of the functional capacity to perform exercise. As CO is indirectly related to exercise performance; CPET allows to indirectly infer cardiac performance. However as direct information about the cardiac contractions is lacking during CPET, cardiac function, and especially the mechanisms of cardiac dysfunction underlying a pathological CPET result, cannot be completely assessed.

Two techniques that allow direct assessment of cardiac function during exercise are radio-nucleotide ventriculography and echocardiography. However, both these techniques have significant limitations in quantification of cardiac volumes and therefore function, as exercise motion and geometrical assumptions result in inaccuracies in volumetric assessment [16]. This has led to a great heterogeneity between studies investigating cardiac behaviour during exercise [2, 4]. As a result, investigations into cardiac response to exercise have so far been limited and, when performed, results are often interpreted cautiously due to the known variability in measurements.

CMR is the current gold standard for the non-invasive quantification of ventricular volumes and blood flow in the great arteries, outperforming both echocardiography and radio nucleotide ventriculography [118, 128]. Especially as cardiac volumes of both ventricles can be reliably assessed, CMR is regarded superior to echocardiography [129]. This makes its use for exercise imaging appealing. However, motion artefacts and unreliable ECG-signals are inevitable during exercise and result in poor image quality when conventional CMR is used [4]. As a result, most researchers have avoided direct imaging during exercise, and instead used pharmacological stress as a surrogate [76, 97, 99, 130], or only obtained imaging

after cessation of exercise [53, 54]. For pharmacological stress, most authors so far have used a dobutamine infusion. Dobutamine (DL-3-4-dihydroxy-N-(3-(4-hydroxyphenyl)-1-methyl-n-propyl), is a synthetic catecholamine that increases cardiac output by increasing contractility via stimulation of the beta-1 receptors in the heart. At high doses, it also increases heart rate and systemic vasodilatation, without a notable effect on the pulmonary vasculature [131, 132]. These effects are similar to the HR and inotropic changes seen during exercise. However, the question is whether pharmacological stress mimics the complete physiological exercise response. The bodily response to exercise encompasses a system of physiological factors that impact cardiac function: sympathetic stimuli directly impact cardiac contraction, heart rate and arterial vascular tone, and skeletal muscular contractions and heavy breathing impact venous return and pulmonary blood flow. The absence of a total systemic exercise response during infusion of dobutamine might therefore result in a stress-state that is not comparable to normal physiology, leading to erroneous conclusions. Only one study so far reported on this issue [133]. This study showed similar SV and HR responses during exercise and high dose dobutamine infusion (20mcg/kg/min), but reported differences in contractility (more pronounced during dobutamine stress) and EDV (a slight fall during dobutamine stress) between the two groups. Unfortunately, the scientific value of this study was poor, as they used two small groups (one undergoing exercise, the other one undergoing dobutamine stress) and, therefore, could not rule out the impact of differences between the two groups on the observed results.

2.3.4.2 Current Exercise CMR Techniques

As explained in the previous sections, CMR provides imaging that allows reliable assessment and quantification of myocardial function and blood flow in a non-invasive manner. To obtain the high quality of CMR imaging, images are not taken in real time, but constructed from *k*-space data obtained over a multitude of heartbeats, during a state of minimal extra-cardiac motion. Consequently, the subject undergoing CMR needs to be completely still during imaging, and often hold their breath, as any bodily motion significantly distorts the acquired images.

To overcome the difficulties with motion and ECG acquisitions, several groups have diverted to measuring cardiac function before, during short breaks and / or immediately after cessation of exercise using conventional or accelerated image acquisition [7, 134, 135]. However, due to changes in heart rate, muscle activity and fast recovery in healthy individuals after exercise, such methods might not provide a true reflection of exercise physiology.

Other groups have used highly accelerated phase contrast flow acquisitions during exercise [8, 136–138]. Mostly in order to obtain a measure of cardiac output during in-MRI cardio-pulmonary exercise tests. Unfortunately validation of these methods during exercise often lacks. Furthermore, they only allow flow assessment and therefore cannot explain the underlying changes in cardiac function.

Recent developments in acceleration techniques now allow imaging at very high temporal resolution (35-50 milliseconds), allowing near *'real time'* dynamic imaging. Imaging at these such speed means that motion does not significantly blurry the images, as the displacement during image-acquisition is only minimal. Whereas image quality suffers due to the high acceleration factors needed for real time imaging, these sequences potentially allow imaging during exercise. Two research groups have been developing strategies for exercise CMR using real time imaging in the last 5 years: Lurz et al. [139] and La Greche et al. [4]. Both groups use real-time, free-breathing, ungated steady state free-precession (SSFP) cine imaging to assess ventricular volumetrics and have shown to be able to quantify cardiac volumes during moderate (Lurz et al.) up to sub-maximal (La Greche et al.) exercise intensities. Lurz et al. developed a customized real time imaging sequence, that utilized a radial sampling pattern and unfolded-SENSE acceleration to achieve high temporal resolution (~30milliseconds) [139]. They acquired a stack of real time images in a short temporal window (2-3 heart beats) in short axis orientation and quantified cardiac volumes without taking into account respiratory motion. La Gerche et al. have a different approach [4]. They modified a routinely available un-gated cartesian sampled SSFP sequence using routine acceleration techniques (half-Fourier transform, half-scan, and SENSE under-sampling) to achieve a temporal resolution of (~35 milliseconds). Furthermore, they developed a dedicated exercise CMR analysis software (RightVol, KU Leuven, Belgium) that allows manual correction of respiratory motion [4]. By acquiring images over at least one respiratory cycle per slice, they were able to identify target end-diastolic and end-systolic images at end-expiration. This way, they avoided a bias in volumetric assessment that results from through plane motion of the heart during respiration.

Both groups also differ in their mode of exercise during CMR. Lurz et al. used an ergometer in which patients move their straight legs up and down. This form of exercise uses only a small part of the leg muscles, which is reflected by a maximal workload (< 22.5 Watts) during the scans that was significantly lower than the maximal workloads that were achieved by La Gerche et al. using a supine bicycle ergometer (218±52 Watts) [4] and upright CPET (225-600 Watts) [140, 141].

The exercise CMR methods discussed above demonstrate the potential feasibility of exercise CMR. Real-time CMR seems to be a good solution to obtain CMR images that are not, or minimally, affected by motion. However, a downside of real time imaging is the large

amounts of images acquired. This results significant variation in quantified volume as instead of a single averaged beat in conventional cine CMR, operators choose new ED and ES target images for each slice out of multiple beats. Furthermore, manual respiratory correction leads to significantly longer processing times for exercise CMR compared to normal cine CMR. These issues demonstrate a clear scope for further development of Exercise CMR imaging and processing techniques in order to facilitate its use in routine clinical research studies.

Part II: Original Contributions

Chapter 3 Exercise CMR set-up

3.1 Introduction

In order to successfully perform Exercise CMR, several adaptions had to be made to the scanner set-up and the image acquisition process. In this chapter, the development of the exercise CMR protocol is described. Firstly, the bicycle ergometer equipment and adaptions to the MRI scanner will be discussed in Section 3.2. Next, a method for acquisition of blood pressure waveforms during exercise CMR is introduced in Section 3.3. Finally, the development of the exercise CMR imaging protocol is described in Section 3.4. Different imaging strategies can potentially be used for exercise imaging. Here the different in-vitro and in-vivo experiments executed to assess CMR and bicycle adaptions for Exercise CMR are described.

3.2 CMR bicycle set-up

In order to allow strenuous physiological exercise during CMR scanning, a bicycle ergometer must first be integrated with the MRI scanner. Several MRI-compatible bicycles have been developed. Whereas these bicycle ergometers could technically be used during MRI-scanning, their use is often restricted to out-of-bore cycling for CMR [142]. The reason for this is the fact that during CMR scanning, with the chest in the iso-centre of the MRI scanner, the knees hit the bore while cycling due to the small size of most MRI bores (60 cm) combined with a relative high position of the bicycle, which is mounted with a frame onto the top of the table, resulting in a relative large angle of the knees. To allow exercise inside the bore, several groups have developed a customized bicycle or adapted existing systems [4, 7, 143].

In King's College London, a Lode MRI compatible bicycle ergometer was available. However, this ergometer could only be used to exercise subjects outside the bore prior to imaging, due to physical restraints when cycling inside the bore (knees hitting the bore) [142]. This system was therefore taken apart and adapted for in-bore exercise. Firstly, the ergometer was migrated from an Achieva 1.5T MRI scanner to an Ingenia 1.5T MRI Scanner (both from Philips, The Netherlands). The Ingenia MRI scanner has a larger bore than the Achieva system, 70 instead of 60 cm. As is illustrated in Figure 3.1, this difference in size

results in a significant larger space at the top of the bore, making more room for the knees during cycling.

Next, adaptions to the bicycle and the mechanism that attaches it to the table were made to further improve the ability to cycle while scanning. In order to lower the bicycle as far as possible, the mounting frame (6 cm high) was disposed and the bicycle was directly attached to a new CMR table, resulting in a dedicated ergometer bed for Exercise CMR. Additionally, the length of the cranks of the bicycle was adapted to decrease the radius of the rotations made during cycling. Altogether, these adaptions resulted in a decrease of maximal knee-height during cycling of 5-12 cm, dependent on the subject's posture.

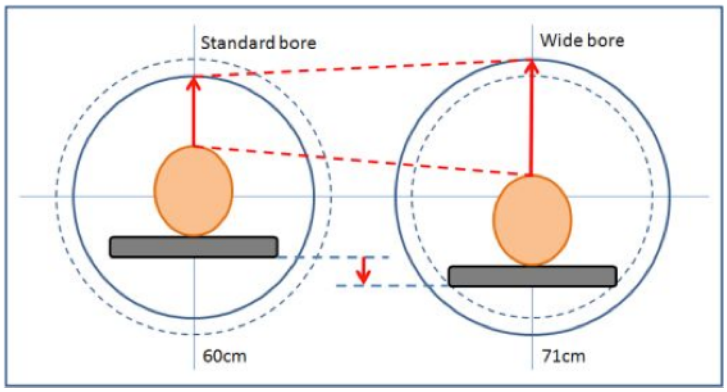

Figure 3.1 Illustration of the effect of increased bore size. A greater bore size significantly improves vertical available space inside the bore, hereby increasing the maximal angle of the legs inside the bore and enabling supine bicycle ergometer exercise.

After the above-described adaptions, the bicycle ergometer system allowed in-bore cycling with the chest in the iso-centre of the scanner in subjects ranging in height from 160 cm to 200 cm. However, strenuous cycling inside the MRI bore was still restricted as the power related to cycling resulted in upward shift of the body, ultimately pushing the participants away from the bicycle. This shift of the body did not only restrict the intensity of cycling, but also resulted in errors in image acquisition as the subject's movement changed the position of predefined target geometries. To restrict the body motion during cycling, a handgrip system was designed. This plastic system was build to fit onto the MRI bed and allowed exercising subjects to hold themselves in place while cycling at high power. Additionally, the imaging protocol was adapted to include a rapid check of geometries prior to imaging at each exercise level. This check was performed using the 'interactive' b-SSFP sequence (a dynamic scan sequence routinely available on Philips MRI scanners to facilitate planning of geometries).

Finally, the coil set-up was changed to reduce image-artefacts. The Ingenia scanner (Philips, the Netherlands) utilizes a large body-coil for CMR. This coil is placed directly on the chest of the subject during CMR. However, cycling movements resulted in significant motion of the coil during exercise, leading to a decreased image quality. In order to stabilize the coil, two plastic coil bridges were designed to hold the coil away from the body. This resulted in a significant improvement of image quality.

Figure 3.2 Exercise CMR set-up. Upper left: bicycle ergometer customization. Upper Right: Custom-build handgrip system that decreased body motion. Below: Exercise CMR set-up with coil bridges and handles.

3.3 Measuring blood pressure during exercise CMR

Afterload of the heart is an important factor influencing cardiac function, especially during exercise [2]. Direct assessment of afterload requires invasive central aortic pressures. However, as such measurements are challenging to obtain, non-invasive brachial blood pressures are often obtained as a surrogate measure for the assessment afterload [144]. In this section, the development and validation of Exercise CMR blood pressure assessment is described.

3.3.1 Introduction

Automated blood pressure cuff measurements allow accurate assessment of mean, systolic and diastolic pressure. In some cases, such as the Centron, a pressure waveform over a full

cardiac beat can be obtained [145]. Unfortunately, automated blood pressure devices often rely on oscillation waves for the measurement of blood pressure. As significant muscle and body motion occurs during exercise these oscillation waves are disturbed. As a result, automated blood pressure devices are notoriously inaccurate during exercise. To overcome this problem, manual assessment of blood pressure using auscultation is often performed during routine clinical exercise tests.

Manual blood pressure measurements are not feasible during exercise CMR, as the subject is positioned inside the MRI bore and there is not enough physical space to measure brachial blood pressures. Furthermore, manual measurements only allow determination of systolic and diastolic pressures, whereas assessment of the full waveform was desired in order to support future work in the development of computational algorithms that allow determination of the central aortic waveform based on peripheral pressure waves [146]. Finapress (FMS, the Netherlands) allows continuous non-invasive radial blood pressure waveform assessment. It uses the so-called volume-clamp technique to determine blood pressure based on the changes in arterial dimensions [147]. The Finapress measurements are less disturbed by bodily movements and therefore allow measurement during exercise [148]. The only downside to this system is that it needs intermittent calibration (using conventional brachial oscillometry) in order to prevent a drift in pressure measurements. As oscillometry has proven not to work during exercise, we aimed to develop a novel method for acquisition and calibration of blood pressure waveforms, based on the Finapress system, that was suitable for use during supine physiological exercise inside the MRI bore.

3.3.2 Developed blood pressure system

In order to obtain adequate calibration of the Finapress blood pressure waveforms, a system was build utilizing the cessation of pulsatile flow in the radial artery during total occlusion of the ipsilateral brachial artery. This total occlusion of the brachial artery was obtained using an inflation oscillometer (Omron IM, the Netherlands), which was reprogrammed to inflate the brachial blood pressure cuff at a continuous rate from 50 – 200 mmHg (ramp: 14 mmHg / second). By simultaneous analysis the Finapress signals and the Omron inflation, the moment of cessation of pulsatility in the Finapress signals could be related to the pressure in the brachial cuff. This allowed calibration of the Finapress signal to a systolic blood pressure.

In order to obtain this point, pressure signals of both the Omron device and the Finapress waveform were transmitted to a desktop computer using a PowerLab analog and digital receiver (AD Instruments, United Kingdom). Brachial cuff pressure was measured directly

from the cuff using a pressure transducer, while the Finapress pressure waveform signal was sourced electronically from the Finapress device. Both signals were displayed simultaneously using LabChart (AD Instruments, United Kingdom). After acquisition, the Finapress waveforms were exported to Matlab (MathWorks, USA) and rescaled based on the obtained systolic measurement. See Figure 3.3A a schematic of the set-up (Fina-method) and Figure 3.3B for an example of the systolic blood pressure assessment.

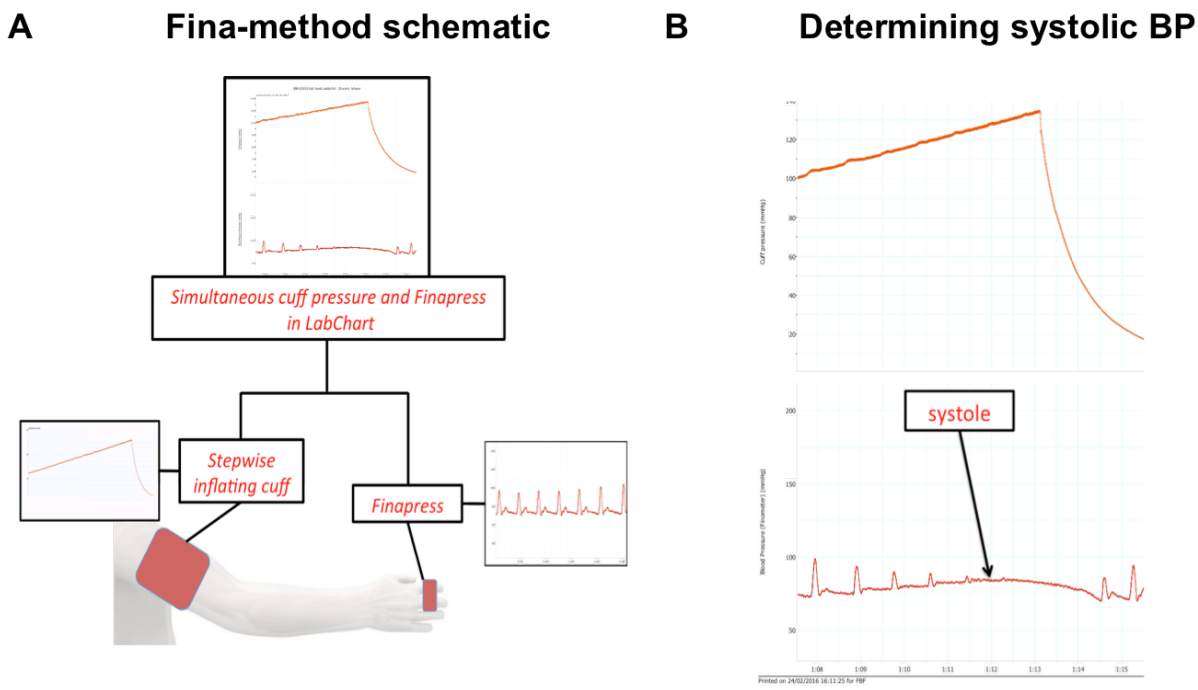

Figure 3.3 Measuring blood pressure during exercise CMR using Finapress (FMS, The Netherlands) combined with a ramped inflation of a brachial blood pressure cuff. A) Schematic of the acquisitions and their integration into one system. B) Using the two aligned signals, the systolic blood pressure can be determined as the pressure in the brachial cuff at which pulsatility is lost in the Finapress waveform.

3.3.3 Validation

The developed set-up was validated against manual blood pressure measurements in 10 subjects during a supine exercise using the set-up of the Exercise CMR. The aim was to investigate how accurate the developed system could identify the systolic blood pressure value, in comparison to the standard manual auscultation. Systolic pressures were measured during low, moderate and sub-maximal exercise, corresponding to a heart rate of 80-90, 100-115 and 140-155 respectively. Blant-Altman analysis of systolic and diastolic blood pressure was performed. The results showed excellent agreement between the two methods, with a mean difference of 0.5±3.87 mmHg. As shown by the Blant Altman plots in Figure 3.4,

individual measurements have some variability, however the limits of agreement of ±7.4 mmHg (±6%) are satisfactory for blood pressure measurements.

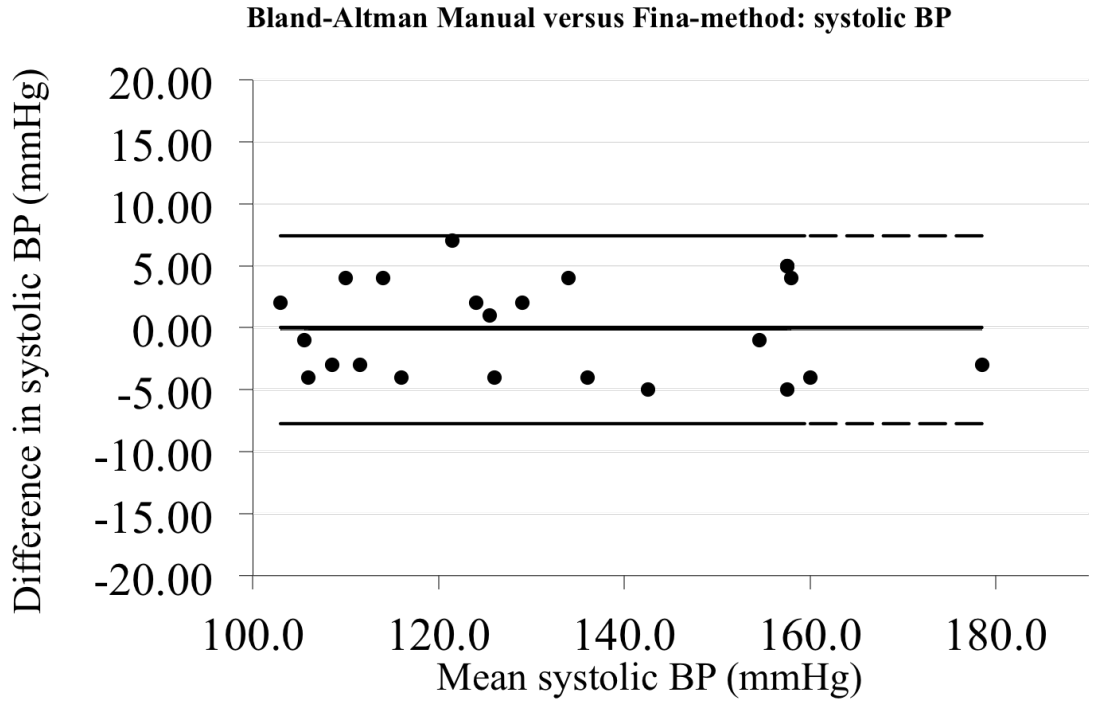

Figure 3.4 Blant Altman Analysis of difference in mean systolic pressure measurement using Fina-method compared to manual auscultation during supine bicycle ergometer exercise. Middle (grey) line represents mean diference, upper and lower thick lines represent limits of agreement.

Subsequently the diastolic pressures obtained from the rescaled Finapress waveforms were compared to the diastolic pressure obtained manually. As shown in Figure 3.5, there is a larger variability in diastolic pressures obtained with the two methods compared to the variability in systolic pressures, with a mean difference of 1.96±4.2 mmHg and limits of agreement of ±8.4 mmHg (±14%). This larger variability in diastolic blood pressures obtained with the two methods could be the result of inaccurate rescaling of the Finapress waveform. However, it can also be due to inaccurate measurements during manual auscultation, which is known to be inherent to the method, and is likely to be exaggerated due to difficult assessment of the diastolic Korotkoff sounds during exercise [149].

Based on these results, it can be concluded that the developed system for blood pressure assessment allows for accurate measurement of systolic blood pressure during supine physiological exercise from low up to sub-maximal exercise intensity levels. Diastolic

pressures were potentially less reliable, but are still within acceptable window of agreement for exercise CMR.

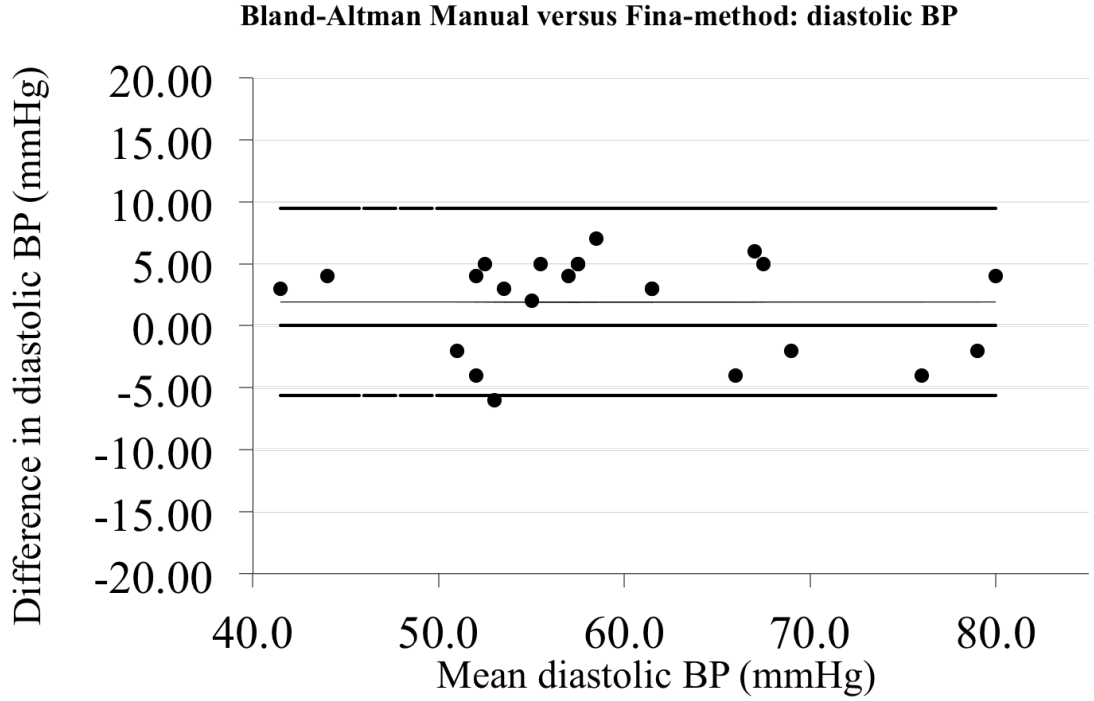

Figure 3.5 Blant Altman Analysis of difference in mean diastolic pressure measurement using Fina-method compared to manual auscultation during supine bicycle ergometer exercise. Middle (grey) line represents mean diference, upper and lower thick lines represent limits of agreement.

3.4 Development of exercise imaging protocol

Part of this work (CASPR-TIGER cine evaluation experiments) was done in collaboration with Dr. M. Usman. Part of the experimental work was publish in [150].

As previously described, the lack of a good ECG signal, the inability to breath hold and bodily motion severely limit the use of conventional imaging during exercise. Real-time imaging can overcome these problems, as these sequences are not ECG gated and can be used during motion without significant distortion of the images. Whereas several real-time imaging protocols have been described, they are not standardly available on each MRI scanner. Furthermore, their performance during exercise has only limitedly been investigated. In order to develop a robust imaging protocol for Exercise CMR, several imaging strategies were tested for their suitability for exercise CMR.

3.4.1 Evaluation of real time imaging

In order to analyse cardiac volumes during exercise, a stack of cine CMR covering the full heart needs to be acquired. As explained previously, real-time imaging is the most suitable option to do this during exercise, as it yields high quality imaging independent of an ECG signal and with limited motion distortion. La Gerche et al. have previously demonstrated the use of a SENSE accelerated balanced steady state free precession (b-SSFP) sequence for exercise imaging [4]. This sequence appeared to be robust, but has reduced image quality compared to conventional b-SSFP cine imaging. Furthermore, this sequence is acquired in real-time without motion correction. As a result, target images need to be manually selected at a fixed point in the breathing cycle from a large series of images per slice (typically >100 frames / slice). This process is time and labour intensive and limits the frequent use of exercise CMR in clinical research.

Recently several more complex acceleration and image-reconstruction techniques have become available that can potentially improve real-time imaging for Exercise CMR. An example of such an acceleration technique is K-T BLAST. K-T BLAST is an adaption to the conventional SENSE sparse sampling of *k*-space [123]. K-T BLAST takes into account not only sparse sampling in the *k*-space of one image (the 'K' factor), but also sparse sampling of data over multiple images (the 'T' factor). By utilizing the similarity between two subsequent images, K-T acceleration needs less 'K' data per image, and therefore higher acceleration factors can be achieved than using normal 'K' only SENSE acceleration. Alternatively, similar acceleration can be achieved with better image quality compared to SENSE alone. K-T BLAST is currently available on all Philips CMR scanners and might potentially improve real-time cine imaging for Exercise CMR by providing better image quality in similar highly accelerated acquisitions.

Although K-T BLAST can improve quality of the real-time imaging, the large amount of images and labour intensive analysis of images remains a drawback for Exercise CMR. Self-navigated acquisitions, acquisitions in which the images are gated before reconstruction based on the *k*-space samples, can potentially solve this problem. Recently, Usman et al. proposed a technique for self-gated, free breathing, ECG-free cine CMR at rest [150, 151]. This technique is based on a golden angle radial *k*-space acquisition and uses a variant of radial / spiral golden angle *k*-space image acquisitions; CArtesian trajectory with Spiral PRofile ordering and TIny Golden angle step for Eddy current Reduction (CASPR-TIGER). The advantage of using a 'golden angle', 111.25°, or one of its variants, is that *k*-space is homogeneously sampled through time. This means that theoretically, even with as little as 3-

4 *k*-space lines, an image can be reconstructed, as information is homogeneously present in all parts of *k*-space. This feature was used during motion correction. Initially, two image sets are reconstructing from the acquired data (one high temporal resolution and one low temporal resolution image). Based on these images, motion is estimated using image-processing algorithms to estimate cardiac and respiratory motion [151]. Based on these motion signals, *k*-space data is reordered and binned into cardiac phases at a desired respiratory state (end-expiration) and the final cine image sequence is reconstructed from the original *k*-space acquisitions without the need of breath holding or an ECG signal. Whereas this sequence is not widely available, its ability to allow real time gating with automated gating can be a significant benefit for the acquisition and analysis of cine CMR during exercise.

3.4.2 Methods

Three different real-time cine acquisition strategies were sequentially tested for their suitability in Exercise CMR in order to find an optimal imaging strategy: 1) a free-breathing self-gating ('CASPR-TIGER') cine imaging, 2) a K-T blast accelerated b-SSFP cine sequence ('K-T BLAST') and 3) the SENSE-accelerated b-SSFP approach of La Gerche *et al.* [4] ('rt-SENSE'). The imaging parameters for each acquisition, including a conventional ECG gated, breath held cine acquisition for reference, are shown in Table 3-1. In short, all imaging sequences were accelerated to obtain a temporal resolution / frame of ~35-40 milliseconds. The rt-SENSE acquisition had the lowest spatial resolution, while CASPR-TIGER had the highest. All imaging was evaluated in a sequential process: 1) Image quality was assessed at rest using the Exercise CMR set-up (including bike and coil n coil bridges), 2) If image quality at rest was sufficient, rest volumes were compared to a conventional ECG gated and breath held cine acquisition ('REFcine'). 3) All acquisitions that scored sufficiently in step two were then assessed of robustness and quality of the images during exercise. Based on these experiments, the 'best acquisition' for exercise CMR was chosen.

Imaging parameters real-time acquisitions and reference standard

	CASPR-TIGER	KT-BLAST	rt-SENSE	REFcine
Rec. Temporal Resolution, ms	~30	~38	~35	~33
Field of View, mm x mm	300 x 300	300 x 300	300 x 300	300 x 300
Acquired Voxel size, mm x mm	2 x 2	3.7 x 3.7	3.5 x 3.5	2 x 2
Rec. Spatial Resolution, mm x mm	1 x 1	2 x 2	2 x 2	1 x 1
Slice Thickness, mm	10	10	10	10
Flip Angle, degrees	50	50	50	50
Echo time, ms	1.7	0.9	0.8	1.8
Repetition time, ms	3.5	1.9	1.9	3.5
Acceleration Technique	Compressed Sensing	KT-BLAST 8	SENSE 2.5	SENSE 2
Additional parameters	none	Training-matrix 13	Half-scan 0.5	none
Net Acceleration Factor	6	4	5	2

Table 3-1 Image parameters of the investigated real time sequences and a ECG gated, breath hold reference sequence (REFcine). Rec. represents reconstructed.

3.4.3 Results

3.4.3.1 Image quality at rest

All three imaging sequences were tested at rest using the bicycle set-up. The presence of the bicycle ergometer was important as potential artefacts on the images caused by the exercise equipment can be anticipated. See Figure 3.6 for an illustration of the images acquired during the different acquisitions. There is a clear loss of image quality in real-time imaging. The CASPR-TIGER sequence came closest to the original imaging quality, despite several streaking effects that are inherent to the acceleration technique used. There was also a mild degree of temporal blurring present in the images. The K-T BLAST suffered significant artefacts. Further investigation showed that these artefacts reduced significantly when the bicycle was turned off, and even more if the bicycle was taken out of the room. The quality of K-T BLAST limited analysis of cardiac volumes. As the artefacts were related to the bicycle, and even at rest imaging was already insufficient, the K-T BLAST sequence was ignored for further assessment. The rt-SENSE acquisition had mildly decreased image quality, but was sufficient for cardiac analysis.

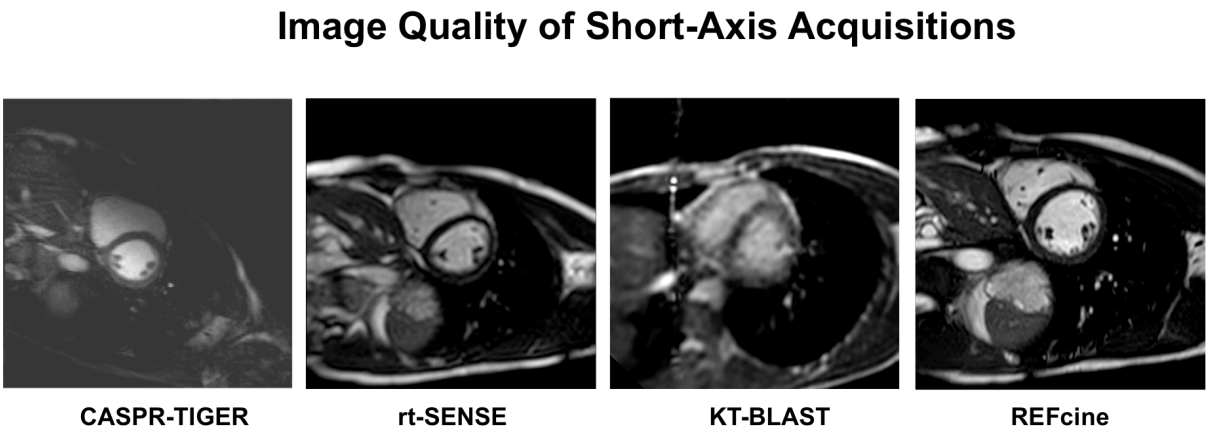

Figure 3.6 Image Quality of the different real-time acquisitions for Exercise CMR. Acquisitions were all made at rest. Most left image is the current standard ECG-gated, breath hold cine acquisition for comparison. Note significant artefacts in K-T BLAST acquisition.

3.4.3.2 Volumetric Analysis at rest

The CASPR-TIGER acquisition showed the best results in the initial image quality screening. Therefore this sequence was tested first for use during real-time imaging. The sequence was evaluated in 8 healthy volunteers. Total acquisition time of a short-axis stack was 1 minute and 10 seconds. Due to the complexity of reconstruction, the images could not be directly viewed on the scanner. After downloading the raw data, a 4,5 hour offline reconstruction was needed before obtaining images. As a result, it was not possible assess planning or potential errors in the acquisition until after the CMR exam had finished. The comparison of cardiac volumes obtained using the CASPR-TIGER and REFcine scans is shown in the Blant Altman analysis in Figure 3.7. As shown, there is a relative large error in end-systolic volumes (limit of agreement: ± 9.4 ml). Inspection of the data showed that this difference was mainly caused by errors in the cardiac gating during reconstruction, resulting in allocation of image data to wrong cardiac phases, combined with the temporal blurring present in the images. The CASPR-TIGER method did perform suboptimal during the imaging trail at rest: the image-processing time was long and did not allow direct quality control during imaging.

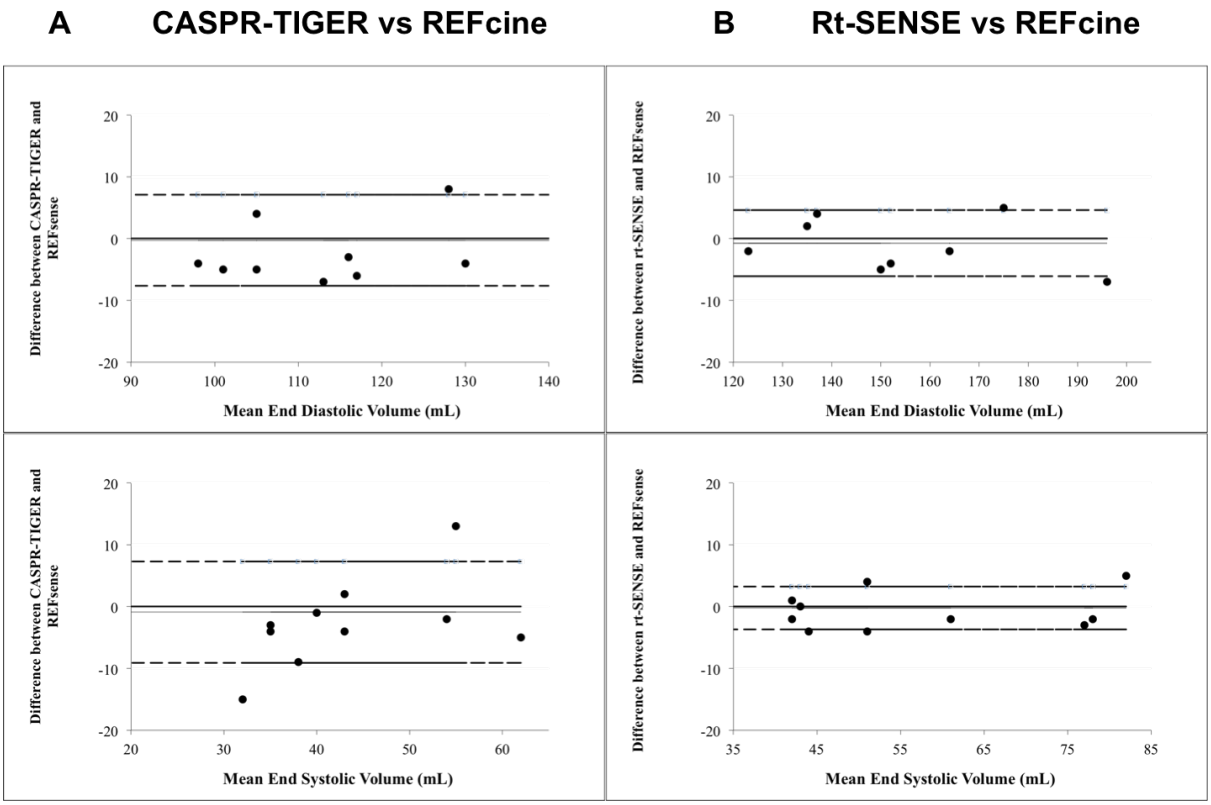

Figure 3.7 Blant-Altman Analysis of cardiac volumes with CASPR-TIGER (A) and rt-SENSE (B) acquisitions versus reference standard acquisition (REFcine). Upper and lower lines are limits of agreement (+2SD and -2SD lines) of the acquisitions with respect to REFcine. Middle line is mean difference from REFcine.

Additionally there were some inaccuracies in volume quantification. Therefore, the rt-SENSE acquisition was evaluated as a potential strategy. Despite the mildly lower image quality, rt-SENSE acquisitions yielded good results for volume quantification with high correlation in obtained cardiac volumes between rt-SENSE and REFcine, see the Blant-Altman analysis. Note that the limits of agreement suggest a smaller error between rt-SENSE and REFcine than between CASPR-TIGER and REFcine. An additional benefit of rt-SENSE was that images were readily available during acquisition, allowing correction of potential errors in planning of images and identification of artefacts.

3.4.3.3 Image quality during exercise

In order to make a final decision which acquisition to use for volumetric assessment during Exercise CMR, the CASPR-TIGER and rt-SENSE acquisitions were assessed for quality

during exercise, see examples in Figure 3.8. Note the significant blurring of the CASPR-TIGER acquisition. In-depth analysis of the origin of this blurring showed that the motion-estimation algorithm in the reconstruction framework, used to detect breathing motion and cardiac beating, failed to accurately detect the cardiac phases during high heart rates. As a result, data was misallocated to the wrong cardiac phases, which led to the observed temporal blurring. The rt-SENSE acquisition is reconstructed frame by frame, each consisting of a complete *k*-space acquisition in 35 milliseconds. Therefore, this acquisition was not sensitive to such problems. rt-SENSE was robust, without significant artefacts and only mild blurring at heart rates >130 bpm.

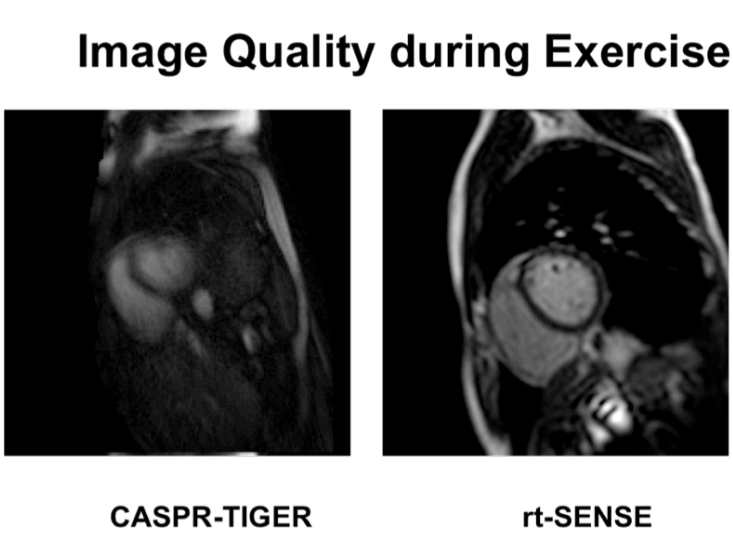

Figure 3.8 Quality of images during supine bicycle ergometer exercise. Note the significant blurrying in the CASPR-TIGER acquisition. There is notably less blurring seen in the rt-SENSE acquisition.

3.4.4 Discussion

In this section, three different real-time (ungated, free-breathing) MRI sequences were evaluated for their potential use for cardiac volume assessment during exercise. In order to capture information at a high enough resolution, all sequences were accelerated to obtain a frame-rate of <40 milliseconds. The first sequence, CASPR-TIGER, used a recently developed golden angle radial *k*-space sampling trajectory combined with compressed sense imaging. This sequence previously showed to allow very high acceleration factors while retaining image quality at rest [150]. Furthermore, during reconstruction of the images, breathing and cardiac motion are automatically corrected, which could have benefited quantitative analysis of Exercise CMR. The second (KT-BLAST) and third (rt-SENSE)

sequences did not have this retrospective motion correction, resulting in a long series of real-time images of the heart over multiple heartbeats and respiratory cycles.

First image quality at rest was evaluated. This test that the KT-BLAST sequence was susceptible for artefacts of the exercise bicycle, resulting in severe distortion of the reconstructed images. Therefore, this technique was abandoned and not included in further analysis. The two remaining sequences, CASPR-TIGER and rt-SENSE showed both to allow reliable quantification of cardiac volumes at rest, agreeing well with a standard (reference) ECG-gated breath hold short-axis cine acquisition. The error in volume assessment in the CASPR-TIGER acquisition was larger than the error of the rt-SENSE acquisition. This was the result of small misallocations of *k*-space data in the cardiac phases, leading to blurring of the images.

After the tests at rest, the CASPR-TIGER and rt-SENSE acquisition were evaluated for their performance during exercise. It was not possible to acquire the reference standard (REFcine) during exercise (due to bodily motion and a lack of ECG). Therefore, only image quality was assessed in this experiment. As expected based on previous work from La Gerche et al. [4], the rt-SENSE acquisition performed well, with nearly no blurring of the images and no significant artefacts. The CASPR-TIGER acquisition, however performed significantly worse. The reconstructed images of the CASPR-TIGER acquisition were significantly blurred. This was caused by a significant increase in misallocation of data in cardiac phases due to the high heart rate and was further worsened, as the algorithm was unable to correct the significant bodily motion during exercise.

Based on these experiments rt-SENSE was therefore chosen as the most optimal image sequence for quantitative assessment for cardiac volumes during Exercise CMR. rt-SENSE allowed robust imaging, even during high exercise intensities. Unfortunately, the downside of this technique is that the acquisition does not include motion correction. This makes analysis of cardiac volumes prone to errors and labour intensive.

3.5 Conclusion

In this chapter, several acquisition methods were evaluated for their suitability for use during exercise CMR. It was demonstrated that rt-SENSE acquisition was the best performing acquisition for cardiac volumes during exercise. Therefore, this sequence was chosen for further development in the Exercise CMR protocol. A downside of the rt-SENSE acquisition is that this acquisition results in a large series of real time images over multiple heartbeats,

without respiratory or cardiac motion compensation. In the next Chapter, this problem is addressed by developing a reconstruction pipeline to yield a conventional cardiac and respiratory-gated cine stack from the rt-SENSE acquisition.

Chapter 4 Retrospectively gated Exercise CMR

This Chapter was adapted from the following publication: Ruijsink et al. LCNS 2017 [152]

4.1 Introduction

As explained in Chapter 1, assessment of cardiac volumes, function and wall motion using cardiac magnetic resonance imaging (CMR) during physiological stress (exercise) has a great potential to improve early diagnosis, treatment evaluation and prognostic stratification in patients with heart disease. In the previous chapter, the initial set-up of Exercise CMR and development of a highly accelerated, near real-time, imaging protocol was explained. The resulting exercise CMR protocol allows imaging during exercise without motion corruption of the images. However, the obtained images are not cardiac nor respiratory gated. As a result, through-plane motion of the heart during respiration and bodily movements during exercise can lead to significant errors in quantification of cardiac volumes and function from the real-time images [9]. The lack of cardiac gating also leads to inconsistent timing of cardiac phases between slices, as imaging is started at each slice in a random point in the cardiac cycle. This further complicates comprehensive analysis of myocardial function, as it does not allow 3-dimensional assessment of myocardial wall motion abnormalities. Finally, instead of reconstructing a single heartbeat, the real time image sequence results in an image sequence of multiple heartbeats. This increases analysis time, as the operator needs to search for a representative beat, and leads to further errors in volumetric analysis as the variation in target images chosen by operators increases inter- and intra observer variability. Altogether, these factors introduce significant challenges to the use of real-time exercise imaging for clinical research applications.

To account for respiratory motion during free-breathing CMR, a navigator echo is typically added to CMR sequences [153]. While valid for CMR at rest, this method reduces temporal resolution of dynamic imaging. This makes it unsuitable for imaging during exercise, as high heart rates require a very high temporal resolution (<40 ms / frame). Several self-navigating

(SG) sequences have recently been developed to account for respiratory and cardiac motion during CMR. In SG, target motion is estimated directly from the acquired data. As a result, most SG techniques do not increase scan-time or reduce temporal resolution. SG techniques can be divided in image-based, k-space based, and model-based approaches.

Image-based SG relies on registration of high quality dynamic images based on motion signals derived from lower temporal or spatial dimensional images reconstructed from the same dataset [151, 154–156]. K-space based methods derive the respiratory signal from central k-space lines [157–159]. Finally, model-based approaches have been proposed for motion detection in CMR. An example of such an approach is described by Yoon et al. [160] who use a low-rank method that separates the background of the image mathematically from the dynamic portions. Although the above described SG techniques have great potential for imaging during exercise, the proposed methods rely on complex k-space trajectories, such as radial [154, 155] or golden angle radial [151, 156, 158] acquisition schemes, and computationally intensive reconstruction frameworks. Such techniques are currently not widely available in a clinical CMR environment, limiting their use for clinical exercise CMR. An exception to this is the method proposed by Hansen et al. [161]. Their image-based method for respiratory gating of cardiac images obtained at rest utilized a real-time CMR sequence that is standardly available on commercial MRI systems. However, proposed technique requires ECG waveforms for cardiac gating; a strategy that is not feasible for imaging during exercise as ECG signals are significantly disturbed due to body motion.

The aim of this chapter is to develop an image-processing framework that reconstructs a respiratory and cardiac gated cine CMR stack from real time CMR data obtained during exercise. Obtaining such a gated cine stack, similar to the ones normally used during rest CMR, would significantly improve the assessment of cardiac volumes, function and wall motion during strenuous physical exercise. To maximise the application of the developed technique in a clinical CMR environment, several criteria were determined prior to development: 1) the method needed to have minimal user interaction, 2) the processing time of the reconstruction framework needed to be minimized to be within clinical standards and 3) the method needed to be able to be flexibly applied to images from all imaging platforms without the need for advanced sequence programming or the use of intensive computing power.

The developed framework is described in 4.2, followed by a validation of the technique in 4.3 and finally a discussion of the technique in 4.4. This chapter shows that the developed technique is able to reconstruct gated cine images with improved image quality and lower

inter-and intra-observer variability compared with non-gated RT imaging. Further, this section demonstrates that the proposed solution allows detection of a pathological cardiac response to exercise in patients with a complex congenital heart disease.

4.2 Methods

The proposed strategy involves (i) acquisition of highly accelerated dynamic (real-time) MRI, as described in Chapter 3 followed by (ii) image-based cardiac synchronisation, (iii) image-based respiratory gating and (iv) motion correction and reconstruction of a 24-30 phase cardiac cine image stack. The main novelty of the proposed method lies in the clinical applicability of our semi-automatic, image-based reconstruction framework that creates respiratory and cardiac gated cine images of the heart during exercise without the need for intensive computing power or advanced cMRI pulse-sequences. The proposed framework is illustrated in Figure 4.1. The reconstruction pipeline was implemented in MATLAB R2015b (MathWorks, Natick, USA) utilizing the signal processing, image processing and statistics toolboxes. This study has been approved by the regional ethics board (REC: 15/LO/522, Bloomsbury London, UK) and informed consent was obtained from all participants.

4.2.1 Highly Accelerated Dynamic CMR

The reconstruction pipeline relies on near real-time (temporal resolution of < 40 ms) dynamic imaging. Such temporal resolution can currently be achieved on all major commercially available MRI scanners using vendor supplied acceleration techniques without the need of advanced user settings. In this work, images were acquired on a 1.5T MRI scanner (Ingenia, Philips Medical, Best, The Netherlands). The real time image sequence used was explained in detail in Chapter 3. In short, steady-state free precession imaging was performed without cardiac gating. 80-100 consecutive frames were acquired per slice in a short axis orientation, with a slice thickness of 8 millimetres. Imaging parameters were: field of view, 300 x 260 mm (approx.); flip angle 50°; SENSE factor 3 (Cartesian k-space undersampling); partial Fourier factor 0.5, repetition time 1.8 milliseconds, echo time 0.9 milliseconds and reconstruction-matrix, 128 x 112, resulting in a reconstructed voxel size of 2.3 x 2.3 x 8 millimetres and a frame rate of ~35 milliseconds. Total acquisition time for a short axis stack was ~55 seconds. After the acquisition, images were automatically loaded into Matlab and a region of interest around the heart (cROI) and a centre point for the LV were manually selected on an average of all images to facilitate the reconstruction process. This is the only manual step of the reconstruction pipeline.

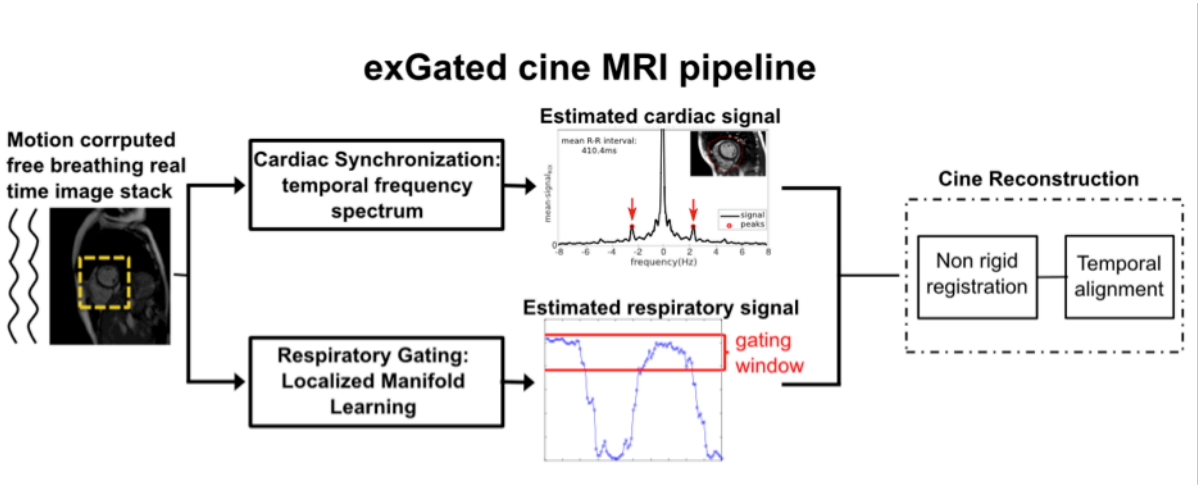

Figure 4.1 Overview of the proposed framework for cardiac and respiratory gated CMR during exercise.

4.2.2 Cardiac Synchronisation

ECG signals, routinely used for cardiac gating in CMR, are significantly distorted during physical exercise. However, the high temporal resolution of the real-time acquisition allows for direct estimation of the cardiac periodicity from the images, as was previously demonstrated by Van Amerom et al. [162]. This proposed technique was integrated in the developed framework in collaboration with Dr Josh van Amerom. In order to obtain cardiac gating, the cardiac periodicity was estimated by detecting the changes in blood pool contrast during ventricular contraction. From the cROI, the mean contrast signals were calculated for each frame and the Fourier transformation was applied to examine the signals in frequency domain. By plotting the frequency spectrum of the signal, the periodic changes in contrast of the blood pool (caused by beating), appear as peaks (local maxima). The local maxima were subsequently detected, as shown in Figure 4.2A, and the heart rate was calculated. A filter was applied to detect only maxima in a range of fundamental frequencies (0.8-2.8 Hz), corresponding to heart rates of 45 to 170 beats per minute (bpm). Subsequently, each frame was binned to an associated cardiac phase based on the cardiac time interval. For HRs < 130 bpm, the cardiac time interval was divided in 30 equally spaced cardiac phase bins, whereas for higher HRs the frames were divided into 24 cardiac phase bins. In both cases, the

temporal resolution (in cardiac phases) of the cine reconstructions was in keeping with routine CMR cine imaging [163].

4.2.3 Respiratory Gating

In order to resolve high quality gated cine imaging of the heart, respiratory motion needs to be corrected. We therefore applied Laplacian Eigenmaps, a Manifold Learning (ML) technique, in order to automatically estimate the respiratory motion in each slice in the imaging stack based on image intensity [151]. ML projects a higher dimensional manifold (e.g., an image of large dimensions) to a corresponding low dimensional representation. By assessing such lower dimensional representation over time, bulk changes in the image states can be assessed. Theoretically, this means that large changes in the images, such as breathing effects, can be identified in the lower dimensional representation of the total image, without the need of locating a navigator signal over the diaphragm, and with little impact of potential local image artefacts resulting from high acceleration factors. Indeed, previous work has shown that the ML technique is able to accurately estimate a 1D representation of respiratory motion from cardiac imaging at rest [151]. The ML respiratory motion estimation was implemented from the previous work in collaboration with Dr Mohammed Usman and adapted for use in highly accelerated dynamic imaging during exercise. As the ML estimated respiratory signal might have cardiac component due to high temporal resolution of real-time images, the acquired ML signal was filtered in the frequency range of 0.1 - 0.5 Hz in order to retain the respiratory component only. The resulting respiratory signal was plotted and a predefined respiratory gating window was used to select the images at end-expiration (20% of respiratory movement from maximal expiration) for further reconstruction, see Figure 4.1. This gating window is equivalent to a ~6-8 mm gating window using respiratory navigator conventionally applied during CMR at rest. Figure 4.2B shows an example of the ML estimated respiratory signal overlaid on a spatio-temporal intensity profile of the real time image acquisition through diaphragm, demonstrating the accuracy of the obtained respiratory signal.

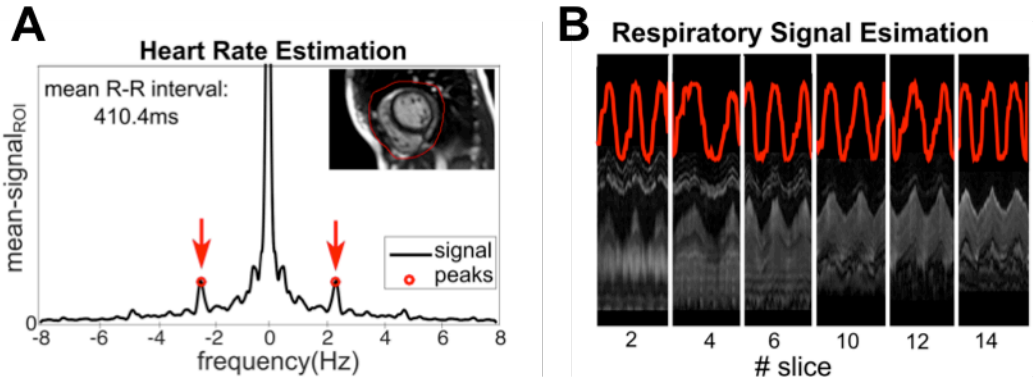

Figure 4.2 (A) Range of fundamental frequencies (0.8 - 2.7 Hz) of the temporal frequency domain, estimated cardiac rate on the ROI appeared as the maxima (red arrows). (B) Estimated respiratory signal (red line) overlay to a spatio-temporal intensity profile through diaphragm.

4.2.4 Cine Reconstruction

The previous cardiac and respiratory gating steps resulted in selection and binning of images into cardiac phases. Within each of these cardiac phase bins, the most representative image was subsequently selected by computing the mean-square error between all image pairs in that bin. The image with lowest error with respect to all other images was selected as the reference image. Subsequently, a Demons non-rigid registration algorithm [164] was used to estimate the set of displacement fields that aligns each image to this reference image. All images were registered and averaged to form a unique image per bin, resulting in a single image per cardiac phase. In order to assure temporal alignment of the cardiac phases between all slices, the LV blood pool was segmented using an automatic segmentation algorithm based on Otsu's method that was guided by the cROI and LV centre point. The smallest segmentation of each slice was selected as the end-systolic frame. Based on this reference frame all slices were temporally aligned so that, for each slice, the first frame of the reconstructed image sequence started at end-diastole. Finally, a rigid body in-plane image registration was performed to register the position of the heart over time and reduce inter-frame exercise motion. This facilitates the interpretation of ventricular contraction and wall motion abnormalities in three dimensions.

4.3 Experiments and Results

4.3.1 Experiments for Evaluation

The developed reconstruction method was evaluated in 10 healthy volunteers and 6 patients with congenital heart diseases (CHD) and exercise intolerance. Dynamic imaging datasets were acquired at moderate and high intensity supine bicycle ergometer exercise corresponding to a heart rate (HR) ~100-110 bpm and ~135-150 bpm, respectively. Image quality was rated using a 5-point Image Quality Score (IQS; 1 = unsuitable for diagnostic use, 5 = similar to conventional cine imaging at rest) by two blinded cardiologists specialized in CMR comparing conventional gated cine sequence, the non-gated RT sequence and our reconstructed exGated cine. As routinely used clinical cine CMR (conventional cine) is significantly distorted during exercise and does not yield enough image quality for analysis, the reconstructed cine exercise CMR images were compared to a previously validated, non-gated real-time imaging protocol (non-gated RT) that uses manual selection of respiratory state using a dedicated cardiac analysis software package (RightVol, KU Leuven) [4]. Agreement between the two methods was compared using Pearson's correlation. Inter- and intra-observer variability in 16 acquisitions of healthy controls (8 moderate, 8 high) were assessed with Bland Altman plots and the difference in inter- and intra-observer variance between the two methods was assessed using the F-ratio. Finally, systolic function was compared between healthy volunteers and patients with CHD during exercise using repeated measures ANOVA with exercise intensity as the within-subject effect. A p-value of $<.05$ was considered statistically significant.

4.3.2 Results

All datasets were successfully reconstructed to exGated cine stacks that allowed volumetric analysis. Figure 4.3 shows an example of conventional cine, non-gated RT MRI and our gated cine approach. Quality of the reconstructed images was significantly better compared to conventional CINE during exercise and non-gated exercise RT cine, with a mean IQS of 1.1±.3 for conventional cine, 3.1±.6 for non-gated RT and 3.9±.5 for exGated cine (cine vs. exGated p-value $<.01$, non-gated vs. exGated p-value = 0.02), see Figure 4.4.

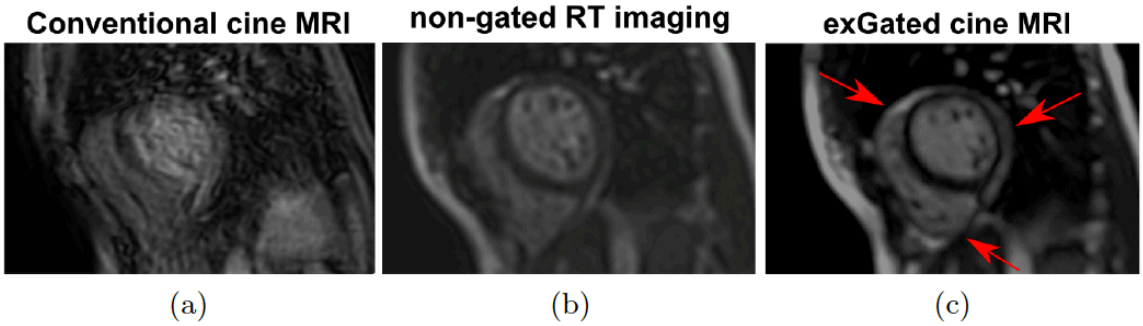

Figure 4.3 Reconstructed MRI images during exercise: (a) conventional cine MRI, (b) non-gated real-time cine MRI, (c) proposed approach – exGated cine MRI. Arrows denote better delineation of pericardium and RV wall of the proposed method.

These images reflect the improved image quality of the proposed exGated cine method with good delineation of pericardial fat and RV-wall obtained by our proposed method.

There was good agreement in ventricular stroke volume (SV) between exGated cine and non-gated RT imaging (R = 0.82). Figure 4.5 shows the Blant Altman comparison between the two methods. This shows that there is a mild degree of underestimation of SV using ExGated cine in comparison to non-gated RT imaging. Next, inter- and intra-observer variability for SV was compared between the two methods. As can be appreciated in Figure 4.6, both the in inter- and intra-observer variability was larger in RT imaging compared to the exGated cine, with larger limits of agreement for RT imaging (intra-observer: ±14.8 mL, inter-observer ±22.6 mL) compared to exGated cine (intra-observer: ±8.8 mL inter-observer ±13.2 mL). Also statistically, the inter- and intra-observer variance of SV was significantly lower in exGated cine compared to RT imaging (intra-observer: $F= 2.75$, $p<.01$ and inter-observer: $F= 3.01$, $p<.01$).

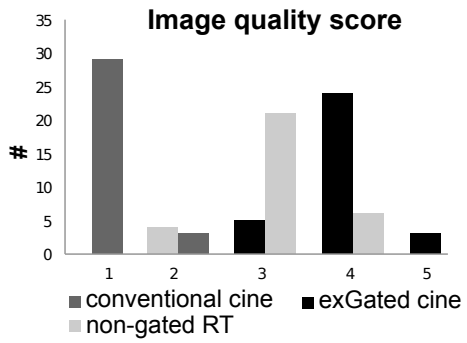

Figure 4.4 Image quality score between conventional cine (white bar), non-gated RT (gray bar) and our proposed approach – exGated cine CMR (black bar) y-values are times score a certain level.

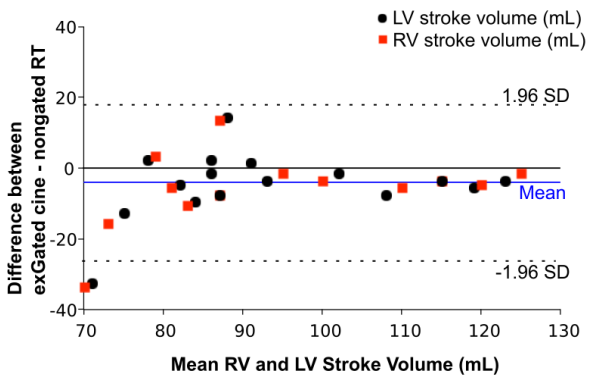

Figure 4.5 Bland Altman plot of agreement in stroke volume (mL) between exGated cine and non-gated RT.

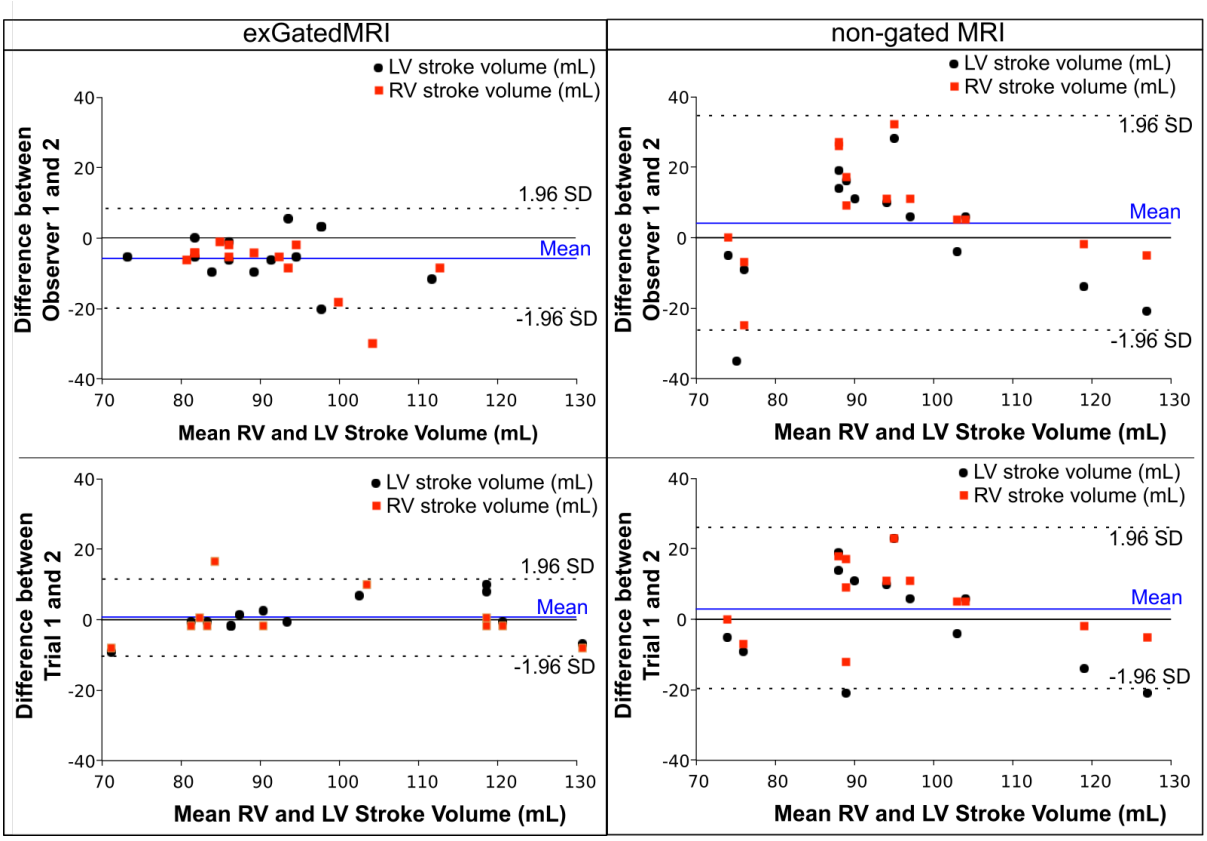

Figure 4.6 Bland Altman plots of inter- and intra-observer variability of stroke volume (mL) of the two methods. Note the smaller limits of agreement and variance in exGated Cine.

Next, intra-observer variability between the two methods was assessed for EDV and ESV. As expected based on the SV results, Blant Altman analysis showed that intra-variability for both EDV and ESV was lower in exGated cine compared to non-gated RT, see Figure 4.7. Limits of intra-observer agreement for EDV in RT imaging were ±15.2 mL and for ExGated cine

±8.8 mL. Analysis of variance using the F-test showed variance in exGated cine was not statistically different from RT imaging, although there was a strong trend towards a lower variance (F = 3.2, p= 0.06). For ESV, intra-observer limits of agreement were for RT imaging were ±10.8 mL than for exGated cine ±5.5 mL. For ESV, analysis of variance using the F-ratio showed a statistically lower variance in exGated cine than RT imaging (F 4.2 p = 0.04).

Lastly, interrogation of the change in LV global systolic function during exercise using exGated cine showed that the increase in LV global systolic function (measured by ejection fraction) was lower in patients with congenital heart disease and exercise intolerance compared to healthy volunteers (p<.01 for both moderate and high exercise), see Figure 4.8

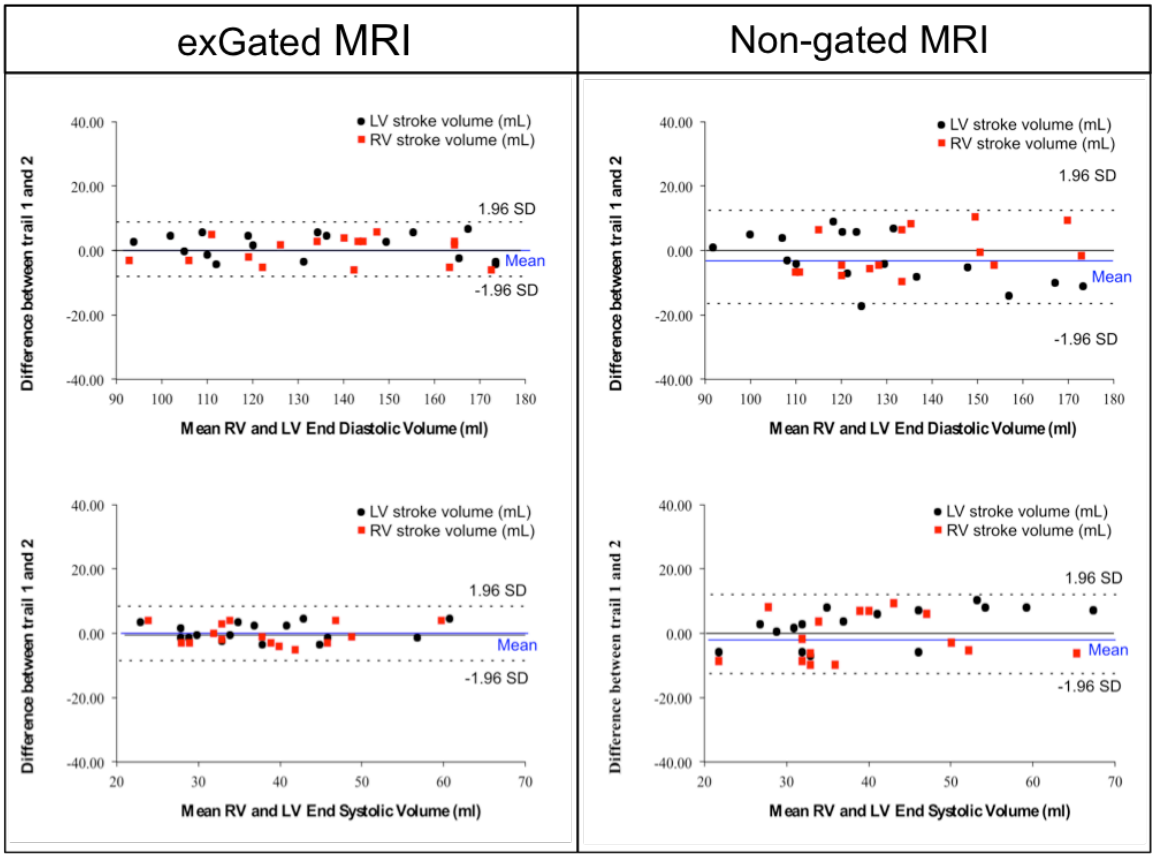

Figure 4.7 Bland Altman plots of inter- and intra-observer variability of EDV (upper two plots) and ESV (lower to plots) of exGated cine compared to non-gated cine. Note the smaller limits of agreement and variance in exGated cine.

LV ejection fraction (%)	Healthy Volunteers (n=10)	Patients with complex CHD (n=10)
Rest	62±5	51±8
Moderate*	68±4	53±6
High*	74±6	55±4

Figure 4.8 Ejection Fraction during exercise for patients with complex congenital heart disease (CHD) and healthy voluneers using the exGated cine MRI. * represents a *p*-value <.05.

4.4 Discussion

In this chapter, a reconstruction pipeline for cardiac and respiratory-gated cine CMR was presented. Our method utilizes standard available imaging sequence for highly accelerated dynamic imaging and computational inexpensive image-processing techniques to obtain a cardiac and respiratory gated cine stack during physiological exercise, without the need for breath holding or ECG triggering. As a result, our proposed framework can be readily applied in most clinical CMR environments using a simple personal laptop computer, independent of MRI vendor MRI.

In the proposed pipeline, the high temporal resolution of these images is exploited for estimation of cardiac and respiratory motion. By applying motion estimation techniques to the reconstructed non-gated real time images, the need for complex *k*-space based reconstruction techniques is avoided. Computational expenses were further reduced by utilizing dimensional reduction of the images in the applied motion estimation techniques. As a result, the proposed framework is able to reconstruct a cine stack of the heart in a clinically acceptable total reconstruction time of ~30-40 minutes using a standard laptop computer.

Manifold Learning was used to estimate motion from the acquired stack of dynamic images. This method has previously been used in combination with complex acquisition schemes for CMR at rest and shown to be both robust and fast in estimating motion from images [151]. By using the entire image as an input to the ML algorithm, it was found that the respiratory motion was accurately estimated, as demonstrated in Figure 4.2. In some cases, ML did also detect a cardiac signal. However, the cardiac periodicity estimation based on this signal proved to be not precise enough for cardiac gating, due to significant shifts in image intensities as a result of through-plane motion of the heart and surrounding fat. Estimation in the temporal frequency domain proved more accurate, but unfortunately only when a cROI was introduced to avoid detection of other (exercise) motion. As a result, the pipeline requires a single manual step: the identification of a cROI and a LV centre point at the onset of processing, just after the images are loaded. Future work might be able to address this single manual step, by implementing recently developed, fully automated deep neural networks for

ventricular segmentation. In collaboration with Dr Puyol-Anton such an algorithm is currently under development, and the preliminary results will be presented at the IEEE International Symposium for Biomedial Imaging 2018 [167].

After development, the proposed framework was implemented in a workflow for exercise CMR in our clinical research CMR facility. Tests of the performance of exGated cine in healthy volunteers and patients with a complex congenital heart disease showed that exGated cine is in acceptable agreement with the only currently available validated standard for non-gated RT imaging in quantification of SV. There is some variability in quantification of SV noted between the two methods. This variability can be a result of underperformance of our technique, or could be part of the inherent variability of the non-gated RT imaging. As previously discussed, non-gated RT imaging suffers from inaccuracies as target images for analysis are manually selected out of a large real time dataset and, despite manual respiratory correction, inconsistencies in respiratory states per slice are hard to avoid [168]. The technique proposed in this chapter utilizes information from multiple heartbeats to reconstruct a single averaged beat, much like conventional cine CMR, reducing the target images for analysis. Furthermore, the automated respiratory correction results in consistent motion states throughout the image stack, both in cardiac phases as well as slices. These advantages were reflected in the superior inter- and intra-observer variability of exGated cine compared to non-gated RT imaging. These results suggest that the observed variability between exGated cine and non-gated RT cine can potentially be a result of inaccurate quantification in the non-gated RT reference standard. Unfortunately, no other standards for quantification of exercise SV are available, except for highly invasive measurements, such as deriving CO using the Fick method, which in themselves have known inaccuracies [169]. The improved accuracy of analysis of cardiac function is an important gain of our technique, as it facilitates implementation of exercise CMR for clinical studies for investigation of cardiac exercise performance. The usefulness of the proposed technique is demonstrated in the subsequent chapters in which the (patho)physiology of the healthy heart and the Fontan circulation are investigated.

4.5 Conclusion

Based on the results presented in this chapter, it can be concluded that the proposed retrospective cardiac and respiratory gating reconstruction framework for non-gated RT imaging improves clinical applicability of Exercise CMR, ensuring better accuracy of volume quantification, while being user-friendly and widely applicable. In the subsequent chapters,

the developed technique will be utilized to investigate the cardiac response to exercise in healthy volunteers and patients with Fontan Circulation.

Chapter 5 Role of the Right Ventricle in SV Augmentation during Exercise

In the previous two chapters, the development, implementation and subsequent validation of Exercise CMR imaging and image-analysis framework was discussed. The following parts of the thesis describe how this framework is utilized to investigate the primary questions of this PhD: *What is the role of the right ventricle in the heart during exercise?* and *How does the absence of the RV impact the (patho-)physiology in the Fontan Circulation?* The present chapter presents the experiments that were executed in order to investigate the role of the RV in cardiac function during exercise, in particular its role in maintaining and augmenting stroke volume (SV). Firstly, in Section 5.1 the rationale behind this work is discussed, especially the importance of SV regulation in cardiac function. Next, in Section 5.2 the used methods are discussed, including the description of the Exercise CMR tests executed and definitions of the biomechanical model used to examine the observed exercise behaviour. In Section 5.3 the results of the executed experiments is discussed. Finally, Section 5.4 discusses the implications of the observations, which show a key role of that the RV in LV function and total cardiac performance during exercise, and concludes this chapter.

5.1 Introduction

In Chapter 2, the cardiac physiological response to exercise was described. As noted there, the healthy human heart increases cardiac output (CO) during exercise by increasing HR while simultaneously sustaining SV. Despite a dramatic reduction in ventricular filling- and ejection-times due to the HR response, SV is maintained or marginally increased up to maximal exercise levels [5, 14, 15, 49]. This allows the heart to effectively increase CO up to 5-fold its resting values, as CO = HR x SV. Although fundamental in cardiac performance, the mechanism of SV preservation (i.e. SV regulation) is not well understood. Anatomical and mechanical differences between the LV and RV [30], and contrasting changes in

ventricular volumes observed during exercise [7, 40] suggest distinct roles for the two ventricles in SV regulation, but too date these roles remain unclear [13].

Traditionally, evaluation of cardiac function in clinical cardiology and physiology has focused on the left ventricle (LV), while the role of the right ventricle (RV) is often neglected. However, advances in medical imaging have improved our ability to assess RV function. Aided by these improvements, new evidence has emerged showing that the RV is not merely a sub-pulmonary pump, but has an important impact on overall cardiac performance. In athletes, RV dysfunction is seen after high intensity endurance exercise [170], while in patients with heart failure, outcomes are poorer if the RV is also effected [11, 12]. Similarly, the absence of a sub-pulmonary pump, as in patients with a single ventricle circulation, results in profound exercise intolerance and pre-mature heart failure [18]. These facts suggest that the RV plays an important role in biventricular pump function for effective cardiac performance.

The impact of the RV on the effective performance of the biventricular heart could potentially be explained by a cooperative, or codependent, mechanism between RV and LV function in SV regulation. Mechanical interaction through the shared ventricular septum is well established. However, this interaction alone cannot explain the impact of RV on LV function and ultimately total cardiac performance. Understanding SV regulation, and in particular the interaction between RV and LV function, is therefore critical for characterizing fundamental cardiac physiology and helps to explain the importance of the RV in the optimization of total cardiac function.

5.2 Methods

In order to investigate the role of the RV in SV augmentation, three Exercise CMR experiments and a biomechanical modeling study were executed. During each Exercise CMR test, the biventricular response to physiological exercise was investigated, by obtaining cardiac volumes at rest and during exercise. In particular, the changes in RV and LV volumes during exercise that determine the SV response were assessed.

First, an Exercise CMR test was performed under normal physiological circumstances in 17 normally active (<4 hrs training per week) healthy volunteers (9 males and 8 females) to evaluate the normal physiological biventricular response to exercise. Next, the same group of volunteers underwent an identical second Exercise CMR test (HR-inhibited test), after pharmacologically induced negative chronotropy (indirect positive inotropy).

CO is closely regulated by oxygen demand of the body. On its turn, oxygen demand is closely related to exercise intensity and load. Exercise levels, exercise time, imaging time, cycle rotations per minute, room temperature and humidity were kept constant between the two Exercise CMR tests. Therefore, selective inhibition of chronotropic response was expected to result in an indirect inotropic drive to increase SV during exercise. This allowed investigation of the changes in LV and RV behavior occurring between the two Exercise CMR tests that underlie augmentation of SV.

Pharmacological inhibition of chronotropy in the HR-inhibited test was obtained by administration of 7.5mg ivabradine orally. This was expected to reduce HR by ~10-15% during exercise [171]. Ivabradine is a selective inhibitor of the I*f* current in the sinusnode. This results in an increased repolarization period, leading to inhibition of the pacemaker frequency of the sinusnode. While decreasing HR, it has no systemic vascular effect, nor any direct pharmacological impact on cardiac inotropy or lusitropy [172]. Ivabradine was administrated directly after the physiological Exercise CMR tests. A three-hour wait was observed between the two Exercise CMR tests in order to allow full recovery and obtain the desired HR-inhibition effect.

Next, the physiological biventricular volume response to exercise was evaluated in a group of 8 competitive endurance-trained athletes (>10 hours of training per week for more than 5 years). All athletes underwent a single Exercise CMR under normal physiological circumstances. Finally, a personalized anatomically correct biventricular biomechanical model of the heart was introduced in order to explain the observed ventricular behavior underlying SV augmentation during exercise and explore its impact on cardiac performance.

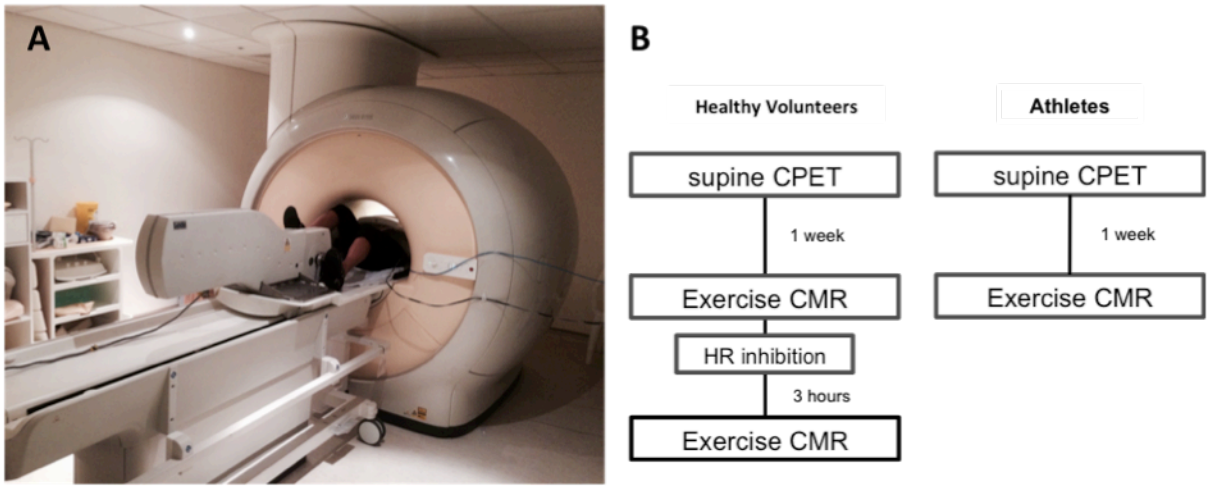

Figure 5.1 Exercise CMR setup and flowchart of Exercise CMR experiments. A) Wide bore 1.5T MRI scanner with a supine bicycle ergometer mounted on a dedicated exercise CMR bed. Wires coming out of the bore are a Finapress continues finger pressure waveform lead and an oscillometry brachial blood pressure cuff used for calibration. B) Flowchart of the exercise CMR experiments.

5.2.1 Exercise CMR's

The set-up of Exercise CMR and a flowchart of the exercise experiments is shown in Figure 5.1. At the start of the study, a supine cardiopulmonary exercise test (CPET) was performed in all participants in order to obtain personalized exercise levels (exercise load in Watts) for the exercise CMR experiments. A week after the CPET, participants underwent the Exercise CMR tests. Imaging was obtained at rest and at two levels of exercise: moderate and sub-maximal exercise. The exercise levels were determined as follows: 'moderate exercise' was defined as the workload corresponding to a HR of 110-120 beats per minute (bpm) during the CPET, and 'sub-maximal exercise' was defined as the workload corresponding to a HR of 145-155 bpm during the CPET. Prior to the CPET and each exercise CMR, a 10-minute training ride was executed in order to avoid training bias between the tests.

During the exercise CMR, a short and long axis image stack were acquired at each exercise level using highly accelerated real time exercise imaging protocol described in Chapter 3 and Chapter 4. End-diastolic volume (EDV), end systolic volume (ESV) and SV were measured in both RV and LV at rest and during moderate and sub-maximal exercise. Real-time 2D phase contrast flows were also recorded in the aorta and, in selected patients, also in the main

and branch pulmonary arteries, and the descending aorta using the real-time flow protocol described in Chapter 3. Furthermore, blood pressure measurements were obtained at each level of exercise using Finapress (FMS, the Netherlands) continuous blood pressure waveform analysis, with calibration of the waveform prior to each measurement using a brachial blood pressure cuff as explained in Chapter 3.

5.2.2 Definition of the biomechanical model

To study the mechanical behavior of the biventricular heart, a biomechanical model was constructed based on previous works by Dr. Nordsletten et al. [173, 174]. The model reference anatomy was personalized based on MRI imaging data collected at end systole from a 30 year old female [21]. While model anatomy was patient-specific, the model was personalized based on values obtained in previous literature [21]. The reduced Holzapfel-Ogden model [173, 174] was used to represent the myocardium, with stiffness parameters (a, a_f) scaled to ensure that model pressure / volume matched predictions based on Klotz et al. [175] (e.g. ensuring $V_{ref} = V_{ED}\ (0.6 - 0.006\ P_{ED})$, with P_{ED} set to $8\ mmHg$). Idealized fibers were introduced into the myocardium as described previously [174], with fiber angles varying transmurally epi to endo +/- 60° in the LV and +/-40° in the RV free wall. Passive stiffness was increased by an order of magnitude around the valve rings to emulate the more collagenous tissue. A length-dependent active tension model [173] was used to enable tissue contraction, with separate activation parameters introduced for LV / septum and RV free wall. To examine the influence of activation and work in the myocardium during sub-maximal exercise, the model was inflated to typical LV / RV exercise afterloads (LVP = 158mmHg (obtained from the data), RVP = 40 mmHg obtained from [15]) and active tension was subsequently introduced into both heart chambers. In the model, aortic and pulmonary valves were fixed, the mitral valve was held in plane but allowed to slide, LV / RV endocardial pressures were set to ramp up and subsequently sustained at estimated sub-maximal exercise afterload, and epicardial boundaries employed zero traction. Active tension was increased in LV / RV at the same rate, with little variance in pressure / volume observed when varying the LV activation or RV activation due to the prescribed model afterload. Increasing contraction parameters, the model exhibited a rapid drop in volume that eventually stagnated. This was a consequence of length-dependence of active tension that reduced the active tension exerted on the model. This result also was a consequence of the

passive / active stiffness interaction at fixed afterloads (Figure 5.6). At zero LV / RV active tension, the load was held entirely by the passive elasticity of the tissue. Contraction subsequently begins to carry the afterload and relieve the passive stretch. However, as the chamber volumes reduced in size passing the reference volume of the heart, the internal wall shear eventually began to resist the activation of the muscle, limiting volume reduction. Reflecting the exponential stress-strain response of the passive myocardium [176], this resulted in an exponential growth in the activation stress / volume curve, therefore requiring increasing amounts of active tension in order to achieve similar volume changes achieved at larger chamber volumes. See Figure 5.6 for an illustration of the impact of these properties on the active tension curves.

5.2.3 Statistics

Data were analysed using IBM SPSS statistics for Mac (version 22, Chicago, IL, USA). Descriptive data for continuous variables are presented as means ± standard deviation. Descriptive statistics for discrete variables are presented as frequencies and percentages. Two-way repeated measures ANOVA was used to compare the biventricular response from rest to sub-maximal exercise between physiological and HR-inhibited tests in healthy volunteers, with exercise intensity and HR inhibition both as within-subject effects. The same test was used to compare athletes versus healthy volunteers, with exercise level as within-subject effect, and athlete vs. volunteer as between-subjects factor. Differences in ventricular volume responses during exercise between groups were expressed as mean effects or mean differences ± standard deviation (SD). Bonferroni post-hoc tests for multiple comparisons were performed. Significance levels are reported after Bonferroni adjustment. A p-value <0.05 was considered statistically significant.

5.3 Results

Exercise CMR's were successfully performed in all included participants. No participant reported discomfort or adverse events from the study.

5.3.1 SV response to physiological exercise

All exercise CMR test results are shown in Table 5-1. During the physiological Exercise CMR, SV increased in healthy volunteers from rest to moderate exercise in both ventricles (+3±3 ml/m^2 p=.04) and was subsequently maintained during sub-maximal exercise (Figure 5.2A). The behavior underlying the increase in SV was different between RV and LV, see Figure 5.2B,C and Figure 5.3A.

EDV fell in both ventricles during exercise, resulting in a negative impact of EDV on SV compared to resting values. However, the fall in LV EDV was less than RV EDV (mean difference: 5.86±1 ml/m^2, p<.01) with RV EDV falling nearly twice as fast from rest – sub-maximal exercise (RV EDV-19±6 ml/m^2 vs. LV EDV -10±4 ml/m^2, p<.01). ESV also fell less in the LV compared to the RV (mean difference: 5.92±1 ml/m^2, p<.01), with a total change of ESV from rest – sub-maximal exercise of -20±6 ml/m^2 and -13±5 ml/m^2 for RV and LV respectively (p<.01). These observations are consistent with other studies investigating RV and LV volumes during moderate intensity supine exercise in healthy volunteers [41, 168, 177], and are in keeping with a larger group of studies that have investigated LV behavior during exercise up to sub-maximal intensity levels [7, 40, 135, 168].

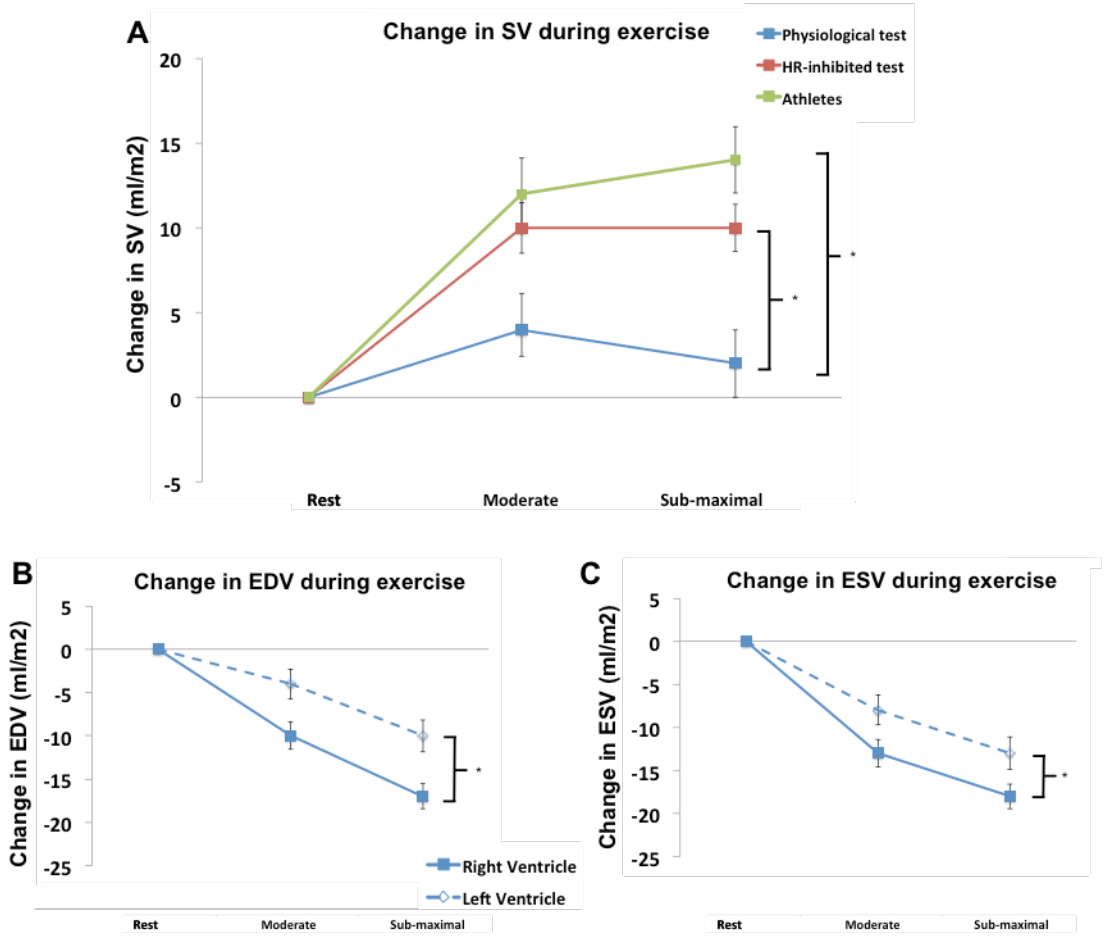

Figure 5.2 RV and LV volumetric changes during exercise. A) Change in Stroke Volume (SV) from rest during physiological (blue) exercise CMR and HR inhibited exercise CMR (red) and in athletes during physiological exercise CMR (green). B) Change in EDV during physiological exercise in the RV (solid blue line) and LV (dotted blue line)during physiological exercise in healthy volunteers. **C)** Change in EDV during physiological exercise in the RV (solid blue line) and LV (dotted blue line) during physiological exercise in healthy volunteers. Mean±SEM. *denotes a significant mean difference in volume response during exercise with $p<.05$ after Bonferroni correction.

The different behavior of LV and RV EDV during exercise is likely to be a reflection of the different preload conditions in the two ventricles. In the human circulation, RV preload is governed by systemic venous return, which in turn is largely determined by factors outside the heart (such as blood flow propagation by active muscle contractions and arterial and venous tone) [178]. Although venous return is enhanced during physiological exercise, the increase in RV preload is not sufficient to compensate for the reduced filling time, resulting in the observed fall in RV EDV [38, 39, 179]. In contrast, the heart is able to manipulate

preload conditions of the LV. The relatively small volume and low resistance of the lung circulation allows increased RV systolic contraction, and the resulting increase in pulmonary artery (PA) flow and pressure, to be transmitted through the pulmonary vascular bed, translating into higher left atrium (LA) pressures during exercise [10, 61]. This fits our observation that LV EDV is better preserved during exercise than RV EDV and that the RV is more dependent on a drop in ESV to augment SV during exercise compared to the LV.

	Healthy Volunteers:						**Athletes**		
	Physiological exercise			**HR-inhibited exercise**					
Exercise Level	Rest	Moderate	Sub-maximal	Rest	Moderate	High	Rest	Moderate	Sub-maximal
Exercise Load (Watts)	0	65±5	121±4.5	0	65±5	121±4.5	0	90±5	174±15
Heart Rate (beats per minute)	68±10	114±14	148±15	65±10	108±12	133±13	52±7	109±9	140±8
Cardiac Output (L/min/m2)	3.5±0.6	6.2±1.1	7.9±1.0	3.2±0.6	6.5±0.9	8.0±1.0	3.37±0.5	8.1±1.3	11.0±1.5
Stroke Volume (ml/m2)	50±7	54±6	53±6	49±6	60±6	60±6	65±8	76±11	79±11
Left Ventricle									
End Diastolic Volume (ml/m2)	81±12	77±12	71±11	80±11	83±12	79±10	108±13	112±13	111±13
End Systolic Volume (ml/m2)	31±7	24±8	18±6	31±7	23±9	19±5	43±9	35±5	31±5
Ejection Fraction (%)	62±4	70±6	75±6	62±4	73±6	77±4	62±4	69±4	71±4
Right Ventricle									
End Diastolic Volume (ml/m2)	91±14	82±11	74±9	90±13	84±10	76±8	125±15	116±13	111±13
End Systolic Volume (ml/m2)	40±10	28±6	22±5	41±9	24±6	16±4	59±8	39±7	32±6
Ejection Fraction (%)	56±6	67±5	71±5	55±5	72±4	78±4	52±4	65±6	71±4

Table 5-1 Changes in heart rate, cardiac output and indexed cardiac volumes during exercise CMR. Exercise CMR test results for healthy volunteers during physiological supine exercise and after HR inhibition and exercise CMR test results for athletes during physiological supine exercise. er physiological Native test versus HR-inhibited test. Expressed are means±SD. Colored boxes refer to a significant mean difference in exercise response between right and left ventricle (blue), physiological and HR inhibited exercise test (red) and healthy volunteers and athletes during physiological exercise using repeated ANOVA, with a significance level of $p<.05$ after Bonferroni correction.

5.3.2 SV response to exercise after negative chronotropy

To gain insight into SV regulation at higher levels of inotropic drive, ivabradine an I_f current inhibitor was given to the healthy volunteers after the physiological exercise CMR to induce selective negative chronotropy (indirect positive inotropy). After a 3hr wait, the exercise CMR study was repeated using identical workloads and exercise times.

Exercise HR decreased significantly between the physiological and HRi-test (mean effect: -7.5±0.8%, $p<.01$) and forced a significant SV response (mean effect: +7.5±1.0%, $p<.01$) while CO was maintained (mean effect: +1.0±1.5% $p=.43$), see Figure 5.2A. The changes between the physiological exercise and HRi tests are shown in Table 5-1 and Figure 5.3A.

In the RV, the increase in SV was obtained primarily by increasing contractility, resulting in a lower RV ESV (mean effect: -9.5±1.6% $p<.01$). The RV EDV response during exercise did

not change between the two tests (mean effect: +1.0±1.0%, p=0.8). In contrast, SV augmentation in the LV stemmed principally from an increase in LV EDV (mean effect +5.3±0.7% p<.01), as the LV diastolic filling rate was significantly increased compare to the physiological test (mean effect: +13±6% p<.01). Whereas the LV ESV response exhibited no change (mean effect: 0.2±2%, p=.91). Interestingly, even during moderate exercise (when the LV still exhibited the ability to decrease ESV), the additional increase in SV seen in the Hr-inhibited test was driven by an increase in LV EDV and not a decrease in ESV.

These findings, combined with the results of the physiological exercise CMR test, highlight that the mechanism of SV augmentation differs between the two ventricles. In the face of a lack of sufficient preload, the RV can only augment SV by contracting down to a lower ESV. The LV is able to augment SV through regulation of EDV and ESV as a consequence of RV's ability to regulate LV preload. However, as shown here, LV SV augmentation during exercise is largely achieved through improved EDV.

The observed improved LV filling could originate either from an enhanced active LV relaxation ('LV pull') or increased support of LV filling through the RV systolic ejection ('RV push') or some combination of these. We propose that the increased RV systolic ejection is the main driver of the observed LV EDV response. LV relaxation is not only a passive elastic recoil phenomenon, but also have an active component. However, as shown in experimental settings, the kinetics of contraction and relaxation are tightly coupled in the cardiac muscle [37] and, likely as a result of this, LV relaxation linearly related to changes in ESV during exercise [14]. This did not change during the HRi test and yet we saw substantial augmentation of LV preload as shown by improved LV diastolic filling rate. This implies that the LV pull is not likely to be a key driver of the observed SV augmentation. Also previous invasive studies show a marked increase in mean pulmonary, and LA pressures during exercise, suggesting that the RV push dominates the improved LV filling response [10, 61]. It therefore seems likely that the enhanced LV filling is mainly driven by the increased RV systolic contraction, which is propagated through the lungs to augment LV filling.

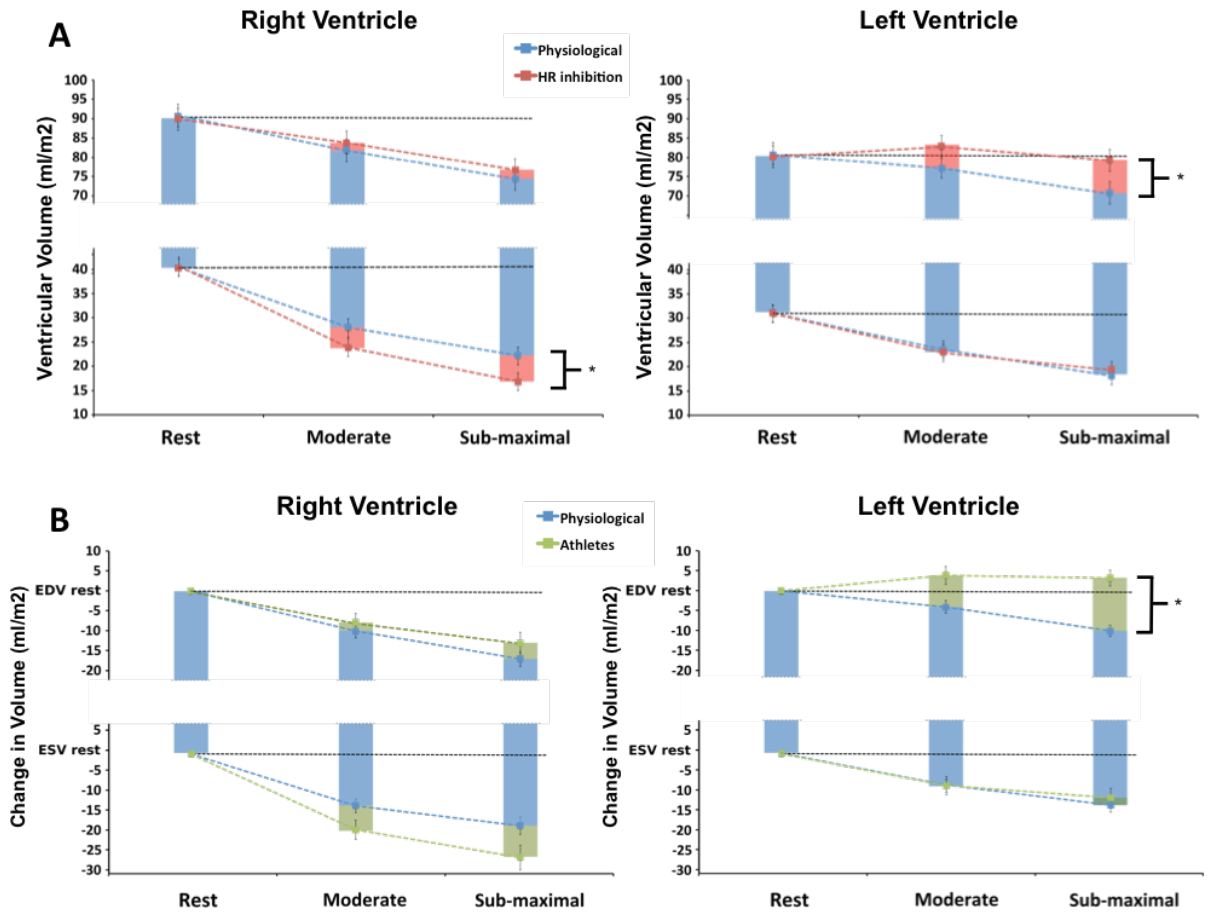

Figure 5.3 Cardiac volume response and stroke volume augmentation during exercise. **A)** Right and left ventricular response to exercise from rest (grey dotted line) to sub-maximal exercise. Stroke Volume (SV) during physiological exercise is depicted (blue box) together with the augmented SV after HR-inhibited (red box). **B)** Change in ventricular volumes from rest during physiological in healthy volunteers and endurance trained athleters. The green box illustrates the mechanism of augmented SV response in athletes compared to healthy volunteers (blue box). Note that SV augmentation during HR inhibition as well as in athletes is achieved is achieved mainly by decreased ESV in the RV whereas in the LV an increase in EDV is the main contributor. Represented are Mean±SEM. *denotes a significant mean difference in volume response during exercise with $p<.05$ after Bonferroni correction.

5.3.3 SV response to exercise in Athletes

In addition to the observations in healthy volunteers under physiological and indirect inotropic conditions, SV augmentation during exercise in endurance trained athletes was evaluated. To determine what underlying LV and RV behavior leads to better SV augmentation in athletes compared to untrained healthy volunteers, the exercise CMR results

of athletes were compared to the physiological exercise CMR test in the healthy volunteers. Because most athletes have very low resting heart rates (between 35 and 50 beats per minute in our cohort), no HR-inhibited test was performed, as this was contra-indicated. Effectively, athletes have due to training remodeled to an augmented SV response similar to the indirect chronotropic response obtained in the healthy volunteers.

As expected, CO increased significantly more in athletes compared to healthy volunteers during exercise (mean difference +1.8±1.5 L/min/m^2, p<.01). This was the result of a larger increase in SV (mean difference: +6.7±1.5 ml/m^2, p<.01), see Figure 5.2A.

In the LV, the larger SV increase was achieved mainly through an enhanced EDV response from rest compared to healthy volunteers (mean difference: +7.3±1.6 ml/m^2, p<.01), whereas the ESV response was not different between the two groups (mean difference: -0.5±1.8 ml/m^2, p=0.7). This behavior is similar to the LV response seen after negative chronotropy in untrained healthy volunteers, as is clearly seen in Figure 5.3.

In the RV, the augmented SV response seemed to be driven mainly by a trend towards a larger decrease in ESV from rest in athletes (mean difference: -3.9±2.1 ml/m^2, p =.06), in combination with a slightly lower fall in RV EDV (mean difference: +2.4±1.98 ml/m^2, p=.15), as also illustrated in Figure 5.3, that is likely caused by improved venous return due to the larger CO in athletes.

The ventricular behavior observed in athletes echo earlier studies that showed that the better LV SV exercise response in athletes compared to sedentary individuals stemmed primarily from an enhanced LV EDV [7, 58, 60], with no, or minimal changes in LV ESV [7, 58, 60] and LV relaxation [180, 181]. Also, previous invasive pressure studies showed even larger augmentations PA and LA pressures during exercise in athletes compared to untrained individuals [10, 61], again suggesting a central role of the RV systolic push in LV SV regulation.

5.3.4 Energetic advantage of biventricular SV augmentation

A core question arising from the results of the exercise CMR experiments is: What drives the heart to improve LV SV by relying on RV supported filling instead of augmenting the LV ESV response? Using a personalised biomechanical model of the biventricular heart, it is

possible to investigate this question by examining the active stress required to generate physiological pulmonary and systemic systolic exercise pressures over a range of different volumes in the RV and LV, respectively. This way, the costs of activation (sum of active stress from EDV - ESV) can be estimated for each ventricle and changes in the energetic cost for increased SV – through some combination of increasing EDV and decreasing ESV – could be explored. These modelling experiments illustrate that the LV has a significant benefit of maintaining an optimal volume state and that maintaining this state during exercise by through RV supported augmentation of LV filling minimizes the costs of biventricular contraction in the heart.

Disregarding overinflated states, where a significant increase in passive stretch diminishes the active tension needed to maintain sub-maximal exercise afterloads, LV active tension is large at sub-maximal LV volumes and decreases with falling volumes, following Laplace's law (see Figure 5.4). At very low volumes, however, costs of activation increase steeply as internal shear deformation of the LV myocardium becomes mechanically limiting. Based on the shape of the LV active tension curve, the LV should ideally work with an ESV close to the active tension minimum in order to optimize costs of contraction. The results of the individualized model show that during exercise the LV operates in this volume range (see the two markers in Figure 5.4A). Albeit minimizing costs of contraction, this volume state of the LV restricts its ESV reserve, as further decreases of ESV result in an exponential increase in contractile costs. As a consequence, the LV becomes increasingly dependent on external sources to enhance EDV in order to maintain or adapt SV during exercise (see insert in Figure 5.4A). On its turn, LV EDV, unable to profit from a further boost in relaxation by augmented elastic recoil from a lower ESV, becomes reliant on effective RV systolic function during increasing exercise intensities.

In the RV, the costs of contraction are significantly lower than the LV (see Figure 5.4 and Figure 5.5), reflecting the reduced stroke work required to overcome the relatively low afterload of the RV. As described above, the RV is limited to decreasing ESV to augment SV. However, the low costs of contraction make increasing contraction to a lower ESV significantly less expensive in the RV compared to the LV. This means that the heart is able to utilize augmentation of SV through contraction to lower ESV in the RV (working against the 'low pressure circulation) to improve filling of the LV, hereby allowing the LV (working against the 'high pressure circulation') to minimize costs of contraction by maintaining an optimal volume state. The costs of RV contraction inevitably increase exponentially at very

low ESV's due to mechanical constraints. However, as shown by the less pronounced changes of the active tension curve in Figure 5.4, RV active tension does not vary as much with volume compared to the LV. As a result, the RV costs of contraction are less dependent on its volume status. This allows larger RV volumes, and thus a larger RV ESV reserve, that improve the ability to augment SV and LV filling. This could explain why the RV is generally larger than the LV in the human heart and why the heart adapts to larger ventricular volumes in endurance athletes [182]. Adjusting the model by increasing rest volumes in both chambers by 10%, we observed that the work required to drive SV indeed improved. With a similar costs of contraction, a ~10% increase in SV was achieved, leading to greater efficiency in pump function. Altogether, these modelling experiments show that the heart, in an attempt to minimize total costs of contraction, operates via a mechanism of RV and LV cooperation that results in a clear dependence of LV SV on RV systolic function during exercise

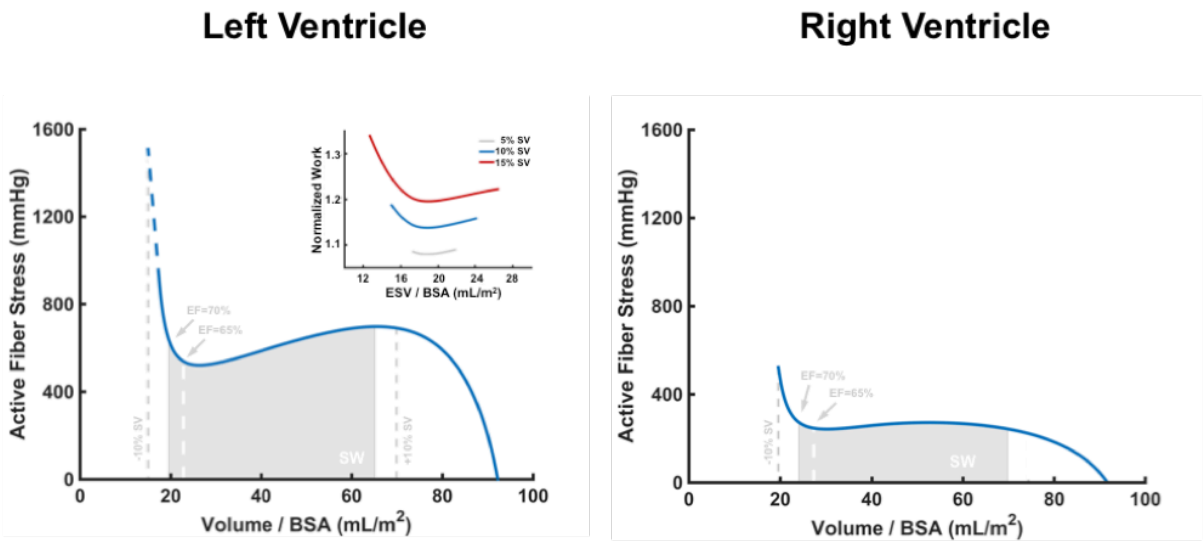

Figure 5.4 RV and LV costs of contraction. RV and LV active tension curves (active stress required to overcome afterload at each volume) in a personalized biomechanical model of a healthy volunteer. In grey volume state during submaximal exercise in a representative volunteer. White Dotted line; volume state at moderate exercise. Grey dotted lines represent a 10% SV increase through decrease in ESV versus an increase in EDV. Insert represents the increase in costs of a SV increase (5%, 10%, 15%) using different strategies with left end of the curves representing SV increase through ESV solely.

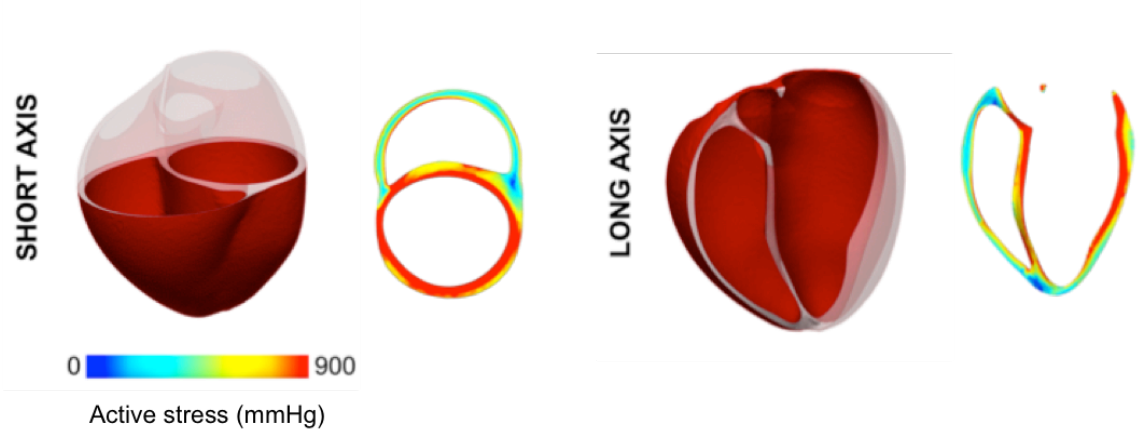

Figure 5.5 Illustration of the personalized biventricular biomechanical model and colour map of active tension needed to overcome exercise-afterload in the ventricles. Note the larger tension needed in the LV compared to the RV.

5.4 Discussion

In this Chapter, the cooperativity between LV and RV in SV regulation during exercise was investigated. The results showed that RV systolic function is pivotal in LV SV augmentation and optimization of total cost of contraction of the heart during exercise. This explains the previously observed, but so far not well understood, impact of the RV on cardiac performance in heart disease and competitive endurance exercise. Furthermore, it means that the RV can be a potential target for optimizing cardiac function in disease and exercise training that should not be ignored during assessment of the heart.

To date, appreciation of ventricular interdependence has largely focused on mechanical inter-ventricular interaction through the septum. While this is a core element of ventricular interaction, the results of this chapter demonstrate that ventricular interaction through SV regulation and preload presents another functional interaction pivotal to cardiac performance during exercise. The importance of this interaction for optimization of cost the cardiac contraction seems to explain the key role of RV function observed during exercise performance and cardiac disease. The described results show that the RV systolic function is exploited to optimize LV SV augmentation during exercise. This explains why transient myocardial injury is observed in the RV after intense endurance exercise, while the LV is not, or to a lesser extend, affected [170]. Furthermore, it helps to understand the mechanism underlying the adverse effects of high intensity training often reported in the RV but not the

LV, such adverse RV re-modeling [170] and its associated RV originating ventricular arrhythmia's [170]. In cardiac disease, the observed importance of RV function in optimizing cardiac performance sheds a new light on diseases typically associated with LV dysfunction. In an already diseased heart, the inability of the RV to optimize LV function is likely to exacerbate the burden of cardiac disease. Whereas previously not well understood, the RV and LV interaction presented in this study seems to be a likely explanation for the reported adverse impact of RV dysfunction on prognosis of systolic and diastolic LV failure [11, 12] and dilated cardiomyopathy and efficacy of treatments, such as cardiac resynchronization therapy [183]. Similarly, our work helps to better understand the inevitable decline of cardiac function and resulting high burden of heart failure in patients with in the single-ventricle circulation, whom lack a sub-pulmonary pump. Heart failure in these patients, rather than originating from distinct events, was previously hypothysed to be the result of slowly progressive exhaustion of the ventricular pump [19]. Our results seem to support this idea, as chronic inability to optimize cost of contraction could have a significant chronic impact on cardiac function. The key role of the RV in optimization of cardiac performance seems to be further supported by the observation that habitual exercise did not improve functional exercise capacity in patients with single-ventricle circulation, while in patients with a biventricular circulation habitual exercise was associated with better exercise capacity [184].

In the light of this existing evidence, our work suggests that the optimization of RV function might provide a valuable new treatment target in cardiac diseases. Similarly, in patients with a single-ventricle circulation (who lack sub-pulmonary ventricle) partial substitution of this mechanism might be vital to maintain cardiac performance in the long-term. Already, some recently developed RV targeted treatments have shown promising results in (pre-)clinical studies. RV assist devices [185] and RV resynchronization therapy [186] have shown immediate improvement of systemic haemodynamics in RV failure. Similarly, implantation of pre-pulmonary impellors [187, 188] seem to improve systemic haemodynamics in the single-ventricle circulation in-vitro and in-vivo experiments. These therapies have focused on severe variants of RV disease. However, our work suggest that optimization of RV function might be a potential target for a much wider range of patients with less severe heart diseases. While monitoring of RV function might provide better prognostic assessment of cardiac

diseases and could provide more insight into optimizing training regimes in athletes aiming for peak performances.

5.4.1 Limitations

The analysis presented in this study assumed that RV afterload did not change significantly enough to explain the RV behavioral changes between the related physiological and HR-inhibited tests. We did not measure invasive pulmonary pressures. However, changes in properties of the pulmonary circulation between the native and HR-inhibited tests are unlikely. Pulmonary pressures and pulmonary capillary wedge pressures are highly correlated with CO [61], which remained unchanged. Furthermore, we recruited healthy non-smoking young adults, without lung or cardiovascular disease nor arrhythmic changes during exercise. At sea-level, maximal pulmonary vasodilatation is reached early in exercise in healthy volunteers and no significant changes in PVR are seen during increasing exercise levels [15, 189]. This makes a sudden drop in PVR as the cause of RV ESV decrease after HR inhibition unlikely. Lastly, a decrease in PA pressures that would result in the observed changes in RV ESV would automatically be translated in lower left ventricular filling pressures, which is counterintuitive in the face of improved LV filling.

HR inhibition itself could potentially result in changes of ventricular behavior during exercise. HR modulation was achieved in this study using ivabradine. Ivabradine is reported to cause no significant cardiac inotropic and lusitropic effects [172]. However, the decrease in HR results in a longer diastole and therefore will have impacted LV and RV EDV. Indeed we observed a trend towards a larger RV EDV, in which preload is largely independent of the heart's actions. A similar effect can thus be expected in the LV. However not only the duration of diastole was longer but also the trans-mitral inflow rate was significantly increased. This showed that HR-inhibition alone did not explain the observed changes in LV EDV.

5.4.2 Conclusion

In this chapter, the pivotal role of RV systolic function in LV SV augmentation during exercise was demonstrated. This role results in a biventricular cooperative mechanism that optimizes cost of contraction during SV augmentation in the biventricular heart. This synergy

in RV and LV function characterizes a fundamental mechanism in cardiac physiology, likely illustrating part of the rationale behind the biventricular design of the human heart. Moreover, it demonstrates that the two ventricles must be viewed as separate entities, as their function is highly interdependent.

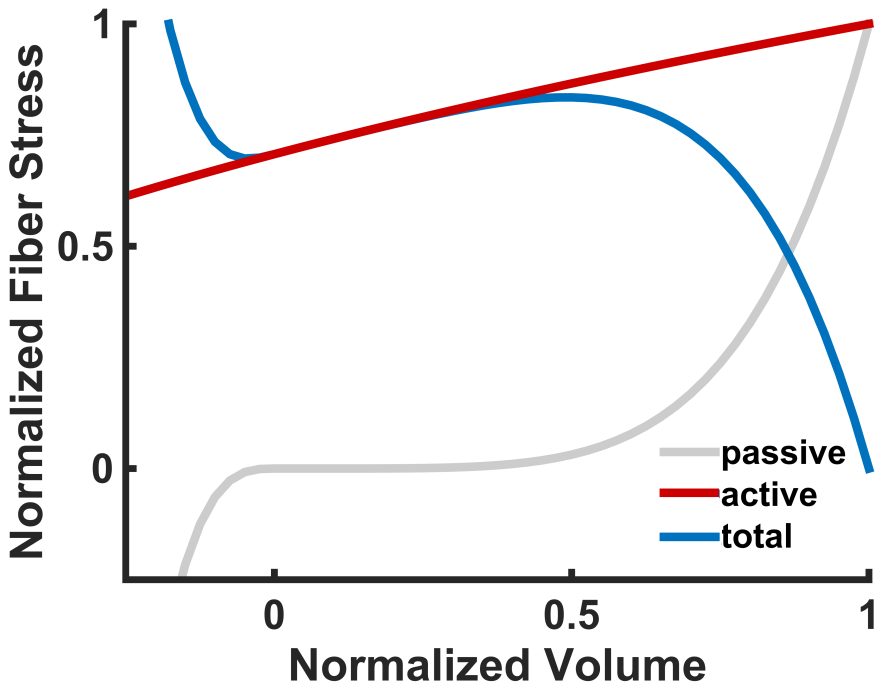

Figure 5.6 Explanation of Active Stress curve LV. The resulting curve is a combination of Laplace's Law and the passive stresses on the myocardium.

Chapter 6 Impact of absence of the RV in the Fontan Circulation

6.1 Introduction

In the previous chapter, Chapter 5, it was demonstrated that the sub-pulmonary (right) ventricle is pivotal in SV augmentation during exercise in the healthy human heart. By supporting LV filling in the face of a striking fall in diastolic filling time in exercise, the RV optimizes total biventricular costs of cardiac contraction. In the Fontan circulation, the sub-pulmonary pump is absent. As discussed in Section 2.2, patients with Fontan circulation experience a seemingly inevitable progressive decline in cardiac performance throughout life, ultimately leading to heart failure and premature death in most patients. The exact pathway of the exhaustion of cardiac performance is not well understood, but it seems clear that a single-ventricular configuration of the circulation does not function as optimal as a biventricular system.

Patients with Fontan circulation have an impaired exercise capacity, even when asymptomatic [190]. In healthy volunteers, CO increases linearly with HR and exercise intensity. In the Fontan circulation, however, the CO response is blunted, due to a fall in SV during increasing HR [88, 90, 191]. As a result, the single ventricle is unable to provide adequate CO to match metabolic demand of the body [192]. The findings in the previous chapter of this thesis may explain these observations; absence of a sub-pulmonary ventricle likely leads to a limit ability to augment systemic ventricular filling. This explains the low preload previously reported during exercise in the Fontan circulation [88, 191, 193]. Moreover, the lack of a sub-pulmonary might significantly alter the efficacy of the physiological HR response to exercise in Fontan patients. The effectiveness of the physiological heart rate response to exercise in the biventricular circulation is build upon the heart's ability to maintain SV. This criterium is not met in patients with Fontan circulation, as SV falls progressively with increasing HR. Whereas there is some adaption of the body to the single ventricle circulation, with altered physiological exercise responses (including a lower

peak exercise HR), the fall in SV during exercise seems suggest these adaptions are incomplete. This could mean that the physiological HR response to exercise and stress in Fontan patients is not optimally accommodating CO augmentation during exercise. Moreover, the sub-optimal filling of the systemic ventricle during exercise could potentially lead to an increase in energetic costs of contraction, see Chapter 5.

In this chapter, the impact of HR on exercise haemodynamics in the Fontan circulation was investigated using exercise CMR. In particular, the ventricular response and its efficiency were evaluated under normal conditions and after selective inhibition of the HR response. Firstly, the cardiac response to exercise was assessed in Fontan patients compared to healthy volunteers under normal physiological conditions. Next, the impact of selective HR inhibition was evaluated in the group of Fontan patients. These experiments illustrated that the HR response during exercise is indeed sub-optimal in Fontan patients compared to healthy volunteers and that HR inhibition leads to a significant improvement in the energetic costs of delivering CO.

6.2 Methods

6.2.1 Subjects

12 patients with Fontan circulation and 12 age- and gender matched healthy volunteers were included in this study.

Patients were recruited from the outpatient clinics of our department of adult congenital heart diseases. All patients were clinically stable, with symptoms corresponding to a New York Heart Association (NYHA) class of <II. Exclusion criteria were: significant AV or VA valve regurgitation, significant arrhythmia's or rhythms other than sinus-rhythm, significant aorto-pulmonary collateral flow or a patent fenestration and an inability to perform exercise during a supine CPET, performed prior to the study.

Healthy volunteers had no history of cardiovascular or pulmonary disease and did not take any medication (except for contraceptives) and were normally active (participation in exercise up to 3 times a week). This study was approved by the London Bloomsbury's regional ethics board (15/LO/522). All participants provided written informed consent.

6.2.2 Data Acquisition Protocol

Fontan patients underwent two exercise CMR exams; one during normal physiological exercise (physiological test) and one after selective HR-inhibition (HRi-test). Data from a

normal physiological exercise CMR age and gender matched healthy volunteers was used for comparison.

In this study, the Exercise CMR setup described in in Chapter 3 and Chapter 4 was used. The protocol of this study was similar to that described in Chapter 5. Briefly, imaging was performed at three stages during the Exercise CMR: at rest, during moderate and during sub-maximal intensity exercise. End diastolic volume (EDV), end systolic volume (ESV), SV, CO and non-invasive brachial blood pressure were obtained at each stage. Additionally, mean diastolic ventricular filling (mDRF) rate was calculated as the ventricular inflow (mL) divided by the diastolic duration (seconds). Intensity levels for the moderate and high exercise levels were obtained from a CPET that was performed one week prior to the Exercise CMR's. Moderate exercise was defined as the wattage level corresponding to a HR of 100-110 bpm, and sub-maximal exercise as the wattage corresponding to a HR of 135-145 bpm during the supine CPET.

After the physiological Exercise CMR, the group of Fontan patients received a single dose of 7.5mg ivabradine (Procolaran, Servier, Suisse) orally. Ivabradine, an inhibitor of sinusnode repolariation, selectively inhibits HR without directly affecting inotropy or lusitropy [194]. After a 3 hour break, to wait for the HR-inhibiting effect and allowing sufficient recovery, a second Exercise CMR (HR-inhibited test) was performed in the Fontan group. Exercise levels, exercise time, imaging time, cycle rotations per minute, room temperature and humidity were kept constant between the two Exercise CMRs. Prior to all Exercise CMR's and the CPET a 10 minute low intensity warm-up was performed to minimize training effect throughout the study.

6.2.3 Data Analysis

First, the difference in exercise response between Fontan patients and healthy volunteers was evaluated by examining the absolute change in HR, systemic ventricular volumes, CO and blood pressure from rest at each exercise level. Next, the impact of HR inhibition on exercise response in Fontan patients was investigated by comparing the change (%) in HR, systemic ventricular volumes, CO and blood pressure within each Fontan patient between the physiological and HRi-test. The use of absolute values for comparison between Fontan patients and healthy volunteers was based on the fact that baseline parameters might differ between individuals. In assessment of HR-inhibition (physiological vs. HR-inhibited test), the Fontan patients act as their own controls and therefore percentage change from their observed physiological exercise response was assessed.

In addition to the changes in HR, cardiac volumes, CO and blood pressure responses after HR inhibition, the impact of HR inhibition on ventricular performance and ventricular efficiency

was investigated in the Fontan patients. To do so, changes in ventricular end systolic elastance (Ees), arterial elastance (Ea), VA-coupling (Ea/Ees), ventricular mechanical efficiency (Meff), energetic efficiency (Eeff) and indexed total systemic vascular resistance (SVRi) were compared between the physiological test and HR-inhibited test, at rest and during sub-maximal exercise. These parameters were obtained based on the pressure-volume relationships. Key components of the pressure-volume relationships in the ventricle are EDV, ESV, end-systolic pressure (P_{es}), Ees (the linear slope between V_0 and P_{es} at ESV), Ea (linear slope between EDV and P_{es}) and V_0(the x-intercept of Ees at zero pressure). See Figure 6.1 for an illustration of the pressure volume relationships.

Ees and V_0 (the x-intercept at zero pressure of Ees) can be estimated with the non-invasive single beat estimation method using cardiac volumes (and ejection fraction), brachial blood pressure readings as well as isovolumetric contraction (PEP) and systolic ejection times (SEP), as described by Chen et al. [144]. This method is based on physiological principle of consistent time-varying normalized elastance in the human heart [144, 195, 196] and has been used in a broad range of cardiac diseases, morphologies and loading conditions, including patients with Fontan circulation [88, 89, 112]. V_0 is commonly regarded as a negligibly small number that does not change by chronotropic [197] or inotropic state [198, 199]. Therefore, after calculating Ees and V_0 at rest during the physiological test, we assumed V_0 to be the fixed for each individual throughout the study. Using the fixed V_0 we could then calculate Ees as the slope between V_0 and Pes. This approach was taken to avoid the influence of errors in serial estimation of Ees and V0 on the analyses of cardiac performance between the tests. Pes was estimated as brachial systolic blood pressure (SBP) x 0.9 as described previously at rest and during exercise [144, 200]. Next, Ea (Pes divided by SV) and the VA coupling ratio were obtained and the PVA graph was constructed, as illustrated in Figure 6.1.

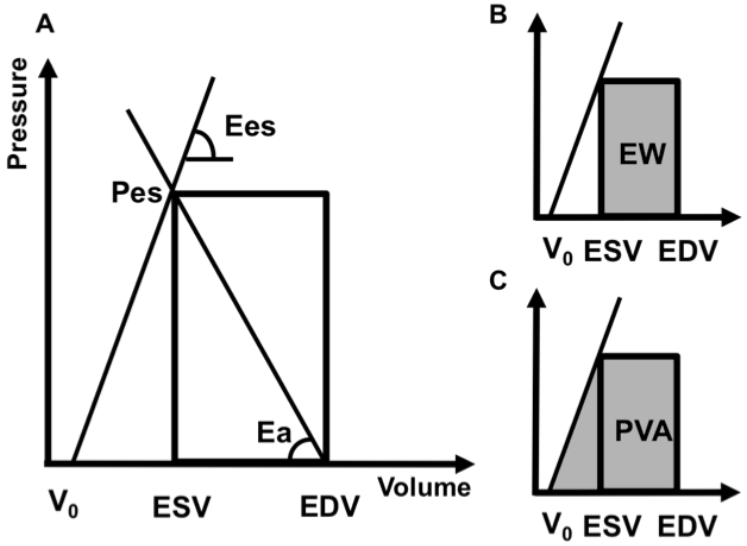

Figure 6.1 Analytical model of the Pressure-Volume relations allow analysis of ventricular performance and ventricular-arterial coupling. A) Components of the pressure-volume area and coupling parameters. B) External Work Area, C) Pressure-Volume Area. Pes; end-systolic pressure, ESV; end-systolic volume, EDV; end-diastolic volume, Ees; ventricular elastance, Ea; arterial elastance, EW; external work, PVA; pressure-volume area.

From the obtained PVA, Meff, Eeff and myocardial oxygen consumption per beat (MvO_2) can be calculated. Meff (%) is defined as follows [201, 202]:

$$(1)\ Meff = \frac{EW}{PVA}$$

With external work (EW in mmHg•ml) and PVA (mmHg•ml) defined as:

$$(2)\ EW = SV \times Pes$$

$$(3)\ PVA = \frac{1}{2}\ Pes \times (ESV - V0)$$

Eeff was subsequently calculated using the method of Burkhoff and Sawage [201] that demonstrated that MvO2 per beat is proportional related to PVA:

$$(4)\ MvO2\ (ml\ O2/beat) = \alpha \times PVA + \beta$$

Where α is a coefficient of the PVA-MvO2 relationship that was fixed for each patient at $1.9e^{-5}$ mL O_2•$mmHg^{-1}$•ml^{-1} (as previously described by Burkhoff et al. [201] and used in a Fontan population by Saiki et al. [89]). And β (mL O_2/beat) was the intercept of the PVA-MvO2 relationship which was dependent on Ees and obtained based on experimental measures as [201]:

$$(5)\ \beta = 0.0032 \times Ees + 0.104$$

After expressing both EW and PVA in Joules (J), using the conversion 1 mmHg•mL = 1.33e^{-4} J and 1 ml O2 = 20 J, energetic efficiency was calculated as:

$$(6)\ Eeff = \frac{EW}{MvO2}$$

Finally, the efficiency of the cardiovascular system in delivering CO to the body (COeff) was evaluated by calculating the myocardial MvO2 consumption per Liter generated CO (ml O2 / L) using the obtained MvO2 per beat, the HR and CO:

$$(7)\ COeff = \frac{MvO2 \times HR}{CO}$$

6.2.4 Statistics

Data was analysed using SPSS (version 22, SPSS, Chicago, IL, USA). Continuous variables were tested for Gaussian distribution using a Kolmogorov-Smirnov test and presented as means±SD or medians (25% - 75%) as appropriate. Discrete variables are presented as frequencies or percentages. To investigate the difference in the cardiac volumetric response to exercise between Fontan patients and healthy volunteers, HR, CO and the change in cardiac volumes and diastolic inflow rate from rest was analysed using two way repeated measures ANOVA [203], with exercise level as the within-subject effect and disease as the between-subject effect. An interaction *p*-value <.05 meant a statistical significant difference in exercise response between the two groups, while the mean effect expresses the mean difference between the groups during exercise.

To evaluate the impact of HR inhibition in Fontan patients, two-way repeated measure ANOVA's was executed for HR, cardiac volume and CO responses to exercise, with both exercise level and HR-inhibition as within-subject effects. In these ANOVA's a significant mean effect (mean percentage change in the analysed parameter between the physiological and HRi-test) is interpreted as a significant difference in exercise response between the physiological and HRi-test. The mean difference in ventricular performance (Ees, Ea, VA-coupling, Meff, Eeff and MvO2/CO) between the physiological and HR inhibited test at rest and sub-maximal exercise was measured using paired *T* tests. Bonferroni post hoc tests were performed during all analysis to correct for multiple comparisons. A *p*-value of <.05 after Bonferroni correction was regarded as statistically significant.

In the light of ethical considerations regarding the use of a drug intervention for the purpose of studying haemodynamics in patients, the study size was kept minimal. Therefore, this study was adequately powered to investigate the impact of HR inhibition on Fontan haemodynamics. The accuracy of Exercise MRI combined with the use of a crossover design, in which patients were their own controls, allowed us to evaluate core haemodynamic differences in this modest sized cohort.

6.3 Results

Baseline characteristics are shown in Table 6-1. Fontan patients were slightly smaller in height and weight compared to healthy volunteers, as expected. All Fontan patients had an intra-cardiac total cavo-pulmonary connection (TCPC). 5 (42%) of the Fontan patients had a systemic LV and 7 (58%) a systemic RV. Underlying cardiac defect, surgical history and age at Fontan completion of each individual Fontan patients is presented in Table 6-2.

Table. Baseline Characteristics

Variable	**Fontan**	**Controls**	*p-value*
Age, y	26±5	27±4	0.54
Male sex, n (%)	7 (58)	7 (58)	1
Height, cm	173±6	178±11	0.05
Weight, kg	64±8	75±16	0.01
BSA, m2	1.76±0.12	1.92±0.25	0.01
Resting HR (bpm)	73±19	66±9	0.36
EDV rest (ml/m2)	88±13	80±12	0.16
ESV rest (ml/m2)	44±10	30±8	<.01
SV rest (ml/m2)	44±8	50±5	0.15
Ejection Fraction (%)	50±6	63±4	<.01
Resting CO (L/min.m2)	2.94±0.52	3.25±0.51	0.25
Systemic RV, n (%)	7 (58)	-	-

Table 6-1 Baseline characteristics of Fontan patients and healthy volunteers (Controls). Expressed are means±SD and count (%). BSA body surface area.

6.3.1 Exercise Response in Fontan versus Healthy controls

HR increased during exercise in both Fontan patients and healthy volunteers with no significant difference in HR increase between the two groups (mean difference -10±14 bpm, interaction p=0.07), although there was a non-statistically significant trend towards lower HR increase in Fontan patients at each exercise stage (HR increase: moderate +43±8 vs. +32±25, sub-maximal +80±13 vs. +61±30 for controls and Fontan patients, respectively).

In Fontan patients, the mean diastolic filling rate of the systemic ventricle was significantly reduced during exercise compared to the healthy volunteers (interaction p=.01). This slower filling resulted in a larger fall in EDV in Fontan patients (mean effect -3.7± ml/m^2, interaction p<.01). There was no significant difference in change in ESV from rest between the two groups during exercise (interaction p=.12). Due to the fall in EDV, SV fell during exercise in Fontan patients whereas SV increased in healthy volunteers (interaction p<.01). Due to the fall in SV with during the increasing HR, CO increase during exercise was blunted in the Fontan patients, whereas it increased linearly with exercise intensity in healthy volunteers (interaction p<.01).

Patient	SV morphology	Underlying defect	Fontan-type	Age TCPC	Surgical History
1	RV	HLHS TA	TCPC	4	BT-shunt, Glenn at 1yr
2	LV	DILV	TCPC	6	BT shunt <1yr, Glen at 1,5 yr
3	LV	DILV	TCPC	4	PA banding <1yr, hemi-Fontan at 1 yr
4	RV	DORV	TCPC	6	Septostomy, Glenn at yr
5	LV	DILV	TCPC	18	atrial switch <1yr
6	RV	DORV	TCPC	7	BT-shunt, Waterstone shunt at 5yrs
7	RV	HLHS TA	TCPC	34	BT-shunt, AP Fontan at 10yr
8	RV	DORV, MA	TCPC	6	BT-shunt, Glenn at age of 4
9	RV	DORV	TCPC	5	BT-shunt, Glenn at 1yr
10	LV	DILV	TCPC	4	not available (surgeries completed abroad)
11	RV	HLHS	TCPC	4	BT-shunt, Glenn at 1yr
12	LV	HRHS	TCPC	22	BT-shunt, AP Fontan age 10

Table 6-2 Surgical history, underlying cardiac defect and age at completion of Fontan for each patient included in the Fontan group. HLHS; hypoplastic left heart syndrome, HRHS; hypoplastic right heart syndrome, TA; tricuspid atresia, DILV; double inlet left ventricle, IAA; interrupted aortic arch, DORV; double outlet right ventricle, PS; severe pulmonary stenosis, MA; mitral atresia. TCPC; total cavopulmonary connection; BT; Blalock-Taussig, ASO; arterial switch operation AP; atriopulmonary, yr; year

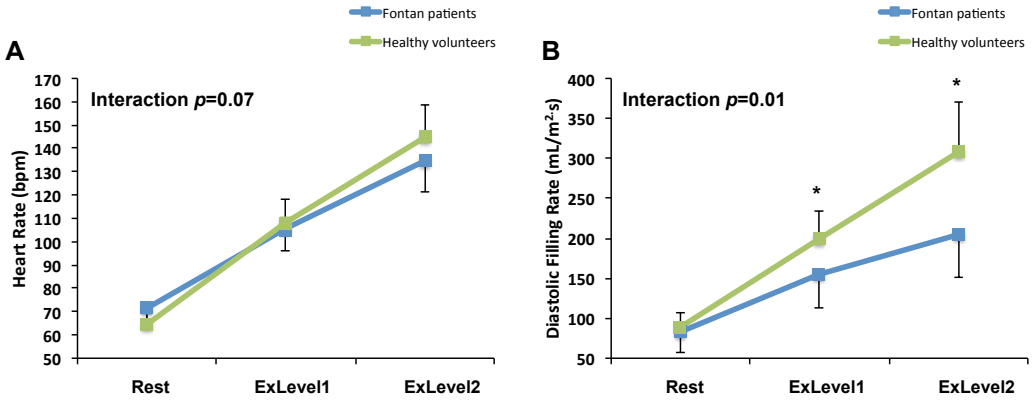

Figure 6.2 Heart rate and mean diastolic inflow rate at rest and during exercise in Fontan patients compared to healthy volunteers. * reflects significant difference in paired T test between the two group at the individual stage. Interaction was calculated using two-way ANOVA.

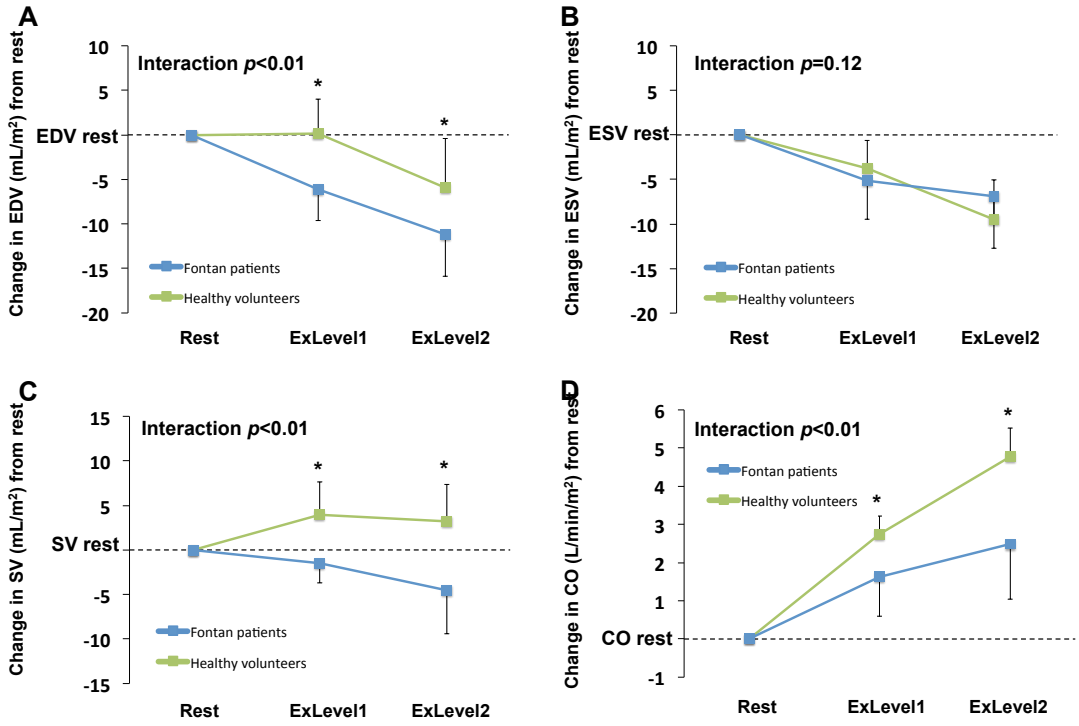

Figure 6.3 Changes in cardiac volumes and cardiac output from baseline rest in Fontan patients and healthy volunteers during exercise.* reflects significant difference in paired T test between the two group at the individual stage. Interaction was calculated using two-way ANOVA.

6.3.2 Theoretical Rationale of HR inhibition

Based on this comparison of exercise response between Fontan patients and healthy volunteers, combined with the existing literature regarding Fontan haemodynamics during exercise, the following observations can be made: 1) augmentation of ventricular filling is limited in the Fontan circulation, resulting in a fall in EDV during increases in HR. As a consequence, SV decreases with increasing HR resulting in a blunted CO response. 2) Due to the fall in SV and CO, Ea increases. This results in VA-uncoupling with increases in HR. Uncoupling of the VA relationship is known to decrease energetic efficiency of the heart [201]. Therefore, it could be hypothysed that HR inhibition, by increasing filling time, might improve SV and subsequently decrease Ea and improve VA coupling. This could lead to improved mechanical and energetic efficiency of the heart during exercise.

6.3.3 Impact of HR inhibition on Fontan Haemodynamics

HR inhibition significantly lowered the HR response during exercise in Fontan patients (mean effect -6±3%, p<.01), see Figure 6.4. The mean diastolic filling rate was unchanged between the two tests (mean effect +3±5%, p=0.13); however the diastolic period was longer (mean effect +5±2% p<.01). Therefore filling was better maintained during exercise resulting

in a smaller fall in EDV (mean effect +5±1%, p<.01). The ESV response during exercise was not altered by HR-inhibition (mean effect +1±2%, p=.24). The larger EDV lead to a significant increase in SV during exercise in the HR-inhibited test (mean effect +6±2% p<.01). As the increase in SV was larger than the decrease in HR, CO was increased during exercise in the HR-inhibited test compared to the physiological test (mean effect: +4±3%, p=.04).

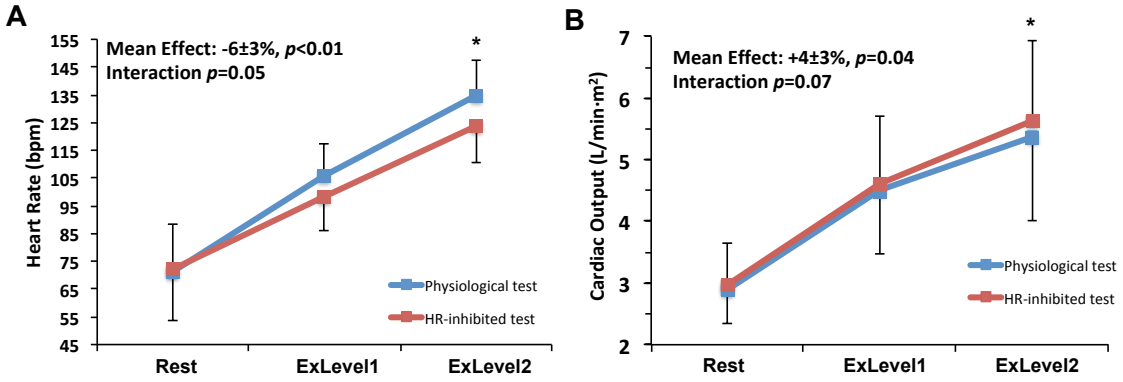

Figure 6.4 Effect of HR inhibition on exercise heart rate and cardiac output in Fontan patients. *Blue line* represents physiological test. *Red line* is after administration of ivabradine (HR-inhibited test). All values are means±SD. An asterix means a significant difference before and after ivabradine. A dagger means a significant increase in baseline response from rest – high exercise.

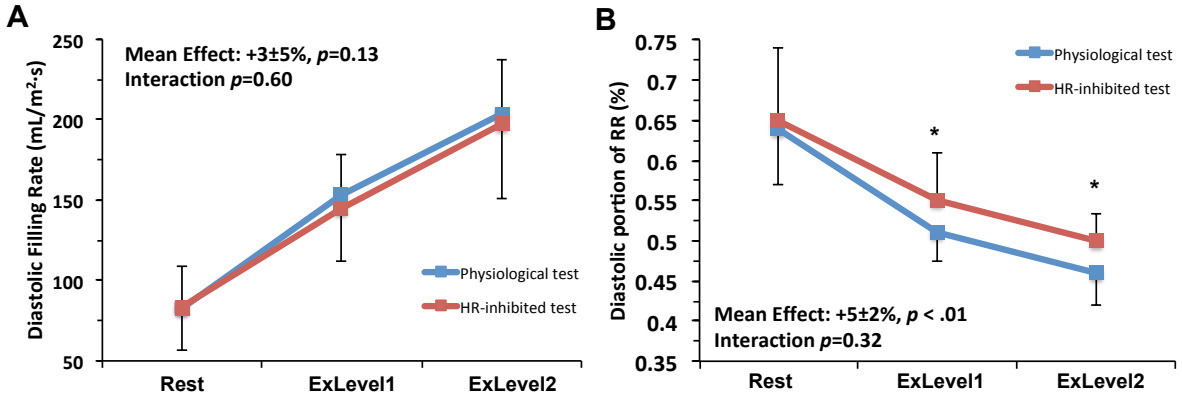

Figure 6.5 Effect of HR inhibition on diastolic filling rate and diastolic time in Fontan patients. *Blue line* represents physiological test. *Red line* is after administration of ivabradine (HR-inhibited test). All values are means±SD. An asterix means a significant difference before and after ivabradine. A dagger means a significant increase in baseline response from rest – high exercise.

6.3.4 Impact on VA-Coupling and Efficiency in Fontan

The impact of HR-inhibition on VA coupling assessment in Fontan patients is presented in Table 6-3. Ees did not significantly change between the physiological and HRi tests. Not at rest (1.25±0.41 vs. 128±0.43, p=0.42), nor at sub-maximal exercise (1.96±0.90 vs. 2.04±1.05, p=0.22). This is not unexpected, as the change in loading due to improved filling should not impact a load-independent measure of contractility. Ea was unchanged at rest, however during sub-maximal exercise Ea was significantly lower in the HRi-test (1.49±0.24 vs. 1.78±0.32 p<.01). Due to the lower Ea, VA coupling ratio improved at sub-maximal exercise in the HRi-test compared to the native test (1.36±0.66 vs. 1.12±0.50 p<.01). Furthermore, mechanical and energetic efficiency, whereas unchanged at rest, improved significantly at sub-maximal exercise from the physiological to the HRi-test (Meff: +6±3%, p<.01 and Eeff: +7±3%, p<.01), see Figure 6.7. The increased Eeff and lower number of heart beats needed to deliver the increased CO at sub-maximal exercise resulted in an improved efficiency of delivering CO, as COeff (the myocardial Mv02 consumption per Liter of generated CO) reduced by 9±4% (p<.01) from the physiological to the HRi-test. Systolic blood pressure at sub-maximal exercise was unchanged between the two tests, despite the higher CO in the HRi-test. This was the result of a fall in SVRi from the physiological to HRi-test (1309±324 vs. 1374±346 dynes•cm^{-5}•m^{2}) that made the vascular system more receptive for the increased CO.

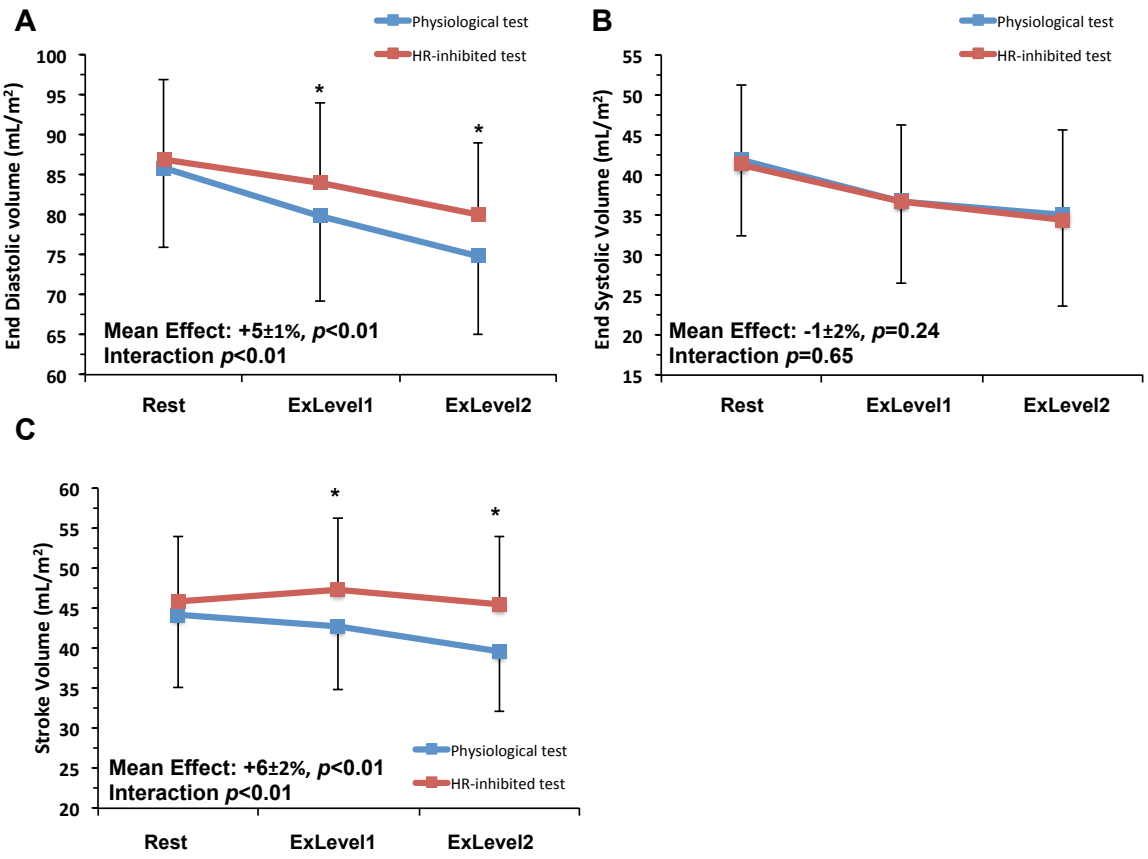

Figure 6.6 Effect of HR inhibition on cardiac function during exercise in Fontan patients. *Blue line* represents physiological test. *Red line* is after administration of ivabradine (HR-inhibited test). All values are means±SD. An asterix means a significant difference before and after ivabradine. A dagger means a significant increase in baseline response from rest – high exercise.

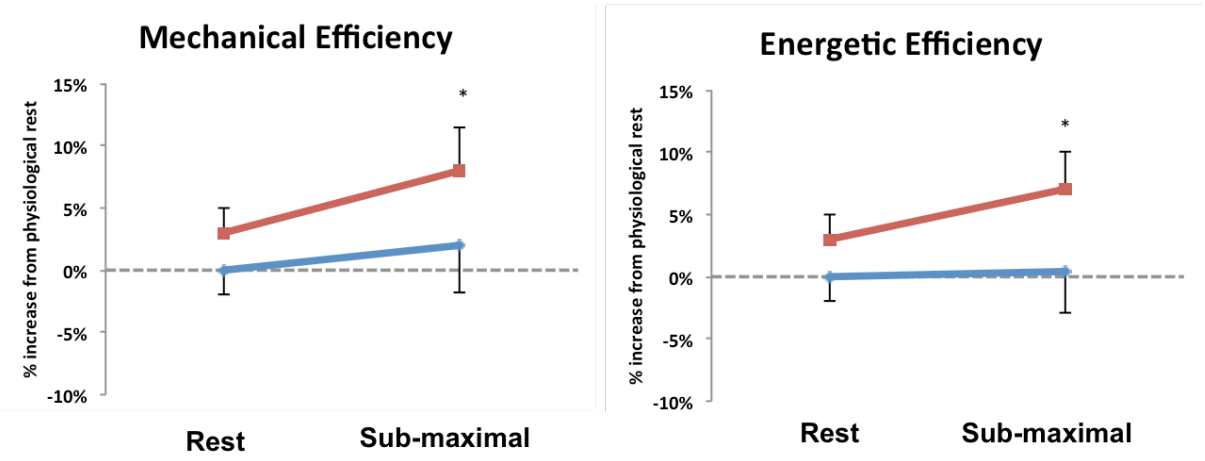

Figure 6.7 Changes in mechanical and Energetic efficiency at rest and during submaximal exercise and after ivabradine (HR-inhibited test) from physiological rest. Means±SD.* denoted *p*-value <.05.

	Fontan Patients			
	Physiological exercise		HR-inhibited exercise	
Exercise Level	Rest	ExLevel2	Rest	ExLevel2
Systolic Blood Pressure, mmHg	116±11	140±8	114±9	137±12
SVRi, Dyne.s.cm-5.m2	2160±390	1374±346	2078±520	1309±324
End-systolic Elastance (Ees), mmHg/mL	1.25±0.41	1.96±0.90	1.28±0.43	2.04±1.05
Effective arterial elastance (Ea), mmHg/mL	1.33±0.36	1.78±0.32	1.25±0.25	1.49±0.24
VA coupling ratio (Ees/Ea)	0.95±0.21	1.12±0.50	1.02±0.24	1.36±0.66
External Work, mmHg.mL	7945±827	8744±1320	8290±861	10005±1538
Mechanical efficiency (EW/PVA), %	0.64±0.05	0.65±0.10	0.65±0.07	0.70±0.10
Energetic Efficiency, %	20±1.6	20±3.0	21±1.9	22±3.0
CO_{MvO2}, Joules MvO2 / Liter CO	70±11	81±11	67±10	74±9

Table 6-3 VA-coupling and ventricular efficiency at rest and during sub-maximal exercise before and after HR-inhibition in patients with Fontan circulation. SVRi; indexed total systemic vascular resistance, VA; ventricular-arterial. A Pink box indicates a significant difference between the physiological and HR-inhibited tests.

6.4 Discussion

In this chapter the role of HR in the pathophysiological cardiac response to exercise was evaluated. The results show that the physiological HR response to exercise is disproportionately high in patients with a Fontan circulation. As the single ventricle circulation lacks an appropriate augmentation of ventricular filling, the HR response to exercise contributes to a fall in SV, resulting in a blunted CO augmentation. Selective inhibition of the HR response partially reverses this fall in SV and hereby improves CO, despite a lower HR. Furthermore, it improves mechanical and energetic efficiency of the ventricle and decreases the estimated oxygen consumption per Liter generated CO. These results present a new insight in physiology of the Fontan circulation and provide a potential novel treatment target for optimizing single-ventricular function.

6.4.1 Abnormal exercise response in Fontan patients

HR is key element of the human physiological response that augments CO in response to stress and exercise [2]. In the biventricular circulation, increasing HR is an effective way to augment CO, as SV is preserved despite a significant fall in diastolic filling time [7, 204]. As shown in the physiological exercise CMR experiments in this chapter, the exercise haemodynamics in Fontan patients are altered, resulting in a sub-optimal effect of the HR response on CO. During exercise, HR increased linearly with exercise in both Fontan patients and healthy volunteers. In healthy volunteers, the increase in HR was accompanied by a similarly large augmentation of mean diastolic LV filling rate. This compensated the shortening of diastole, allowing LV EDV to be maintained. Only at sub-maximal exercise, LV EDV fell mildly. In Fontan patients, the increase in filling rate was much lower. As a result, EDV fell progressively while HR increased. Interestingly, the ESV response during exercise was not significantly different between Fontan patients and healthy volunteers, suggesting that the contractile response of the Fontan cohort was not significantly impaired. However, this ESV response was not enough to compensate for the large drop in EDV, resulting in a progressive fall in SV during exercise. In contrast, SV increased during exercise in the healthy volunteers. As a result the CO response to exercise was significantly blunted during exercise, compared to the linear increase observed in healthy volunteers.

So far, the mechanism behind the falling SV remains incompletely understood. Decreased contractile response and diastolic dysfunction could potentially play a role, however the current accepted view seems to be that the main factor limiting the increase in CO in the Fontan circulation is a lack of sufficient ventricular filling during exercise [19, 72]. This theory was build upon the observation that preload is low in adult Fontan patients during exercise [8] and, in children, during dobutamine stress [191]. However, no comprehensive exercise imaging study has so far confirmed the abnormal ventricular behaviour in relation to the healthy biventricular heart. Moreover, the role of heart rate in this abnormal response has been overlooked. The fall in EDV that we report during exercise is in keeping with the observations by Bruaene et al. [96], who executed a exercise CMR study to investigate the impact of Sildenafil on exercise haemodynamics in Fontan patients. We show that, compared to healthy volunteers, this fall is indeed abnormal and is owed to a lack of augmentation of filling. Interestingly, the ESV response was not significantly different between healthy volunteers and Fontan patients, suggesting that contractile dysfunction did not contributed to the low SV. Indeed, a relatively preserved contractile reserve in Fontan patients has been previously reported by multiple groups [88, 90, 207]. The preserved contractile function during exercise suggests that the single ventricle could potentially generate more SV, were it not limited by sub-optimal filling. Sub-optimal ventricular filling as a result of shortening of diastole, in combination with preserved contractile function, can be a contributing factor in

the previously observed more pronounced adverse impact of HR on ventricular mechanical and energetic efficiency of the single-ventricle compared to healthy volunteers [88, 191].

Contrary our results, Van den Bruaene et al. did not observe a decrease in ESV from rest [96]. However, resting cardiac index in their study was relatively for Fontan patients (4.1 L/min/m^2). This was almost 40% larger than the resting cardiac index in our study and might have influenced further contractile augmentation.

6.4.2 The role of HR in Fontan haemodynamics

In the physiological test, it was observed that a lack in augmentation of ventricular filling limits SV and CO augmentation during exercise. However, whether this is caused by the decreased HR time or intrinsic diastolic dysfunction remains unclear. To investigate the impact of HR on ventricular behaviour during exercise, in its role in ventricular filling and efficiency, we performed a second test under selective HR inhibition using ivabradine.

During the HR-inhibited test, the mean diastolic filling rate of the ventricle was not significantly different from the physiological test, which is contrary to augmentation in diastolic filling rate seen after HR inhibition in the healthy volunteers in Chapter 7. This reflects the relative inability of the single-ventricle circulation to impact ventricular filling during exercise. However, due to the longer duration of diastole, ventricular filling was increased in the HR-inhibited test, as illustrated by the increased EDV response (see Figure 6.5 and Figure 6.6). Moreover, SV increased from the physiological to the HR-inhibited test, leading to a seemingly contradictory increase in CO despite a lower HR.

This series of events induced by HR-inhibition can be interpreted as follows: Firstly, diastolic time is the limiting factor in filling of the ventricle during exercise in this group of Fontan patients. Whereas diastolic dysfunction is frequently reported in Fontan patients, this observation seems to suggest that such dysfunction is either not present or not a limiting factor. Secondly, SV increases with improved filling. This demonstrates that impaired filling and not impaired / inadequate systolic function limits SV augmentation in Fontan patients. Even more, the increase in SV was obtained without an increase in contractility, as shown by the unchanged ESV and Ees responses. This suggests that myocardial contractile function is not well utilized during exercise of the single ventricle circulation due to relative underfilling, an observation also previously suggested by Senzaki et al. [88] and that the improved filling during HR-inhibition allowed the ventricle to make more optimal use of the Frank-Starling forces. Finally, these experiments therefore illustrate that passive filling of the ventricle, in particular diastolic filling time, is pivotal for the delivery of CO in the Fontan circulation.

The inhibition of the HR response resulted in a significant improvement in ventricular efficiency during exercise, as shown in Figure 6.7. The more efficient ventricular contractions, combined with the lower heart rate also significantly reduced the estimated oxygen consumption needed to deliver CO (COeff) during exercise in the HR-inhibited test. At rest, a statistical significant effect was not reached, but there was a strong trend towards improved VA coupling and ventricular energetic efficiency due to HR-inhibition, see Table 6-3 and Figure 6.7. As exercises work of the heart, the changes are more exaggerated, it is likely that in a larger study, powered for studying impact at rest, a positive effect of HR-inhibition might also be present a resting state. The improved ventricular and total efficiency of the heart was the consequence of a range of improvements in the system. Firstly, the increased length of diastole resulted in better filling. This likely improves utilization of the Starling mechanism in the heart and resulting in a larger SV without an increase in contractility, as observed in our HR-inhibited test. Secondly, due to the larger SV, CO is delivered using less beats, reducing the number of times the heart has to overcome aortic pressure (afterload). As volume work is less energy costly than pressure work, oxygen consumption per Liter of CO generate decreases [208, 209]. Thirdly, Ea increased due to the larger SV. This improved VA-coupling. Better coupling of ventricular and arterial elastance results in increased mechanical and energetic efficiency of the ventricle [201, 210]. In total, these factors together are likely to explain the significant decrease of estimated myocardial oxygen consumption per Liter generated CO (-9%). Additionally, although not assessed in this study, the prolongation of diastole in the HR inhibited test provides more time for coronary blood flow and oxygen supply to the myocardium of the single ventricle.

Despite the increase in CO, blood pressure did not significantly change between the physiological and HR inhibited test. This was the result of a fall in SVRi, which matched the increase in CO, see Table 6-3. In Fontan patients, resting and exercise SVRi are high compared to healthy volunteers. This is partly a consequence of the two circulations in series. However, it has also been suggested that the high SVRi, and especially limited drop in SVRi during exercise, is an important secondary mechanism in Fontan patients to ensure adequate systemic pressure, and therefore perfusion and flow through the circulation, in the light of a low CO [19]. We observed that SVRi fell with improving CO. Furthermore, the magnitude of this fall matched the CO increase and therefore left blood pressure unchanged. This suggests that in our cohort of asymptomatic Fontan patients, at least part of the high SVR during exercise can be explained by a deliberate self-regulated response of the body to maintain adequate body organ perfusion pressure in the face of a blunted CO increase. This observation is important in the light of afterload reducing treatment strategies in patients with Fontan circulation. While such strategies have been suggested in the light of the high SVRi [111], our work seems to suggests that it might counteract a useful protective response of the body to low CO. This would explain the unsatisfying clinical results of long-term ACE-

inhibition on functional capacity in Fontan patients [111, 211] and therefore our observations provide further evidence against routine ACE-inhibiting treatments in asymptomatic Fontan patients. These findings are made in a small cohort of TCPC Fontan patients and therefore might not be generalizable to a larger population and across all Fontan patients. However, these results demonstrate that cautious consideration of the potential protective mechanism of increased SVR remains important while determining treatment.

6.4.3 Implications for clinical management

The results of this study demonstrate the importance of HR and filling time in optimization of haemodyanmics of the Fontan circulation. Whereas the concept of limited preload in Fontan patients due to the lack of a sub-pulmonary ventricle has been well described [19, 20, 72, 88], its implications, i.e. the importance of filling time and thus HR, for adequate function of the Fontan circulation has so far been overlooked.

In order to minimize the seemingly inevitable functional decline of patients with Fontan circulation, optimization of cardiac and circulatory function has become a central goal in treatment of Fontan patients. While all patients seem to be affected by declining functional status, there is currently no scientifically backed routine treatment available that effectively prevents or slows down the functional decline. Recently, promising results have been booked with regard to pulmonary vasodilator therapies (PVD). Both in the short and long-term, improvements of functional status have been reported [117, 212–214]. However, it is hard to see such treatment as a routine option in all Fontan patients. Most patients do not have an elevated pulmonary vascular resistance. We have previously shown children with HLHS rarely had an elevated PVR, despite being symptomatic, and that PVD did not improve pulmonary blood flow or filling [98]. In such patient the efficacy of PVD might be questionable. Therefore, the potential side effects and costs of PVD might outweigh potential benefits in asymptomatic patients [114, 115, 117]. Another important consideration is that PVD, especially Sildenafil, can result in a degree of systemic vasodilatation. Careful analysis of the impact of Sildenafil on Fontan haemodynamics in the Exercise CMR study by van Bruaene et al. [96] shows that PVD did not improve blood flow towards the heart or ventricular, filling despite a lower PV, but did result in a significant decrease in SVRi. This drop SVRi was only partly compensated by an increase in HR and lower ESV, resulting in decrease in systemic blood pressure and, more importantly, increased arterial lactate levels and a decreased arteriovenous oxygen difference, suggesting a deterioration of blood flow towards the working muscles. In the light of the self-regulation of SVRi found in our study and the unsuccessful trails of afterload reducing treatments [211] this suggests that one needs to be cautious of the systemic vasodilation effect of Sildenafil. Whereas this in the short-term

increasing CO, which might explain the acute effects in improved functional capacity, in the long term, Sildenafil could potentially an adverse effect on the Fontan haemodynamics.

It is clear from both in vivo experiments [88–90] and computational modelling [77, 88, 89, 91] studies that the single-ventricular circulation is an inefficient pump in which, even at rest, HR adversely affects ventricular efficiency more significantly than in healthy controls [89]. While the absence of a sub-pulmonary ventricle is inherent to the Fontan circulation, HR and filling time can potentially be targeted. As this study showed, selective modulation of HR results in an acute improvement of CO and efficiency of cardiac performance in a group of patients with Fontan circulation during exercise. These findings are only done in a small group of patients, which do not include all the different variants of Fontan modifications. Whether they therefore apply to the general to the principles of single-ventricular haemodynamics in all Fontan patients remains unclear. However this proof-of-concept study seems to suggest that selective HR inhibition could be potentially have a role in optimization of ventricular performance in the Fontan circulation. Selective HR inhibition does not exhibit the negative inotropic effect of beta-blocker treatments. It therefore suits the potential target of treatment in Fontan patients, reducing HR and filling time targets, instead of restraining all facets of cardiac function to minimize metabolic demand (the main target in ischaemic heart disease).

This study was set up to investigate the role of HR in the exercise response of the Fontan circulation and therefore merely assessed the direct effect of HR-inhibition using ivabradine on exercise in a subgroup of patients with TCPC Fontan circulation. To determine the value of selective HR inhibition as a realistic treatment option, randomized controlled trials, designed for this assessment, are needed.

6.4.4 Limitations

Previous studies have highlighted the importance of respiratory and muscle pump in Fontan haemodynamics during exercise [216]. Our methodology did not allow us to investigate the impact of HR-inhibition on these factors separately. However, respiratory correction was used for analysis of cardiac volumes, avoiding the potential confounding of impact of respiration on cardiac volumes between the two tests and between individuals. Non-invasive estimates of VA-coupling were used in this study. The values for V_0 and α were obtained only at one initial stage (physiological rest) to calculate all VA-coupling and efficiency in the other stages. This approach was taken to avoid the impact of errors in estimaton of Ees on the assessed changes in VA-coupling over the stages. V_0 and α are related to inherent myocardial structural properties and have previously been reported to be constant for an individual independent of inotropic or chronotropic drive [197, 199, 201].

Most studies obtaining non-invasive measures of VA coupling disregard V_0, assuming its value is neglectable [217, 218]. However, others have argued a potential change of V_0 during exercise [219]. It was felt that utilizing a single estimate and hereby avoiding an estimation error outweighs the potential adaptions of V_0, especially as only relative changes between two exercise tests within individual subjects were assessed. For calculation of Ees at physiological rest state, systolic time intervals were obtained from high temporal resolution cine imaging (~17ms per frame). Cine CMR uses averaging over multiple beats, which is different than the real time assessment during echocardiography. However, the other parameters included in the calculation, blood pressure and volumes, were also obtained over multiple beats. Furthermore, real time echocardiographic measurements are in essence also averaged, as good practise described taking the mean of at least 3 separate measurements. Altogether, we therefore think the use of high temporal cine CMR did not result in significant errors in measurement of systolic intervals.

Due to the physical constraints of the CMR, the exercise CMRs were performed in a supine position. Therefore the gravitational forces on the body are different to an upright position, most likely influencing the observed cardiovascular function and haemodynamics. It is likely that venous return towards the heart in an upright position is more impaired, potentially further reducing the ventricular filling reserve, in particular in Fontan patients. These results can therefore not directly be extrapolated to an upright position.

Lastly, invasive central aortic pressures were not measured during this study. Therefore, Pes was defined as 0.9 x SBP. This method has often been described and has also been used before during exercise [200] However it is not validated, and might result in an error with increased exercise level. Radial tonometry might have provided a better estimate of Pes, however such methods are not MRI-compatible. Furthermore, as we assessed the relative changes in parameters between two exercise CMRs in individual patients, we felt that most of such error would be systematic and, whereas it most likely impacted the estimated real values, the impact on the relative changes will be small.

6.5 Conclusion

In this chapter, the experiments are described that aimed to investigate the impact of HR on haemodynamics of the Fontan circulation during exercise. The results of this work show that the physiological HR response to exercise is inappropriately high in the Fontan circulation, as the lack of a sub-pulmonary ventricle does not allow ventricular filling to be maintained during increasing HR. As a result, the CO response is blunted and ventricular efficiency deteriorates. Selective inhibition of the HR response improved filling, CO and ultimately

cardiac efficiency during exercise. Selective HR inhibition might be a potential target for optimizing Fontan haemodynamics.

Chapter 7 Computational Modelling of the Dobutamine Stress Response in Fontan Patients

The computational modelling work presented in this chapter was executed in close collaboration with Dr. R. Chabiniok, who developed the model and supervised me during the implementation.

In the previous chapters, several experiments were executed to demonstrate the role of the RV during exercise and impact of its absence on exercise haemodynamics in adult asymptomatic patients with Fontan circulation. These experiments gave a fundamental insight into Fontan physiology and the negative impact of the inappropriately increase in HR during exercise. In this chapter, the focus of explaining (patho)physiology is shifted from the general perspective to a patient-specific approach. The aim of the following set of experiments was to explore the added value of a closed loop heart-circulation biomechanical modelling framework for diagnostic assessment of the stress response in patients with Fontan circulation and symptoms of progressive exercise intolerance.

7.1 Introduction

As discussed in Section 2.2, the Fontan circulation is burdened by a progressive decline in cardiac function resulting in a high incidence of heart failure. Unfortunately, the mechanism of failure in individual patients is often hard to detect. Routine diagnostic investigations used in cardiology clinics, such as echocardiography or cardiac magnetic resonance imaging (CMR) are frequently unable to identify the cause of failure. As a result, determining effective treatment is challenging. Exercise intolerance is a relatively common early symptom of the failure of the single ventricle. In several specialized clinics, simultaneous cardiac

catheterization and CMR (XMR) at rest and during pharmacological stress is used to simulate an exercise response in order to better understand causes of failure in Fontan patients. Rich datasets of combined pressure, flow and ventricular volume measurements are obtained during these exams. However, the complex physiology of Fontan circulation and large inter-individual variations make it difficult to obtain direct conclusions from these investigations.

7.1.1 Modelling Fontan Physiology

Biophysical modelling has in recent years advanced into clinical applications by assisting diagnosis [21] and therapy planning [220, 221] in non-congenital heart disease patients, see also a recent review by Chabiniok et al. [24] and references therein. It allows for integration of various data-modalities into a single framework. As opposed to image or signal analysis, the physical and physiological principles of these models have the potential to assess the tissue properties of the heart and vascular system – quantities not directly measurable from the image and pressure data but accessible via constitutive relations and equilibrium equations. Such modelling techniques have also been previously applied to investigate Fontan physiology. Most work so far has focused on predictions of flow characteristics in the total cavo-pulmonary connection (TCPC) and the impact of geometrical shapes of the surgically created TCPC on blood flow through the system [222]. Recently, several authors investigated overall circulatory function of Fontan circulation using lumped parameter networks resembling the single ventricular circulation. Kung et al. used a closed loop lumped parameter network of the Fontan circulation during exercise to investigate exercise intolerance in patients with Fontan circulation [22]. Their proposed model was tuned based on population trends and available clinical data during model development. By adapting only a few input parameters of their predefined model based on individual patient characteristics (HR and exercise capacity), this method allowed insight in disease processes, however it lacks the detailed patient specific input that would be needed to predict absolute output parameters. Puelz et al. recently used a similar closed loop circulation to study the impact of anatomical variations of the Fontan circulation in general, without considering specific patients [23]. While useful in assessment of general characteristic of the Fontan circulation in individual patients, these models lack the detail to assess patient-specific causes of failure or guide treatment decisions.

7.1.2 Aims of this work

The goal of this work was to develop a patient-specific modelling framework to augment the diagnostic value of the XMR dobutamine stress studies. Integrating XMR data (flow, pressure, ventricular behaviour and vascular function) into a closed looped computational model of the heart and circulation allows access to key clinical parameters of cardiovascular function (such as myocardial stiffness, contractility and venous return) in individual patients. This potentially aids the identification of the pathophysiological mechanisms underlying heart failure in individual patients. In this work, the value of using such computational models in diagnostic assessment of XMR dobutamine stress exams was evaluated. Additionally, the potential use of the calibrated models for investigating the impact of therapeutic interventions was explored.

The heart model employed was a reduced-dimensional (0D) biomechanical model detailed in previous work [223, 224]. In order to interpret the acquired XMR data in varying physiological conditions in a relatively short time (or possibly nearly real time), the actual 3D anatomy of patients' ventricles was reduced into a sphere together with a complete reduction of biophysical model as described in Caruel et al. [225]. While the geometry and kinematics of the heart were simplified, all the constitutive relations were preserved, i.e. the model used is a full biophysical model. The principal unknowns of the reduced model are therefore the displacement of the ‘spherical ventricle’ in the radial direction (capturing the variations of ventricular volume and systolic wall thickening during the cardiac cycle) and pressure in the ventricular cavity.

The continuum mechanics based model of the ventricle was connected to a Windkessel-type model of circulation to obtain arterial characteristics (peripheral and distal resistance and capacitance). A closed loop circulation was created by modelling the venous return flow to the systemic ventricle according to a venous return law that was linearly proportional to the distal venous and atrial pressure. This venous return law, that assumes an equilibrium between the cardiac output and venous return, is a generally accepted concept used in cardiovascular physiology [178] and was put into the modelling context in previous work by Chabiniok et al. [221]. This closed loop circulation of the cardiac, arterial and venous systems creates a representation of the patient's cardiovascular system suitable for the analysis of inotropic and chronotropic changes, i.e. changes in myocardial contractility and heart rate. This therefore allows investigation of stress and exercising responses using the model. See Figure 7.1 for a schematic representation of the coupled heart-Windkessel circulation and venous return model.

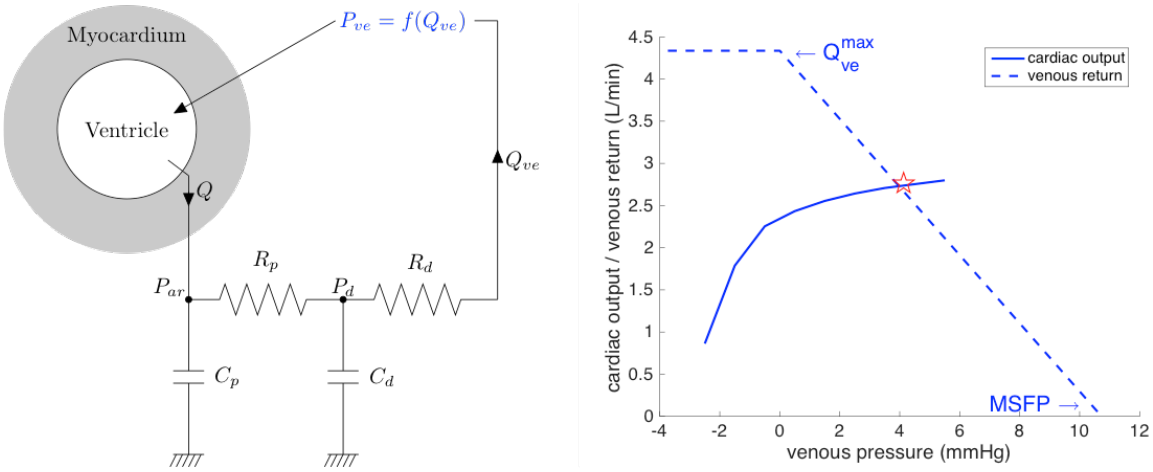

Figure 7.1 Left: Scheme of 0D heart model connected with a 2-stage Windkessel model (R_p, C_p, R_d, C_d stand for proximal and distal resistances and capacitances, P_{ar} and P_d stand for proximal aortic, distal circulation pressure). Right: Closing of the heart-circulation circuit by a linear venous return law defining the preload of systemic ventricle according to the cardiac output (MSFP stands for mean systemic filling pressure and $Q_{ve\text{-}max}$ for maximum achievable venous flow).

In this chapter, the type of data acquired during the XMR procedure and the model used are first presented in Sections 7.2.1 and Section 7.2.2. Next, the step-wise method for calibration of the model using the obtained patient data is discussed in Section 7.2.3. After this, it is demonstrated in Section 7.3.1 that the proposed modelling framework successfully represents the cardiovascular system of Fontan patients at rest and provides physiological parameters related to the properties of myocardial tissue, hereby translating the image and pressure data into functional properties of myocardium, such as passive tissue stiffness and active contractility. Next, the performance of the modelling framework in improving diagnostic assessment of exercise intolerance in individual patients during the dobutamine stress XMR are presented in Section 7.3.2. Finally, the potential predictive value of the model for investigating the impact of a therapeutic intervention (heart rate inhibition) was explored in one of the cases in Section 7.3.3 and the obtained results are discussed in Section 7.4.

7.2 Methods

7.2.1 Acquired Data

Five patients with Fontan circulation that underwent a clinically indicated XMR dobutamine stress exam for progressive symptoms of exercise intolerance were included in this study. In

all patients, the underlying congenital heart defect was hypoplastic left heart syndrome. Additionally, two 'controls' with a biventricular heart and normal circulation were studied to compare the model estimates in Fontan patients to model predictions in a biventricular heart. These control patients had Allagile's syndrome and mild branch pulmonary artery stenosis and underwent an XMR dobutamine stress study for risk assessment prior liver transplantation [226]. One of the cases (control 2) had a clinically unremarkable cardiovascular response to dobutamine ('good stress response') whereas the other (control 1) had an impaired stress response, which was indicated by an insufficient increase in cardiac output (<30% increase from rest).

During the XMR exams, pressure signals (aortic, ventricle, venae cavae, and pulmonary capillary wedge pressures) were obtained at rest, and under continuous infusion of dobutamine 10 mcg/kg/min (dob10) and 20 mcg/kg/min (dob20) mimicking moderate and strenuous exercise stress, respectively. Simultaneously, CMR imaging data was recorded, consisting of a stack of ventricular volumes throughout the cardiac cycle and 2D flow data (ascending aorta, descending aorta, venae cavae, and branch pulmonary arteries). The obtained CMR data were post-processed into 0D signals of time-versus-flow or time-versus-ventricle volume, and these signals were temporally aligned with the time-vs-pressure, see Figure 7.2.

This study was performed under the ethical approval of our regional research ethics committee (Ethics Number 09H0804062) and all participating patients (or their parents) gave written consent for participation in the study.

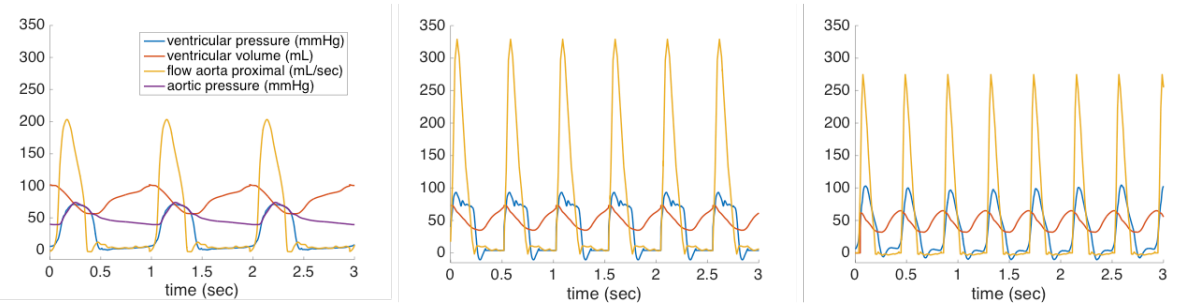

Figure 7.2 Data of Fontan patient 1 acquired at rest (left) and during low- and high-dose dobutamine infusion (center and right).

7.2.2 Biomechanical model

The reduced order heart model used in this work was in detail described in [225]. The main ingredients of the model are described below.

The passive part of myocardium is modelled by an exponential law inspired by Holzapfel et al. [227] as a hyperelastic material, while taking into account anisotropy given by the direction of the myocardial fibres. The ventricular volume at reference configuration V_0 (the volume of the ventricle at zero pressure) was assumed to correspond to 50% of the end diastolic volume (EDV) at rest, which is close to values described in previous experimental studies in hearts with a wide range of geometries (both normal and dilated) [228]. Using V_0, EDV and preload, the end-diastolic pressure volume relationship (EDPVR) was obtained according to the experimentally defined single-beat method of Klotz et al. [228].

The active component of the heart was modelled by a system of ordinary differential equations representing chemically controlled actin-myosin interactions – formation of cross-bridges – generating active stress and active stiffness in each sarcomere at a certain sarcomere length [224]. The symptomatic active stress, σ_0, generated by the sarcomere is in related to myocardial contractility. Contractility was modeled to be dependent on actin-myosin overlap (sarcomere length) based on the Frank-Starling law, as shown in Figure 7.3 (left panel). Activation of the cardiac myocytes was modeled by an activation function based on ECG signals, see Figure 7.3 (right panel).

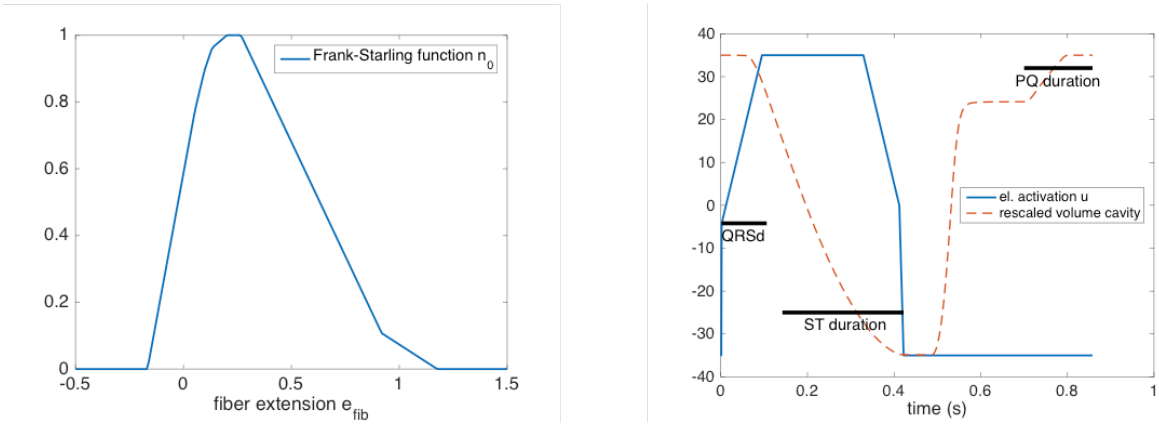

Figure 7.3 Left: Frank-Starling function n_0. Right: Profile of the electrical activation function u with a rescaled ventricular volume plot. The measured durations of QRS, PQ and ST segments of ECG at rest are used to impose timings for the electrical activation function and for the atrial contraction.

The peripheral circulation receiving flow (Q) from the heart was modeled using a 2-stage Windkessel model (see schematics in Figure 7.1). The proximal part of the circulation (aorta and large arteries) was represented by a proximal capacitance and resistance (C_p and R_p). The peripheral circulation was represented by a distal resistance and capacitance (R_d and C_d).

The final modeling ingredient – the venous system – provides the preload to the systemic ventricle, closing the cardiovascular circuit. The venous return is governed by the physiological state of the circulatory system and cardiac output. The relationship between distal venous pressure P_{vs} and venous return flow Q_{ve} has previously been described by Chabiniok et al. [229]. This model of venous return is based on Guyton's law [178]. This law describes that cardiac output is a function of venous return, which itself can be modeled as a linear relationship between P_{vs} and venous flow, see Figure 7.1. The x-axis intersect of the venous law represents the pressure at zero flow, the so-called *mean systemic filling pressure* (MSFP), while the maximum venous return flow $Q_{ve\text{-}max}$ is reached at a venous pressure of 0 mmHg, with no further increase at lower venous pressure due to collapse of the large veins [178].

7.2.3 Model calibration

The biomechanical model was calibrated following a fixed step-by-step protocol that minimizes the chance of a non-unique set of parameters describing the data.

First, the geometrical relations of the 0D model (the ventricular volume and myocardial mass) were prescribed based on the MRI derived values for EDV and ventricular mass. After this, each component of the full heart-circulation was calibrated as described below:

1) Windkessel calibration: the Windkessel model was decoupled from the heart and MR derived aortic flow was directly imposed into the system. Resistances and capacitances were adjusted to match the aortic pressure waveform in the data. The distal properties, R_d and C_d, were calibrated to obtain the height of the dicrotic notch and the time constant of the diastolic pressure decay. The proximal part was then tuned to obtain peak systolic pressure. Figure 7.4 shows the result of calibration in a patient with excellent agreement of the simulated aortic pressure in the proposed Windkessel system with the data. The parameters of the Windkessel model were then fixed for the rest of the study (both at rest and during dobutamine stress). Whereas dobutamine might have an effect on the peripheral resistance [132] we did not have aortic pressure data during the dobutamine stress stages of the CMR study, as the pressure catheter was left in the ventricle.

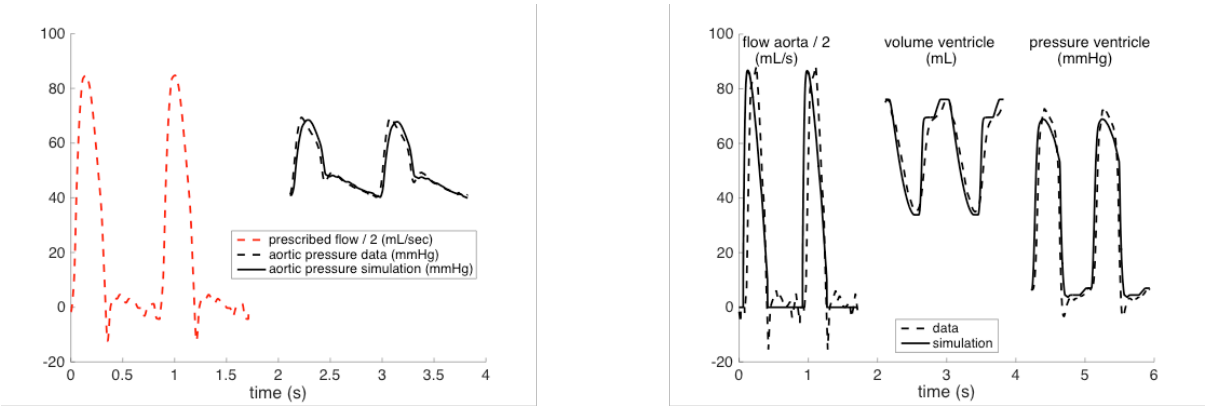

Figure 7.4 Calibration of the Windkessel model (left), and of the heart model at rest with prescribed level of preload (right).

2) Calibration of the passive component of the heart: The passive tissue properties of the myocardium in the heart model were adjusted based on end-diastolic pressure and volume data. End diastolic pressure was imposed onto the ventricle and the hyperelastic potential of the ventricular model was adjusted by multiplying the linear stiffness coefficients C_1 and C_2 by a 'relative stiffness' parameter to obtain the right end-diastolic volume. This relative stiffness parameter was based on Klotz et al. [228] and allows comparison of stiffness values between patients (see Table 7-2).

3) Calibration of the active component of the heart: Active calibration consisted of adjustment of electrical activation and myocardial contractility, σ_0. In this step, the heart model is connected to the previously calibrated Windkessel system while imposing preload as measured at end-diastole. The activation function *u* is calibrated based on the QRS and ST durations measured from the ECG at rest. Likewise, the atrio-ventricular activation delay in the model was adjusted according to the PQ-interval, see Figure 7.3(right panel) for the profile of the activation function. After obtaining the personalised activation function, contractility at rest was adjusted to reach the same SV and aortic flow as observed in the data. Figure 7.4 demonstrates the results of calibration steps 1-3 in a patient, showing excellent agreement between the heart model and the data.

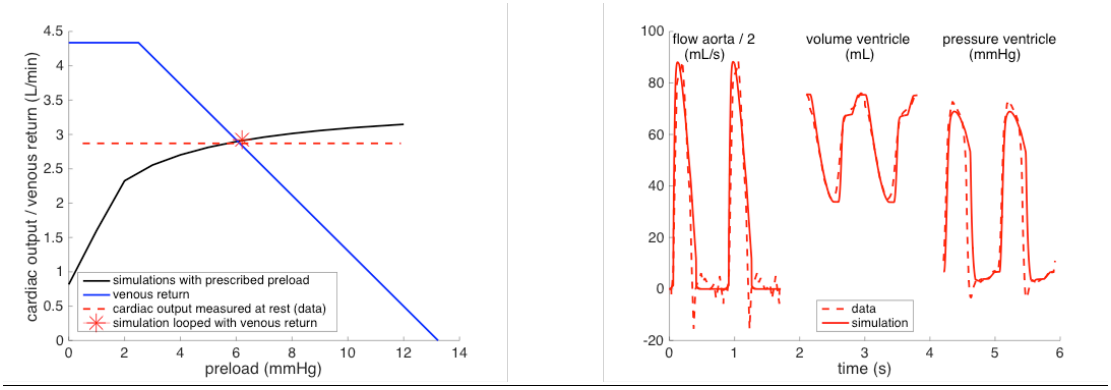

Figure 7.5 The complete heart model looped with venous return calibrated at rest.

4) Venous return calibration: The last step of the calibration of the close loop heart-circulation model and consists of identifying the parameters of the effective volume V_{eff} and capacitance C_{vs} of the venous system. The linear venous return law can be uniquely parameterized using the working point of the heart at rest (intersection of the measured preload and cardiac output) marked by the rest star in Figure 7.1 and the assumption that maximum venous return $Q_{ve\text{-}max}$ is 150% of cardiac output at rest. This assumption lead in all cases to a mean systemic filling pressure between 10-20 mmHg, values which are physiologically to be expected [178].

Patient #	Age (years)	EDV (mL)	EF %	ventricle mass (g)	contractility (kPa)	relat. passive stiffness	preload (mmHg)
1	7	103	44	49	70	1.1	7.0
2	4	58	42	27	77	0.9	5.5
3	10	76	46	38	70	1.1	7.0
4	10	71	44	39	73	1.3	10.0
5	12	82	52	34	65	0.9	8.5
Control 1	4	44	73	42	85	1.1	11
Control 2	1.5	20	59	21	65	1.3	15

Table 7-1 Measured indicators and parameters of calibrated models at rest.

7.3 Experiments and Results

7.3.1 Coupled heart-circulation model at rest

By following the calibration process described in section 7.2.3 models of the rest state were set up for all the cases. Table 7-1 shows the main model output parameters in all patients. Notably, contractility at rest seems to be equal in Fontan patients compared to the healthy

control case 2, whereas the clinically used, load-dependent parameter, EF, suggested impairment of systolic function in all Fontan patients. The preload measured at rest was higher in the two control cases than in any of the Fontan patients Figure 7.5 illustrates an excellent level of accuracy of the closed-loop heart-circulation model calibrated at rest conditions with respect to measured data.

7.3.2 Coupled heart-circulaton model under dobutamine stress

After calibration at rest, the effects of dobutamine stress were introduced into the model to obtain the stress states observed in the data. First, the chronotropic effect was accounted for. We adjusted the cardiac cycle duration according the heart rate at dob10. As the ECG device was not MR compatible, a detailed ECG was only available at rest. While we assumed PQ and QRS durations did not change significantly from rest, the ST interval is known to shorten with increasing heart rates [230]. Therefore, the ST interval was adjusted in order for the simulated pressure waveform to match the one observed in the catheter data. The purple plot in Figure 7.6 demonstrates the prediction of the model at dob10 after only adjusting the chronotropic effect (heart rate and ST segment duration). As can be seen, such a hypothetical scenario would not lead to an actual increase of cardiac output, and the maximum systolic pressure and maximum aortic flow would be much below the measured values at dob10 stress. By adding the inotropic effect into model – by increasing contractility with a factor of 1.75 in this particular case – the simulation reached the level of cardiac output observed in the data (blue plots in Figure 7.6). Note that the simulation did not capture the high pressure spike in the data at dob10 (blue dashed line). Review of the pressure traces revealed a typical pattern of overshooting resulting in overestimation of the peak systolic pressure and the model-predicted pressure might actually be closer to the real value.

Figure 7.7 demonstrates the result of model calibration for both low and high level of dobutamine stress in an example Fontan patient. This well matched calibration was achieved by adjusting the cycle duration and ST interval (chronotropic effects), and tissue contractility (by a factor of 1.75, and 2.75, for low and high dobutamine levels, respectively) without any adjustments of the venous return law, which was kept identical to the rest state (black line in panel A of Figure 7.7). A direct interpretation of this result is that in this individual patient the myocardial contractile reserve appears to be good. However, venous return augmentation seems to be limited and negatively impacts filling and stroke volume of the ventricle during higher heart rates and inotropic activation.

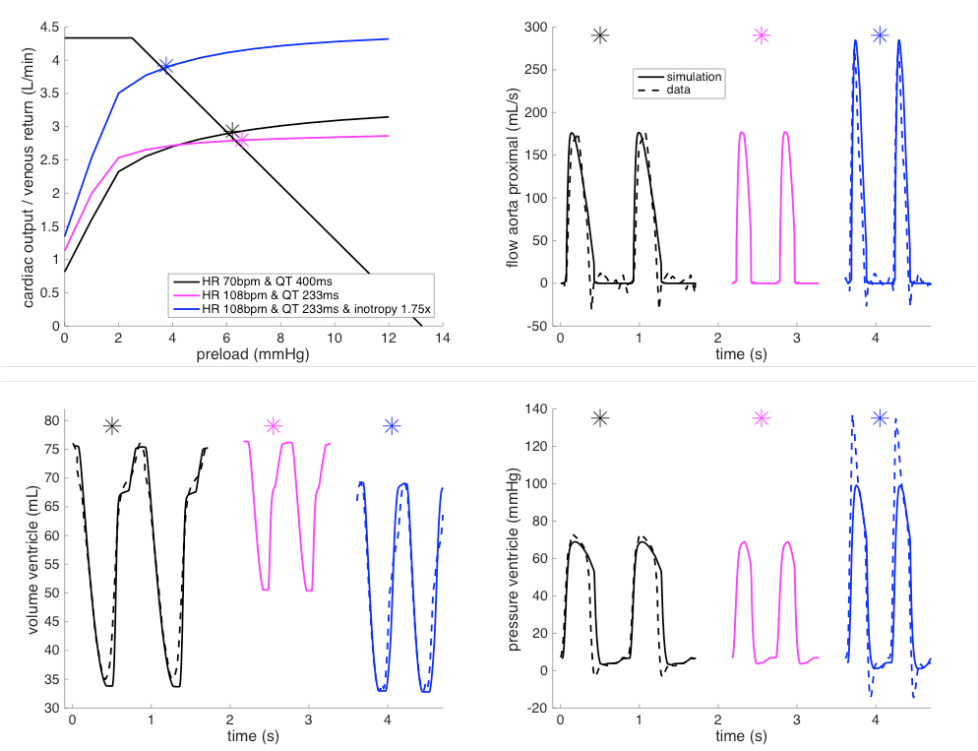

Figure 7.6 The full heart-circulation model for Fontan patient 3 calibrated at rest (black) and the predicted chronotropic effect for heart rate as during low-dose dobutamine stress (purple). The additional inotropic effect (blue) brings the simulation close to the data. The asterisks represent the cardiac output-venous return equilibrium points of the closed-loop system.

The assumption of a fixed venous return law from rest to dobutamine stress was valid for all Fontan cases, except for patients 2 and 4. In these cases, a fixed venous return law resulted in a lower end-diastolic volume and preload than observed in the clinical data. As demonstrated in Figure 7.7 for patient 2 and 4, the venous return law therefore had to be adapted (a right and upward shift of the venous return relationship) to match the behaviour observed in the data. Both these patients had a patent fenestration (a shunt between the systemic venous system and common atrium that allows a portion of the blood to bypass the pulmonary circulation and therefore improve preload). The model accurately predicted the existence of such a boost in preload, and it is clear that during stress this leads to an improvement in venous return to the heart due to the increase in venous pressures. The change in venous return in the cases with fenestration are in keeping with the pattern seen the biventricular control cases as illustrated in Figure 7.10, suggesting augmentation of venous return, which is normally seen to an even larger extend in the healthy biventricular heart during exercise [178].

Table 7-2 summarizes the adaptions in model parameter estimates needed to match the obtained clinical data of the dobutamine stress exam. All the patients were able to increase the contractility by factor 2-3, except for control 1. Control 1 had a higher contractility at rest compared to the others and only increased contractility during dobutamine by a factor of 1.5.

As shown in Table 7-3, the changes in *Dp/Dt* from rest, a surrogate measure of changes in contractility, showed similar behaviour as the predicted contractility changes in the model. Augmentation of venous return during dobutamine stress was present in both control cases and the two Fontan patients with a patent fenestration, while in Fontan patients~1, 3 and 5 venous return was fixed.

Altogether, these results suggest that our model was able to characterise the different components of the dobutamine stress response in individual patients, allowing patient-specific investigation of the factors causing an impaired stress response.

Patient #	contractility at rest σ_0^{rest} (kPa)	σ_0 at low dobutamine stress	σ_0 at high dobutamine stress	Q_{max}^{ve} increase at stress (%)
1	70	2.0 x σ_0^{rest}	2.5 x σ_0^{rest}	0
2	77	2.0 x σ_0^{rest}	2.5 x σ_0^{rest}	30
3	70	1.75 x σ_0^{rest}	2.75 x σ_0^{rest}	0
4	73	3.25 x σ_0^{rest}	data not available	20
5	65	2.25 x σ_0^{rest}	2.75 x σ_0^{rest}	0
Control 1	85	1.4 x σ_0^{rest}	1.5 x σ_0^{rest}	25
Control 2	65	2.5 x σ_0^{rest}	2.5 x σ_0^{rest}	50

Table 7-2 Summary of the changes in cardiovascular systems in patients and controls during dobutamine stress.

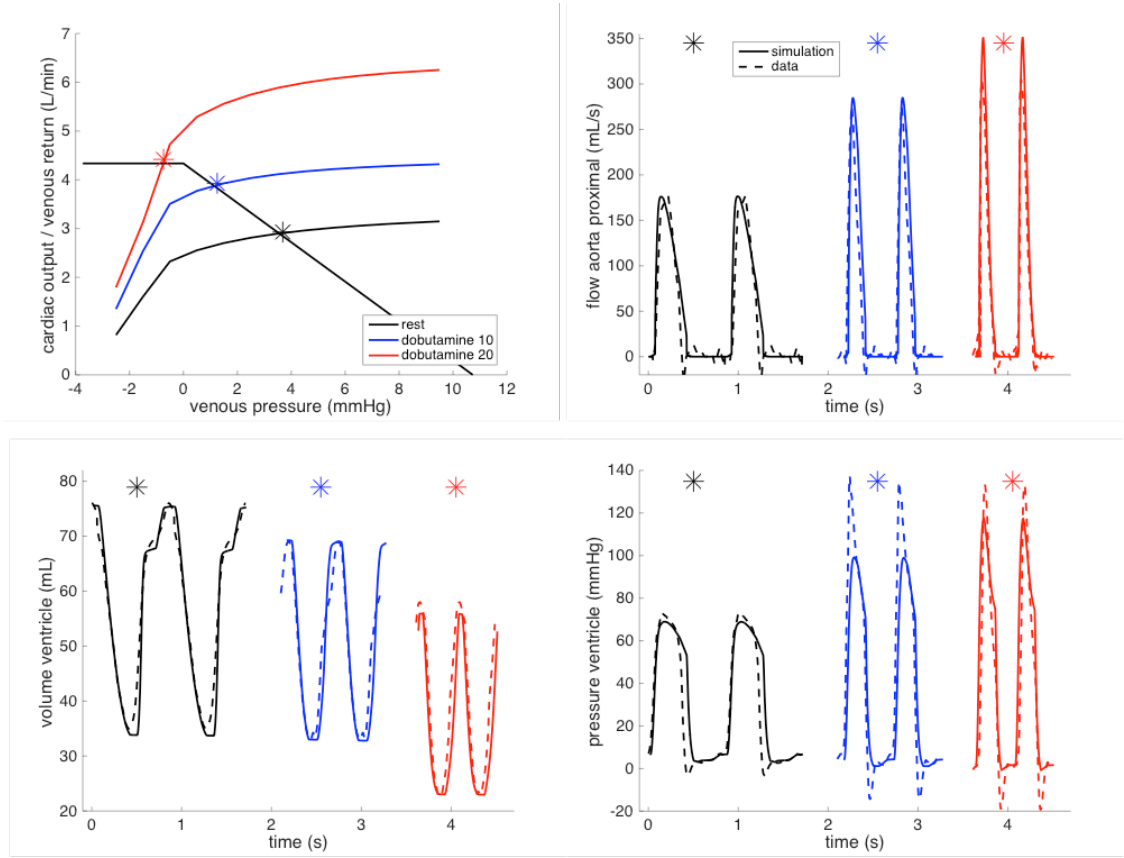

Figure 7.7 Simulations for Fontan Patient 3 at rest and during two levels of dobutamine stress: low (dobutamine 10 mcg/kg/min, blue) and high (dobutamine 20 mcg/kg/min, red). The asterisks represent the cardiac output-venous return equilibrium points of the closed-loop system.

7.3.3 Prediction for therapeutic intervention: heart rate inhibition

In patients~1,3 and 5 our model estimates suggest that the dobutamine exercise response was limited due to a lack in augmentation of venous return, while the contractile reserve seemed to be unaffected. An inability to augment venous return significantly impacts ventricular filling and subsequently SV and CO during increases in HR. As became clear from the previous chapter, Chapter 6, selective inhibition of the heart rate response can improve haemodynamics of the Fontan circulation. Therefore, the potential of the model to reflect the impact of this therapeutical intervention was explored.

The patient-specific calibrated model of patient 3 was used to investigated the impact of HR modulation in the setting of a fixed venous return law at each observed stress stage. A closed loop simulation was run with varying heart rates for multiple levels of inotropy (rest, dob10, dob 20 and two levels in-between). From each simulation, the model's predicted end-diastolic volume, SV and CO was obtained and these values were plotted against HR. The results are shown in Figure 7.8. Each colour represents one ``iso-inotrope'' curve – a set of simulations at a given contractility level differing only in chronotropy (heart rate and duration of ST; linearly interpolated between the values at rest, low and high level of dobutamine). The asterisks represents the measured data at rest, dob10 and dob 20 (recall Figure 7.7).

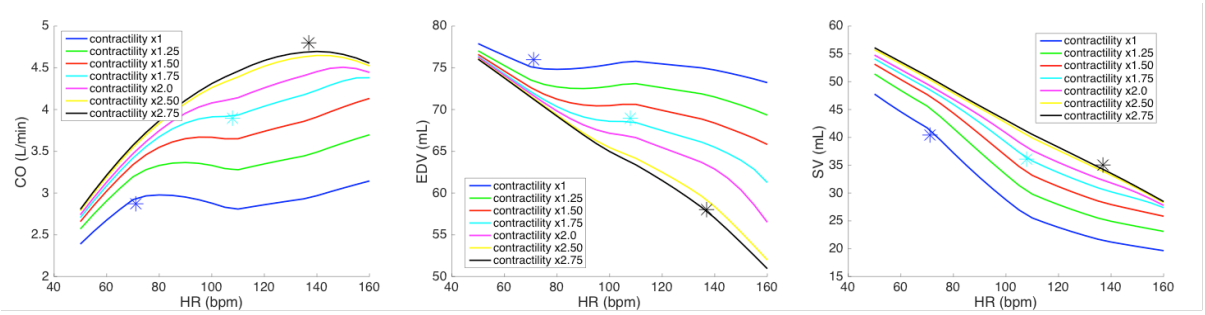

Figure 7.8 Functional indicators of cardiac output (CO), end-diastolic volume (EDV) and stroke volume (SV) for simulated cardiac cycles with heart rates varying between 50 and 160bpm (x-axis) for inotropic states increasing from the level of contractility at rest (dark blue). The asterisks (*) shows the actually measured data at rest, low and high dose of dobutamine.

As explained in the previous chapters and control cases 1 and 2, CO and HR are linearly related in the healthy heart during exercise, as SV is maintained due to augmentation of LV filling by the RV. This relation was not linear for Fontan patient 3 during dobutamine stress. As shown in the left panel of Figure 7.8 the contribution of heart rate to CO is limited above

100-110 bpm, as can be appreciated by the decrease in slope CO curves after this heart rate. In the middle and right panel of the figure it is shown that this is the result of a significant decrease in end-diastolic filling and stroke volume with increasing HR. From these plots, it can be appreciated that at the two stress stages (light and dark blue star for dob10 and dob20 respectively) a 10% decrease in the heart rate would not significantly impact CO, as filling of the ventricle is better with a lower heart rate.

These simulations suggest that for both dob10 and dob20, at heart works at a point (asterisks) where the CO – HR relationship is very flat, as a result of the increasing fall in EDV and SV with HR. Based on this, a hypothetical decrease in HR by ~10%, the postulated effect of selective HR-inhibition, would lead to an improvement in EDV and SV, while not resulting in a significant fall in CO.

Patient #	DpDt at rest (mmHg/msec)	DpDt at low dobutamine stress	DpDt at high dobutamine stress
1	1743	2.5 x $DpDt^{rest}$	2.5 x $DpDt^{rest}$
2	1817	2.7 x $DpDt^{rest}$	3.0 x $DpDt^{rest}$
3	1893	1.75 x $DpDt^{rest}$	2.75 x $DpDt^{rest}$
4	1763	3.25 x $DpDt^{rest}$	data not available
5	1610	3.6 x $DpDt^{rest}$	3.8 x $DpDt^{rest}$
Control 1	2500	1.5 x $DpDt^{rest}$	1.6 x $DpDt^{rest}$
Control 2	1960	2.5 x $DpDt^{rest}$	2.8 x $DpDt^{rest}$

Table 7-3 Summary of peak ventricular pressure increase (Dp/Dt, mmHg/msec) from rest in Fontan patients and controls during dobutamine stress.

7.4 Discussion

In this study, the applicability of the 0D reduced model [225] looped with venous return [221] was demonstrated for investigation of cardiovascular haemodynamics at rest and during dobutamine stress in patients with Fontan circulation. We showed that employing this modelling technique improves the interpretation of XMR dobutamine stress exams by allowing evaluation of the impact of key components of the cardiovascular system on the dobutamine stress response.

Firstly, the model with prescribed preload was used to characterize stiffness and contractile state of the single ventricle at rest in each individual patient. Such quantities are normally not

directly accessible from the clinical data. The modelling results showed that in all Fontan patients, the contractile state at rest was comparable to the measurements in the two control cases and was not lower than values for healthy myocardium obtained from the literature [231]. This is clinically relevant as the conventional MRI derived measures of systolic function, EF, suggested a decreased systolic function in the Fontan cases, see Table 7-1. EF is load- and geometry-dependent and it is widely known that it does not accurately reflect systolic function in patients with Fontan circulation. The modelling results might even suggest an increased contractility in these young Fontan patients. Contractility values were similar to the control case 1, an Allagile's patient. Patients with Allagile's are likely to be in a mildly excited contractile state as a consequence of the hyperdynamic circulation that accompanies their liver disease [226]. This is reflected by the high cardiac index at rest in the control cases (control 1: CI 5.5 L/min/m^2, control 2: CI 4.1 L/min/m^2), in particularly in control case 1, who had a high contractile state at rest, see Table 7-2 and Table 7-3. This could mean that the Fontan patients, as a consequence of ventricular dilatation, low myocardial mass and the abnormal circulation, require larger levels of contractility to maintain cardiac output. Whereas the study population is too small to be certain, this would be in keeping with previous observations by Saiki et al. [89] and Szabo et al. [232], who showed that contractility in the Fontan circulation is increased to match the higher afterload.

Using the closed-loop model, it was also possible to investigate the response to dobutamine stress in individual patients. By evaluating the parameter changes from baseline, the individual components that make up this response – such as the heart rate, contractile reserve and venous return augmentation – could be evaluated. We showed a good contractile reserve in all Fontan patients. During exercise contractility increased 2-3 fold, similar to the reserve observed in the control case (control 2). This increase was also in keeping with the changes in Dp/Dt and estimates of ventricular elastance obtained using pressure-volume loops in the same cohort in a previous study [191]. This was again contrary to the clinical data that suggested a reduced systolic reserve. The model was also able to detect abnormalities in contractile response. It marked a blunted contractile response observed in control 1, whom clinically was suggested to be already in a high cardiac output state at rest, and identify the oversensitive response to dobutamine in patient 4. In the latter, a clinical over-reactivity for dobutamine was observed, with a large increase in heart rate and blood pressure at dob10 (systolic blood pressure rose to 180mmHg), resulting in abortion of the XMR exam. Altogether, these results suggest that the closed-loop reduced order model is able to accurately estimate contractility and contractile reserve using data obtained from clinical examinations, providing additional diagnostic information to the exam.

Using the closed-loop simulations of the dobutamine stress response, it was also possible to investigate changes in venous return. As discussed in Chapter 5 and Chapter 6, the lack of a sub-pulmonary ventricle is likely to reduce augmentation of venous return, affecting ventricular filling and thus CO [72]. In the biventricular case with a good dobutamine response (control 2), venous return increased by ~50% during exercise. However, in Fontan patients 1, 3 and 5 the venous return was completely fixed. Only in Fontan patients 2 and 4 venous return was mildly augmented. These patients had a patent fenestration, that allowing blood to bypass the pulmonary circulation and flow directly towards the atrium. Using the models, it is possible to investigate the impact of venous return on the individual patients. Figure 7.9 shows a summary of the calibrated model of patient 3. As can be observed, the fixed venous return (black line upper panel) results in a significant fall in EDV and SV during dobutamine (lower panel; volume curves), as the CO line moves towards lower preload. On the other hand, Figure 7.10 shows that in control case 2, venous return was augmented during dobutamine (upper panel black to blue and red line) and preload was maintained resulting in preserved EDV, higher SV and a larger increase in CO.

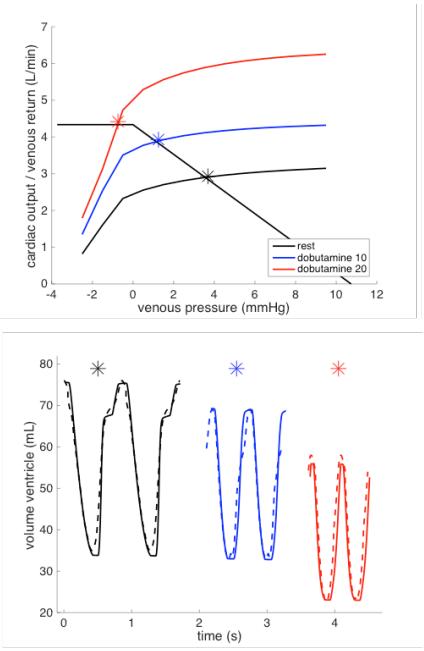

Figure 7.9 Simulations for Fontan Patient 3 at rest and (black) during two levels of dobutamine stress: low (dobutamine 10 mcg/kg/min, blue) and high (dobutamine 20 mcg/kg/min, red). Note the fall in ventricular volume during dobutamine stress (lower right) due to the fixed venous return (upper right).

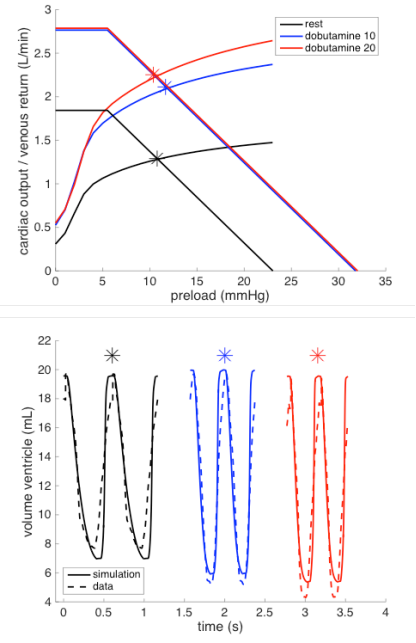

Figure 7.10 Simulations for Control2 at rest (black) and during dobutamine stress: low (dobutamine 10 mcg/kg/min, blue) and high (dobutamine 20 mcg/kg/min, red). Note the upward shift in the venous return curve that maintains EDV and significantly improves the ability to augment CO.

Figure 7.11 shows the model results for Fontan patient 2, with a patent fenestration. This figure shows that if, hypothetically, venous return would have been fixed (e.g. fenestration

closed; purple curves) preload during dobutamine would have significantly fallen, resulting in a decrease in EDV and a lower CO. However due to the augmented venous return through the fenestration, preload was maintained during dobutamine in the actual patient and EDV, SV and CO were higher.

Together, these examples illustrate that the patient-specific analysis venous return using the model can help guiding potential therapies in Fontan patients, such as enlargement or closure of a fenestration (or other shunts such as veno-venous collaterals). The impact of desaturation of the systemic blood due to mixing of deoxygenated and oxygenated blood should also be taken into account for such decisions. Integration of this information into the model using oxygen saturation levels is an aim of future work.

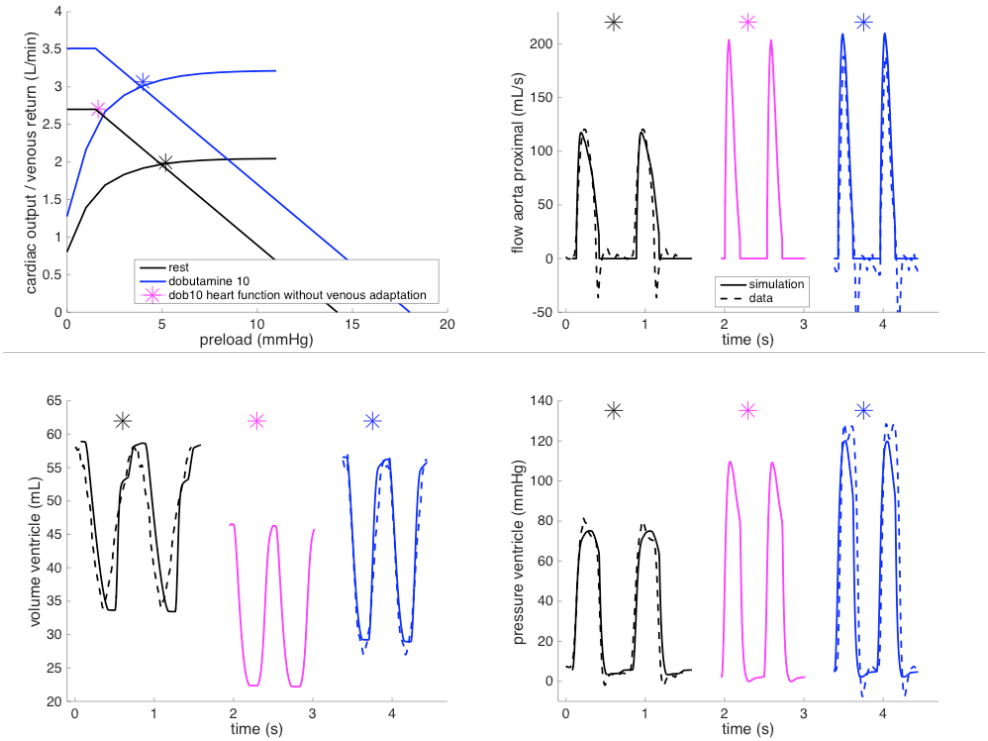

Figure 7.11 Cardiac output curves of Patient 2 at rest (black) and during low dobutamine stress (blue) with the cardiac output-venous return equilibrium points of the closed-loop system marked by asterisks – purple for the cardiac output at stress and the venous return kept as at rest, and blue allowing an increase of venous return during dobutamine stress.

Using the personalized model of Fontan patient ~3, it was shown that this modelling framework simulations potentially allows exploration of treatment effects in individual patients *in-silico* in Fontan. These simulations suggested that a hypothetical decrease in HR

by ~10% would lead to an improvement in EDV and SV, while not resulting in a significant fall in CO. These results are in keeping with the in vivo results of HR-inhibition seen in our adult cohort of asymptomatic Fontan patients, described in Chapter 6. This shows that our modelling framework is able to grossly predict the impact of treatment. Ofcourse, such treatment simulations are only estimates, as the simplified heart-circulation model does not take into account all the complex regulatory and response mechanisms of the human body. However, treatment predictions using a well-calibrated, personalized heart-circulation model, like the one shown here, can provide a helpful first assessment to better understand the consequences of potential treatment options. This is especially the case in patients Fontan circulation, as rationale behind and impact of treatment in these patients is often not well understood.

7.5 Limitations

In this work, a simple linear venous return model was used to allow closed-loop simulations of the dobutamine stress response. This is a simplification reality. However, the changes represented in the our modelling framework fit the physiological expectations in the the different circulations included in this work [178]; in patients without a fenestration augmentation of return was almost fixed, in patients with a fenestration some augmentation (20-30%) of venous return was suggested and in a biventricular control case with an unremarkable dobutamine stress response this response was even better. This suggests that the simplified model of venous return might be sufficient to represent physiology of stress responses. The two points defining the linear venous return law (the maximum achievable venous return, $Q_{ve\text{-}max}$, and MSFP) are unknown. The assumption of $Q_{ve\text{-}max}$ being 150% higher than the cardiac output at rest is reasonable taking into account physiological experiments [178]. As the working point for cardiac output at a measured EDP is also known, the venous law could be modelled. Using these points all modelled cases had a MSFP between 10-20 mmHg at rest, values that are in the range of previously published physiological experiment in humans [233, 234]. Whereas average values of MSFP in patients with Fontan circulation are unknown, they are likely to be increased as a consequence of decreased venous capacitance and compliance [85]. An estimate of MSFP might be obtained during the intervention by varying the level of positive end-respiratory pressure and can be a potential subject of study in future works.

The 2-stage Windkessel model used here did not allow separation of the impact of the systemic and lung vasculature in the model in Fontan patients. Such separation can help investigating targeted therapies, such as pulmonary vasodilators, in patients with raised

pulmonary vascular resistance. Including a more detailed Windkessel network into the heart-circulation model is therefore another aim for future work.

The clinical data obtained to inform the models was highly detailed. This resulted in accurate calibration of the models. However, slight discrepancies between the simulations and data were expected due to the inherent differences in CMR and pressure data acquisitions (e.g. averaging of data over several heart beats in CMR and real-time acquisition of pressures). Furthermore, these measurements can carry inherent errors, such as overshooting of the ventricular pressure trace due contact between the tip of the fluid filled catheter and the ventricular wall, as shown in Figure 7.7 or errors in volume segmentations from cine CMR (e.g. due to a limited temporal resolution or suboptimal data quality). This last issue was demonstrated in the case of Fontan patient 4 (Figure 7.12) where the model-predicted end-systolic volumes lower than measured from the data. The stroke volume obtained by processing the aortic flow phase contrast CMR data however suggests that the end-systolic volume might have been overestimated in the cine CMR data. Such potential errors illustrate the need for careful verification of the data prior to model-calibration. Biomechanical models, possibly coupled with atlas based statistical methods, can potentially automatically filter out these errors once sufficiently validated.

7.6 Conclusion

This chapter described the use of a heart-circulation model for interpretation of XMR dobutamine stress exams in patients with Fontan circulation. The experiments described were aimed to evaluate the usefulness of such a framework in augmenting diagnostic capabilities of the XMR stress exam. The results showed that the heart-circulation model supplied additional information to the XMR exam by allowing evaluation of key features of the cardiovascular stress response, such as contractility at rest, contractile reserve and venous return. Furthermore, it was shown that the calibrated models could be used to estimate the gross effects of potential treatments on the stress response in individual patients. This work was a proof of concept of the model's ability to accurately represent Fontan physiology using highly detailed clinical data. Future investigations will look at the capability of the modelling framework to represent patient specific physiology using less detailed (potentially totally non-invasive) data. This could potentially allow detailed investigation of the stress response with physiological techniques such as exercise CMR.

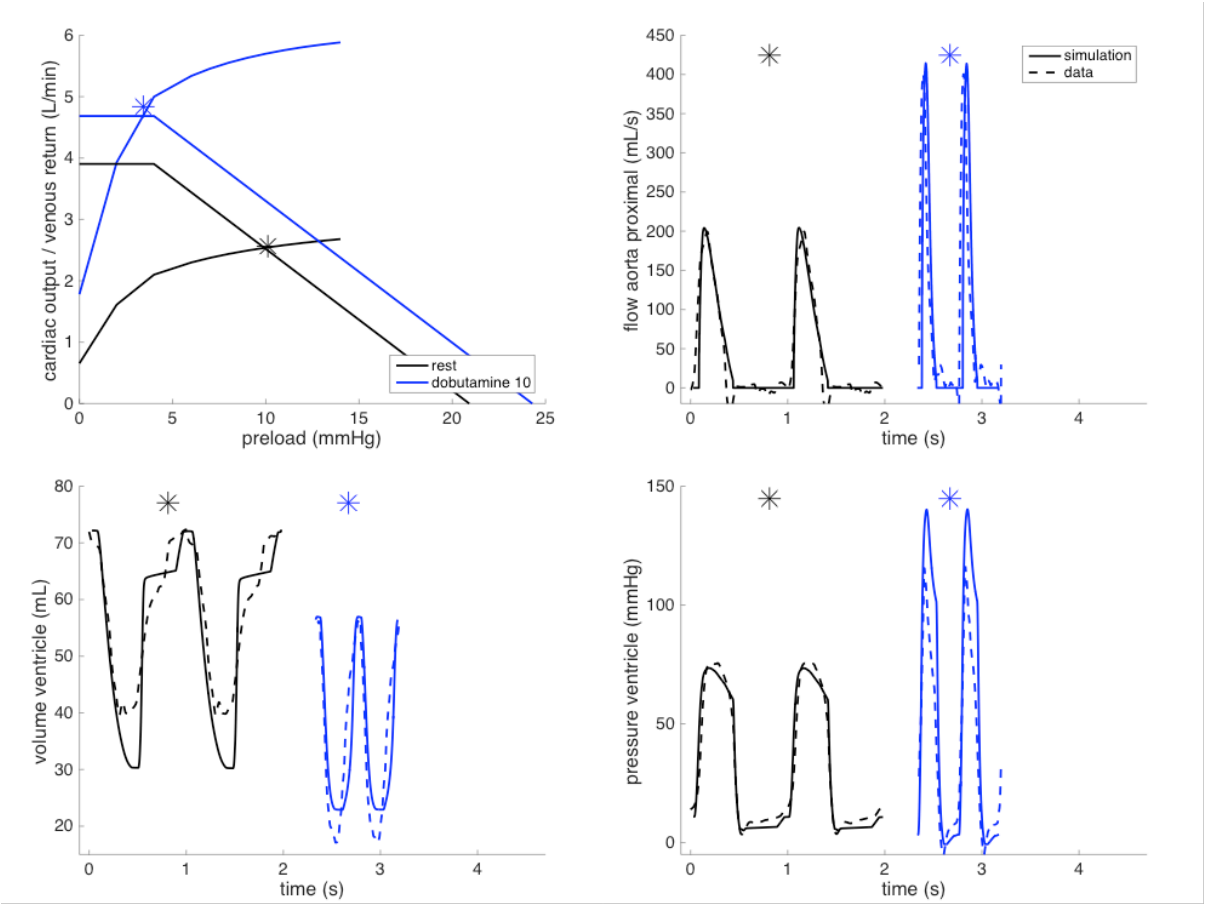

Figure 7.12 Simulations and data for Patient 4, for whom only low dose of dobutamine data was available, however increasing the contractility as for the high dose and with the increase of venous return by 20%.

Chapter 8 Conclusion and Perspectives

In this last chapter of the thesis a summary of the original contributions is given in Section 8.1, combined with an assessment of their clinical impact. Next, an analysis of the current limitations of both Exercise CMR and the obtained experimental results are provided in Section 8.2, along with possible future directions to address these limitations. Finally, an overall conclusion will be drawn in Section 10.4

8.1 Summary and Clinical Impact

This thesis focused on investigation of the role of the sub-pulmonary ventricle (the RV in a healthy heart) in overall cardiac function during exercise and the impact of its absence in patients with Fontan circulation. As was described in the introductory chapters, the role of the RV in overall cardiac performance has so far been unclear. This is the result of a lack of adequate imaging techniques that allow investigation of the biventricular cardiac function when it is most visible, i.e. during physiological exercise. In order to investigate the role of the RV, a comprehensive method for CMR imaging during exercise needed to be developed. Previous published work illustrated the potential of real-time imaging to overcome the problem of bodily motion and disturbances in ECG signals during exercise [4, 6–8, 135]. However, due to the lack in motion compensation, significant inaccuracies can occur in quantification of cardiac volumes using these techniques [9], unless time-intensive manual respiratory correction is used [4]. Moreover, none of the existing exercise CMR studies reported a methodological examination of the best available technique for real-time image acquisition.

Therefore, the first major contribution of this thesis was the development of a comprehensive framework for Exercise CMR. As shown in Chapter 3, first several different real-time acquisition techniques were evaluated for their potential use during exercise. It was shown that a real-time acquisition using relatively standard acceleration techniques, rt-SENSE, was the most robust imaging method for Exercise CMR. Two more advanced acceleration and acquisition techniques, KT-BLAST and CASPR-TIGER, performed worse. Whereas the latter techniques would theoretically result in a lower loss of image quality for the acceleration needed, due to their more complex reconstruction algorithms, the irregularity

and severity of exercise motion impacted the reconstruction significantly more in these cases compared to the simpler rt-SENSE images. This illustrates that, while these acceleration techniques have shown to deliver fast and high quality imaging at rest, their use during exercise is not directly beneficial, as motion and machinery can significantly impact the complex reconstruction algorithms.

After establishing the most appropriate acquisition technique for exercise CMR, the aim was to develop an automated method for correction of breathing and exercise motion. As shown in Chapter 4, a retrospective cardiac and respiratory gating technique was developed to reconstruct a conventional cine image stack of 24 to 30 cardiac phases from the real-time motion corrupted image-sequence. The framework utilized the high temporal resolution of real-time imaging to estimate cardiac periodicity and breathing motion. Based on these motion signals, the images at end-expiration were selected and subsequently reordered and resampled in predefined cardiac phases. In order to make this technique accessible in clinical CMR environments, special attention was given to speedy, relatively computer-inexpensive motion estimation techniques that were not vendor-specific nor dependent on complex *k*-space based reconstructions or advanced image-processing software. The resulting pipeline can be run relatively fast on a standard personal computer. As shown in the validation stage, a significant improvement in image quality and inter- and intra-observer variability for quantitative assessment of cardiac volumes was obtained with this technique, as the respiratory motion was eliminated and the real time data was averaged to a single beat Altogether, the developments presented in Chapters 3 and 4 resulted in a methodologically developed, clinically accessible and accurate framework for Exercise CMR.

The second contribution was the demonstration of the pivotal role of the RV in optimizing performance of LV during exercise. The experiments in Chapter 5 were executed in order to investigate the mechanism of SV preservation and augmentation during exercise. To do so, the normal physiological cardiac responses during exercise in healthy volunteers was observed and compared to two situations of an augmented SV response; firstly in the same healthy volunteers using selective heart rate inhibition as a pharmacological intervention to increase inotropic drive in the heart and secondly by evaluating the SV response in endurance trained athletes. These experiments demonstrated that LV SV augmentation during exercise relies on increased LV filling, which is supported by increased contraction in the RV. A personalized anatomically correct biventricular biomechanical model of a volunteer was used to further explain this behaviour. This showed that during exercise the LV is dependent on augmentation of LV filling during SV augmentation to prevent an excessive increase in contractile costs. By utilizing increased contractility in the RV, which pumps against a low afterload, to augment LV filling the heart optimizes the total cost of contraction (in active stress). These experiments demonstrate a fundamental principle of cardiac function. It shows

that the RV and LV do not act as individual entities, but cooperate in an integrated synergetic system to optimize efficiency of total cardiac performance. This observation explains why RV function has an independent impact on prognosis and treatment efficacy of typical LV diseases [11, 12, 183], and proves previous suspicions that the RV plays a central role in athletic performance [13, 170]. More importantly, it illustrates that the two ventricles cannot be regarded as individual entities, but must be viewed as one synergetic system in the organ with a high interdependency of ventricular function. This notion suggests that current clinical practice in cardiology, in which the two ventricles are often assessed and treated separately, should shift towards a more integrated assessment of biventricular function.

After establishing the role of the sub-pulmonary ventricle (RV) in the healthy circulation, the impact of absence of this ventricle in patients with Fontan circulation was assessed in Chapter 6. The aim of these investigations was to better understand the Fontan haemodynamics and potentially find new targets for treatment to improve Fontan haemodynamics. Using the Exercise CMR, the cardiac response to exercise in Fontan patients was evaluated and compared to the behaviour in age and gender matched healthy controls. As expected based on the results in Chapter 5, patients with a TCPC-type Fontan circulation suffered from a fall in ventricular filling with increasing heart rates, as filling rate was not sufficiently augmented during exercise compared to the healthy controls. Subsequently, it was shown that selective inhibition of the heart rate response during exercise improved filling, by allowing a longer filling time. As a result, SV increased. This led to an increase in CO, even despite the lower heart rate. Based on these results it can be concluded that in healthy asymptomatic Fontan patients, the physiological heart rate response during exercise is inappropriately high, due to the lack of a sub-pulmonary ventricle. Furthermore, the results of the experiments showed that selective heart rate inhibition significantly improved mechanical and energetic efficiency of the single ventricle, resulting in lower estimated oxygen consumption per litre of generated CO. The higher CO, combined with the improved efficiency of the heart suggests that HR-inhibition can potentially be a target for treatments aimed at improving efficiency of the Fontan circulation.

Finally, in Chapter 7 an initial step was taken to evaluate the potential use of a computational modelling framework to augment the diagnostic value of stress / exercise exams in individual patients with Fontan circulation. In collaboration with Dr. R. Chabiniok a computational modelling framework was developed to integrate the data obtained during combined cardiac catheterisation and cardiac CMR (XMR) exams. Subsequently, this framework was used to create patient-specific models of 5 Fontan patients and 2 biventricular control patients. The aim of this work was to investigate the potential of this modelling framework in improving

diagnostic assessment during stress. In particular, the ability to identify key factors of cardiovascular function (contractile reserve, myocardial stiffness and venous return) was assessed. These factors cannot be readily assessed using the clinical data alone. The results showed that the model allowed detection of impaired and preserved contractile responses. It also allowed to determine the impact of venous return on the exercise response in Fontan patients. Furthermore, it was illustrated that the impact of treatments can potentially be evaluated using this simple model. The work presented in Chapter 7 showed that the diagnostic value of XMR stress exams could be improved using computational modelling. This means that there is a scope for further development of this modelling framework in order to enhance diagnostic value of exercise and stress examinations.

8.2 Current Limitations and Future Directions

In this section, the main limitations of the presented works are analysed. For each limitation, possible solutions that could represent future investigations are discussed and presented.

Quantitative flow assessment during Exercise CMR. In the currently developed CMR set-up, quantification of blood flow was not integrated. Several real-time sequences have been explored during this PhD (data not presented here). During phantom tests and in-vivo dobutamine stress exams real time phase contrast flow sequences revealed good correlation with routine ECG gated sequences. However, during exercise large discrepancies in quantified volumes between flow measurements were noted. This was likely a combination of 1) the effect of bodily motion on flow encoding, 2) the need to acquire images outside of the isocentre, resulting in magnetic field inhomogeneity's, and 3) artefacts arising from the exercise bicycle ergometer. Other groups such as Muthurangu et al. and Quinlan et al. have reported the use of real time flow sequences during exercise [6, 8]. However, these are available only on Siemens CMR systems. Furthermore, their flow measurements were not validated during exercise and were only used in the ascending aorta and not in smaller vessels. More advanced flow acquisitions, for example the compressed sensing flow acquisitions described by Kwak et al. can provide better real time flow quantification during exercise and are worth evaluating [235, 236]. Also, development of a motion-correction and reconstruction framework, similar to the one described in Chapter 4 for cine imaging, could potentially provide more accurate flow quantification.

Influence of training on biventricular function during exercise. In Chapter 5 the pivotal role of the RV in cardiac function was demonstrated. Endurance trained athletes were part of the evaluated study cohort. This group clearly had an improved interventricular cooperation leading to larger increases in SV during exercise. The total cohort of healthy volunteers undergoing Exercise CMR was not large enough to investigate whether habitual

exercise also influences the interventricular cooperation. Qualitative assessment of the cardiac volume responses during exercise in individuals seems to suggest such an improved cooperation in more fit participants. In order to assess this, a larger population needs to undergo exercise CMR. This is one of the many questions to address based on the presented conclusions.

Clinical impact of heart rate inhibition on functional status of Fontan patients. In Chapter 6 the acute impact of selective heart rate inhibition on exercise haemodynamics in Fontan patients was presented. These results suggest a significant beneficial impact on cardiac output and efficiency of the heart in a small group of patients with TCPC-type Fontan circulation. This raises the question whether selective heart rate inhibition can potentially positively impact ventricular function in the long term, by preserving efficiency. Selective heart rate inhibition is a low-cost drug with minimal side effects. Therefore, such treatment could provide a valuable option for routine maintenance therapy. In order to address this question, a multi-centre randomized controlled trial needs to be undertaken that evaluates the impact of routine administration of selective HR inhibition over multiple months and in larger cohorts of Fontan patients.

All exercise studies in this thesis were perfomed in a supine position. The different gravitational forced on the body in this position, in comparison to upright exercise, impact haemodynamics, in particular venous return towards the heart. The observations in these studies can therefore not directly be extrapolated to exercise in an upright position.

Intergration of computational modelling frameworks into clinical practise. In Chapter 7 the first steps were taken to integrate a modelling framework into diagnostic assessment of the XMR stress exam for patients with Fontan circulation who undergo evaluation for symptoms of heart failure. This work only encompassed a limited number of patients. Whereas the first results are promising, several steps need to be undertaken before such a framework can be readily implemented in clinical practice. Firstly, the computational model could be expanded. In the current model, the systemic and pulmonary circulations were not separately modelled. While this reduced the amount of model parameter to be estimated, and thus decreases the chance of errors in model calibration, it does not allow investigation of pulmonary circulation as an individual entity. Current treatment of patients with failing Fontan circulation often involves pulmonary vasodilation, and therefore assessment of this circulation could provide meaningful insights into treatment efficacy. Furthermore, there is currently no option to model fenestration or collateral flow in the system. While this flow is detected as increased venous return (as shown in Section 7.3.2)

this does not allow separation of the two mechanisms (fenestration vs. collateral flow). Expansion of the model to include such the pulmonary circulation and potential R-L shunts is likely to improve the usability of the model. Lastly, the process for obtaining CMR parameters could be improved. Currently, manual segmentation of all cine frames is needed to get accurate cardiac volume and flow curves. This is time-consuming. Recently, several highly accurate automated segmentation pipelines have been developed, using deep learning algorithms. In collaboration with Dr Puyol-Anton, it was shown in preliminary work that such networks could be adapted to allow segmentation of cardiac volumes over time [167]. Further adaptions to also allow automated flow quantification will significantly simplify the use of computational models in clinical research, hereby allowing larger studies that will support future integration into clinical practice.

8.3 Conclusions

In thesis, the role of the sub-pulmonary ventricle on cardiac function during exercise and the impact of its absence were investigated. Fundamental principles in cardiac function are best assessed when the heart is under stress. Therefore, investigation during physiological exercise is vital. The work in this thesis therefore started with the development of a comprehensive technique for Exercise CMR using MRI and image-processing techniques. This was followed by utilization of this technique during clinical research studies in the healthy heart and patients with Fontan circulation. These experiments demonstrated a new fundamental physiological mechanism of biventricular cardiac function in the healthy heart and provided a new insight into the pathophysiological exercise response in the Fontan circulation. Finally, the use of advanced computational biomechanical modelling framework in providing additional diagnostic value to a clinical stress examination in patients with Fontan circulation developing exercise intolerance was presented. This sequence of studies is a demonstration of cross-disciplinary, translational project aimed at answering clinical questions using new technology. As scientific knowledge has grown, so have the borders between different disciplines in science. Therefore, developing knowledge across different fields of science has become key for rapid and effective translational development. This thesis hopefully displays the opportunities of such cross-disciplinary efforts.

References

1. Plein S, Greenwood J, Ridgway J (2011) Cardiovascular MR Manual, 1st ed. Springer International Publishing, London

2. Wigmore D, Fernhall B, Smith D (2011) Cardiovascular response to acute aerobic exercise. In: Advanced Cardiovascular Exercise Physiology. Human Kinetics, Champain, pp 139–62

3. Tune JD, Gorman MW, Feigl EO (2004) Matching coronary blood flow to myocardial oxygen consumption. J Appl Physiol 97:404–415 . doi: 10.1152/japplphysiol.01345.2003

4. La Gerche A, Claessen G, Van de Bruaene A, et al (2013) Cardiac MRI: a new gold standard for ventricular volume quantification during high-intensity exercise. Circ Cardiovasc Imaging 6:329–38 . doi: 10.1161/CIRCIMAGING.112.980037

5. Warburton DER, Haykowsky MJF, Quinney HA, et al (1999) Reliability and validity of measures of cardiac output during incremental to maximal aerobic exercise. Part I: Conventional techniques. Sport Med 27:23–41 . doi: 10.2165/00007256-199927010-00003

6. Muthurangu V, Lurz P, Critchely JD, et al (2008) Real-time assessment of right and left ventricular volumes and function in patients with congenital heart disease by using high spatiotemporal resolution radial k-t SENSE. Radiology 248:782–91 . doi: 10.1148/radiol.2482071717

7. Le T-T, Bryant JA, Ting AE, et al (2017) Assessing exercise cardiac reserve using real-time cardiovascular magnetic resonance. J Cardiovasc Magn Reson 19:7 . doi: 10.1186/s12968-017-0322-1

8. Quinlan M, Jaijee S, Marvao A, et al (2016) Exercise CMR: real-time assessment of cardiac performance with phase contrast imaging. J Cardiovasc Magn Reson 18:T2 . doi: 10.1186/1532-429X-18-S1-T2

9. Claessen G, Claus P, Delcroix M, et al (2014) Interaction between respiration and right versus left ventricular volumes at rest and during exercise: a real-time cardiac magnetic resonance study. Am J Physiol Heart Circ Physiol 306:H816-24

10. La Gerche A, Heidbuchel H, Burns AT, et al (2011) Disproportionate Exercise Load and Remodeling of the Athlete's Right Ventricle. Med Sci Sport Exerc 43:974–981 . doi: 10.1249/MSS.0b013e31820607a3

11. Meyer P, Filippatos GS, Ahmed MI, et al (2010) Effects of right ventricular ejection fraction on outcomes in chronic systolic heart failure. Circulation 121:252–258

12. Kjaergaard J, Akkan D, Iversen KK, et al (2007) Right ventricular dysfunction as an

independent predictor of short- and long-term mortality in patients with heart failure. Eur J Heart Fail 9:610–616 . doi: 10.1016/j.ejheart.2007.03.001

13. Wasfy MM, Baggish AL (2016) Endurance exercise and the right ventricle: weak link, innocent bystander, or key ingredient? Circulation 133:1913–5 . doi: 10.1161/CIRCULATIONAHA.116.022418

14. Stöhr EJ, González-Alonso J, Shave R (2011) Left ventricular mechanical limitations to stroke volume in healthy humans during incremental exercise. Am J Physiol - Hear Circ Physiol 301:H478–H487

15. Higginbotham MB, Morris KG, Williams RS, et al (1986) Regulation of stroke volume during submaximal and maximal upright exercise in normal man. Circ Res 58:281–91

16. Warburton DE, Haykowsky MJ, Quinney HA, et al (1999) Reliability and validity of measures of cardiac output during incremental to maximal aerobic exercise. Part II: Novel techniques and new advances. Sports Med 27:241–60

17. Fontan F, Baudet E (1971) Surgical repair of tricuspid atresia. Thorax 26:240–8 . doi: 10.1136/THX.26.3.240

18. Khairy P, Poirier N, Mercier L-A (2007) Univentricular heart. Circulation 115:800–12 . doi: 10.1161/CIRCULATIONAHA.105.592378

19. Redington A (2006) The physiology of the Fontan circulation. Prog Pediatr Cardiol 22:179–186 . doi: 10.1016/j.ppedcard.2006.07.007

20. Pushparajah K, Wong JK, Bellsham-Revell HR, et al (2016) Magnetic resonance imaging catheter stress haemodynamics post-Fontan in hypoplastic left heart syndrome. Eur Heart J Cardiovasc Imaging 17:644–51 . doi: 10.1093/ehjci/jev178

21. Hadjicharalambous M, Asner L, Chabiniok R, et al (2017) Non-invasive model-based assessment of passive left-ventricular myocardial stiffness in healthy subjects and in patients with non-ischemic dilated cardiomyopathy. Ann Biomed Eng 45:605–618 . doi: 10.1007/s10439-016-1721-4

22. Kung E, Perry JC, Davis C, et al (2015) Computational modeling of pathophysiologic responses to exercise in Fontan patients. Ann Biomed Eng 43:1335–47 . doi: 10.1007/s10439-014-1131-4

23. Puelz C, Acosta S, Rivière B, et al (2017) A computational study of the Fontan circulation with fenestration or hepatic vein exclusion. Comput Biol Med 89:405–418 . doi: 10.1016/J.COMPBIOMED.2017.08.024

24. Chabiniok R, Wang VY, Hadjicharalambous M, et al (2016) Multiphysics and multiscale modelling, data–model fusion and integration of organ physiology in the clinic: ventricular cardiac mechanics. Interface Focus 6:

25. Rhoades R, Tanner G (2003) The cardiac Pump. In: Medical Physiology, 2nd ed. Wolters Kluwer Health, pp 237–250

26. Zaffran S, Kelly RG, Meilhac SM, et al (2004) Right ventricular myocardium derives from the anterior heart field. Circ Res 95:261–8 . doi: 10.1161/01.RES.0000136815.73623.BE

27. Chin KM, Kim NHS, Rubin LJ (2005) The right ventricle in pulmonary hypertension.

Coron Artery Dis 16:13–18

28. Duncker DJ, Bache RJ (2008) Regulation of coronary blood flow during exercise. Physiol Rev 88:1009–86 . doi: 10.1152/physrev.00045.2006

29. Zong P, Tune JD, Downey HF (2005) Mechanisms of oxygen demand/supply balance in the right ventricle. Exp Biol Med (Maywood) 230:507–19

30. Haddad F, Hunt SA, Rosenthal DN, Murphy DJ (2008) Right ventricular function in cardiovascular disease, part I: Anatomy, physiology, aging, and functional assessment of the right ventricle. Circulation 117:1436–48 . doi: 10.1161/CIRCULATIONAHA.107.653576

31. Friedberg MK, Redington AN (2014) Right versus left ventricular failure: differences, similarities, and interactions. Circulation 129:1033–44 . doi: 10.1161/CIRCULATIONAHA.113.001375

32. Burgess MI, Mogulkoc N, Bright-Thomas RJ, et al (2002) Comparison of echocardiographic markers of right ventricular function in determining prognosis in chronic pulmonary disease. J Am Soc Echocardiogr 15:633–9 . doi: 10.1067/MJE.2002.118526

33. Sheehan F, Redington A (2008) The right ventricle: anatomy, physiology and clinical imaging. Heart 94:1510–5 . doi: 10.1136/hrt.2007.132779

34. Sequeira V, van der Velden J (2015) Historical perspective on heart function: the Frank-Starling Law. Biophys Rev 7:421–447 . doi: 10.1007/s12551-015-0184-4

35. Fukuda N, Terui T, Ohtsuki I, et al (2009) Titin and troponin: central players in the frank-starling mechanism of the heart. Curr Cardiol Rev 5:119–24 . doi: 10.2174/157340309788166714

36. Bombardini T, Gemignani V, Bianchini E, et al (2008) Diastolic time - frequency relation in the stress echo lab: filling timing and flow at different heart rates. Cardiovasc Ultrasound 6:15 . doi: 10.1186/1476-7120-6-15

37. Janssen PML (2010) Kinetics of cardiac muscle contraction and relaxation are linked and determined by properties of the cardiac sarcomere. Am J Physiol Heart Circ Physiol 299:H1092-9 . doi: 10.1152/ajpheart.00417.2010

38. González-Alonso J, Mortensen SP, Jeppesen TD, et al (2008) Haemodynamic responses to exercise, ATP infusion and thigh compression in humans: insight into the role of muscle mechanisms on cardiovascular function. J Physiol 586:2405–2417 . doi: 10.1113/jphysiol.2008.152058

39. Mortensen SP, Svendsen JH, Ersbøll M, et al (2013) Skeletal muscle signaling and the heart rate and blood pressure response to exercise: novelty and significance. Hypertension 61:

40. Steding-Ehrenborg K, Jablonowski R, Arvidsson M, et al (2013) Moderate intensity supine exercise causes decreased cardiac volumes and increased outer volume variations: a cardiovascular magnetic resonance study. J Cardiovasc Magn Reson 15:1 . doi: 10.1186/1532-429X-15-96

41. Mols P, Huynh CH, Naeije N, Ham HR (1991) Volumetric response of right ventricle during progressive supine exercise in men. Am J Physiol - Hear Circ Physiol 261:H751–H754

42. Gerche A La, Roberts T, Claessen G (2014) The response of the pulmonary circulation and right ventricle to exercise: exercise-induced right ventricular dysfunction and

structural remodeling in endurance athletes (2013 Grover Conference series). Pulm Circ 4:407–416 . doi: 10.1086/677355

43. Kovacs G, Olschewski A, Berghold A, Olschewski H (2012) Pulmonary vascular resistances during exercise in normal subjects: a systematic review. Eur Respir J 39:319–328

44. Naeije R, Chesler N (2012) Pulmonary circulation at exercise. Compr Physiol 2:711–41 . doi: 10.1002/cphy.c100091

45. Gerche A La, Claessen G, Dymarkowski S, et al (2015) Exercise-induced right ventricular dysfunction is associated with ventricular arrhythmias in endurance athletes. Eur Heart J 36:446–452 . doi: 10.1093/eurheartj/ehv202

46. Reeves JT, Linehan JH, Stenmark KR (2005) Distensibility of the normal human lung circulation during exercise. Am J Physiol Cell Mol Physiol 288:L419–L425 . doi: 10.1152/ajplung.00162.2004

47. Mortensen SP, Dawson EA, Yoshiga CC, et al (2005) Limitations to systemic and locomotor limb muscle oxygen delivery and uptake during maximal exercise in humans. J Physiol 566:273–285 . doi: 10.1113/jphysiol.2005.086025

48. Rowland TW, Roti MW (2004) Cardiac responses to progressive upright exercise in adult male cyclists. J Sport Med Phys Fit 179–85

49. Plotnick GD, Becker LC, Fisher ML, et al (1986) Use of the Frank-Starling mechanism during submaximal versus maximal upright exercise. Am J Physiol - Hear Circ Physiol 251:H1101–H1105

50. Vella CA, Robergs RA (2005) A review of the stroke volume response to upright exercise in healthy subjects. Br J Sports Med 39:190–5 . doi: 10.1136/bjsm.2004.013037

51. Nottin S, Vinet A, Stecken F, et al (2002) Central and peripheral cardiovascular adaptations during a maximal cycle exercise in boys and men. Med Sci Sports Exerc 34:456–63

52. Kimball TR, Mays WA, Khoury PR, et al (1993) Echocardiography determination of left ventricular preload, afterload, and contractility during and after exercise. J Pediatr 122:S89–S94 . doi: 10.1016/S0022-3476(09)90050-6

53. Holverda S, Rietema H, Westerhof N, et al (2009) Stroke volume increase to exercise in chronic obstructive pulmonary disease is limited by increased pulmonary artery pressure. Heart 95:137–41 . doi: 10.1136/hrt.2007.138172

54. Holverda S, Gan CT-J, Marcus JT, et al (2006) Impaired stroke volume response to exercise in pulmonary arterial hypertension. J Am Coll Cardiol 47:1732–3 . doi: 10.1016/j.jacc.2006.01.048

55. Epstein SE, Beiser GD, Stampfer M, et al (1967) Characterization of the circulatory response to maximal upright exercise in normal subjects and patients with heart disease. Circulation 35:1049–62

56. Rowland T, Whatley Blum J (2000) Cardiac dynamics during upright cycle exercise in boys. Am J Hum Biol 12:749–757 . doi: 10.1002/1520-6300(200011/12)12:6<749::AID-AJHB4>3.0.CO;2-W

57. González-Alonso J, Calbet JAL (2003) Reductions in systemic and skeletal muscle blood flow and oxygen delivery limit maximal aerobic capacity in humans. Circulation 107:824–30

58. Seals DR, Hagberg JM, Spina RJ, et al (1994) Enhanced left ventricular performance in endurance trained older men. Circulation 89:198–205

59. Fagard R, Van Den Broeke C, Amery A (1989) Left ventricular dynamics during exercise in elite marathon runners. J Am Coll Cardiol 14:112–118 . doi: 10.1016/0735-1097(89)90060-0

60. Schairer JR, Stein PD, Keteyian S, et al (1992) Left ventricular response to submaximal exercise in endurance-trained athletes and sedentary adults. Am J Cardiol 70:930–3 . doi: 10.1016/0002-9149(92)90741-G

61. Bossone E, Rubenfire M, Bach DS, et al (1999) Range of tricuspid regurgitation velocity at rest and during exercise in normal adult men: Implications for the diagnosis of pulmonary hypertension. J Am Coll Cardiol 33:1662–1666 . doi: 10.1016/S0735-1097(99)00055-8

62. Gabrielli L, Bijnens BH, Brambila C, et al (2016) Differential atrial performance at rest and exercise in athletes: Potential trigger for developing atrial dysfunction? Scand J Med Sci Sports 26:1444–1454 . doi: 10.1111/sms.12610

63. Santoro A, Alvino F, Antonelli G, et al (2016) Left atrial strain after maximal exercise in competitive waterpolo players. Int J Cardiovasc Imaging 32:399–405 . doi: 10.1007/s10554-015-0786-8

64. Schnell F, Claessen G, La Gerche A, et al (2017) Atrial volume and function during exercise in health and disease. J Cardiovasc Magn Reson 19:104 . doi: 10.1186/s12968-017-0416-9

65. National institute of Cardiovascular Outcomes Research. www.nicor.gov.uk. Accessed 26 May 2016

66. de Leval MR, Kilner P, Gewillig M, Bull C (1988) Total cavopulmonary connection: a logical alternative to atriopulmonary connection for complex Fontan operations. Experimental studies and early clinical experience. J Thorac Cardiovasc Surg 96:682–95

67. Norwood WI (1989) Hypoplastic left heart syndrome. Cardiol Clin 7:377–85

68. d'Udekem Y, Iyengar AJ, Cochrane AD, et al (2007) The Fontan procedure: contemporary techniques have improved long-term outcomes. Circulation 116:I157-64 . doi: 10.1161/CIRCULATIONAHA.106.676445

69. Krasemann T, Fenge H, Kehl H-G, et al A decade of staged Norwood palliation in hypoplastic left heart syndrome in a midsized cardiosurgical center. Pediatr Cardiol 26:751–5 . doi: 10.1007/s00246-005-0908-5

70. Delmo Walter EMB, Hübler M, Alexi-Meskishvili V, et al Staged surgical palliation in hypoplastic left heart syndrome and its variants. J Card Surg 24:383–91 . doi: 10.1111/j.1540-8191.2008.00759.x

71. de Leval MR (2005) The Fontan circulation: a challenge to William Harvey? Nat Clin Pract Cardiovasc Med 2:202–8 . doi: 10.1038/ncpcardio0157

72. Gewillig M, Brown SC, Eyskens B, et al (2010) The Fontan circulation: who controls cardiac output? Interact Cardiovasc Thorac Surg 10:428–33 . doi: 10.1510/icvts.2009.218594

73. Stickland MK, Welsh RC, Petersen SR, et al (2006) Does fitness level modulate the cardiovascular hemodynamic response to exercise? J Appl Physiol 100:1895–901 . doi: 10.1152/japplphysiol.01485.2005

74. Takken T, Tacken MHP, Blank AC, et al (2007) Exercise limitation in patients with Fontan circulation: a review. J Cardiovasc Med 8:775–81 . doi: 10.2459/JCM.0b013e328011c999

75. Shachar GB, Fuhrman BP, Wang Y, et al (1982) Rest and exercise hemodynamics after the Fontan procedure. Circulation 65:1043–8

76. Schmitt B, Steendijk P, Ovroutski S, et al (2010) Pulmonary vascular resistance, collateral flow, and ventricular function in patients with a Fontan circulation at rest and during dobutamine stress. Circ Cardiovasc Imaging 3:623–31 . doi: 10.1161/CIRCIMAGING.109.931592

77. Sundareswaran KS, Pekkan K, Dasi LP, et al (2008) The total cavopulmonary connection resistance: a significant impact on single ventricle hemodynamics at rest and exercise. Am J Physiol Heart Circ Physiol 295:H2427-35 . doi: 10.1152/ajpheart.00628.2008

78. Hsia T-Y, Migliavacca F, Pittaccio S, et al (2004) Computational fluid dynamic study of flow optimization in realistic models of the total cavopulmonary connections. J Surg Res 116:305–13 . doi: 10.1016/j.jss.2003.08.004

79. Gewillig MH, Lundström UR, Bull C, et al (1990) Exercise responses in patients with congenital heart disease after fontan repair: Patterns and determinants of performance. J Am Coll Cardiol 15:1424–1432 . doi: 10.1016/S0735-1097(10)80034-8

80. Darst JR, Vezmar M, McCrindle BW, et al (2010) Living at an altitude adversely affects exercise capacity in Fontan patients. Cardiol Young 20:593–601 . doi: 10.1017/S1047951109990357

81. Bridges ND, Mayer JE, Lock JE, et al (1992) Effect of baffle fenestration on outcome of the modified Fontan operation. Circulation 86:1762–9

82. Lemler MS, Scott WA, Leonard SR, et al (2002) Fenestration improves clinical outcome of the fontan procedure: A prospective, randomized study. Circulation 105:207–212 . doi: 10.1161/hc0202.102237

83. Mertens L, Hagler DJ, Sauer U, et al (1998) Protein-losing enteropathy after the Fontan operation: an international multicenter study. PLE study group. J Thorac Cardiovasc Surg 115:1063–73

84. Kreutzer J, Lock JE, Jonas RA, Keane JF (1997) Transcatheter fenestration dilation and/or creation in postoperative fontan patients. Am J Cardiol 79:228–231 . doi: 10.1016/S0002-9149(96)00723-0

85. Krishnan US, Taneja I, Gewitz M, et al (2009) Peripheral vascular adaptation and orthostatic tolerance in Fontan physiology. Circulation 120:1775–83 . doi: 10.1161/CIRCULATIONAHA.109.854331

86. Giardini A, Hager A, Pace Napoleone C, Picchio FM (2008) Natural history of exercise capacity after the Fontan operation: a longitudinal study. Ann Thorac Surg 85:818–21 . doi: 10.1016/j.athoracsur.2007.11.009

87. Anderson PAW, Sleeper LA, Mahony L, et al (2008) Contemporary outcomes after the Fontan procedure: a Pediatric Heart Network multicenter study. J Am Coll Cardiol 52:85–98 . doi: 10.1016/j.jacc.2008.01.074

88. Senzaki H, Masutani S, Ishido H, et al (2006) Cardiac rest and reserve function in patients with Fontan circulation. J Am Coll Cardiol 47:2528–35 . doi: 10.1016/j.jacc.2006.03.022

89. Saiki H, Eidem BW, Ohtani T, et al (2016) Ventricular-arterial function and coupling in the adult fontan circulation. J Am Hear Assoc Cardiovasc Cerebrovasc Dis 5: . doi: 10.1161/JAHA.116.003887

90. Cheung MMH, Smallhorn JF, McCrindle BW, et al (2005) Non-invasive assessment of ventricular force-frequency relations in the univentricular circulation by tissue Doppler echocardiography: a novel method of assessing myocardial performance in congenital heart disease. Heart 91:1338–42 . doi: 10.1136/hrt.2004.048207

91. Haggerty CM, Restrepo M, Tang E, et al (2013) Fontan hemodynamics from 100 patient-specific cardiac magnetic resonance studies: A computational fluid dynamics analysis. J Thorac Cardiovasc Surg 1–10 . doi: 10.1016/j.jtcvs.2013.11.060

92. Diller G-P, Giardini A, Dimopoulos K, et al (2010) Predictors of morbidity and mortality in contemporary Fontan patients: results from a multicenter study including cardiopulmonary exercise testing in 321 patients. Eur Heart J 31:3073–3083 . doi: 10.1093/eurheartj/ehq356

93. Fernandes SM, Alexander ME, Graham DA, et al (2011) Exercise esting identifies patients at increased risk for morbidity and mortality following Fontan surgery. Congenit Heart Dis 6:294–303 . doi: 10.1111/j.1747-0803.2011.00500.x

94. d'Udekem Y, Cheung MMH, Setyapranata S, et al (2009) How good is a good Fontan? Quality of life and exercise capacity of Fontans without arrhythmias. Ann Thorac Surg 88:1961–9 . doi: 10.1016/j.athoracsur.2009.07.079

95. Troutman WB, Barstow TJ, Galindo AJ, Cooper DM (1998) Abnormal dynamic cardiorespiratory responses to exercise in pediatric patients after Fontan procedure. J Am Coll Cardiol 31:668–673 . doi: 10.1016/S0735-1097(97)00545-7

96. Van De Bruaene A, La Gerche A, Claessen G, et al (2014) Sildenafil improves exercise hemodynamics in fontan patients. Circ Cardiovasc Imaging 7:265–73 . doi: 10.1161/CIRCIMAGING.113.001243

97. Robbers-Visser D, Jan Ten Harkel D, Kapusta L, et al (2008) Usefulness of cardiac magnetic resonance imaging combined with low-dose dobutamine stress to detect an abnormal ventricular stress response in children and young adults after fontan operation at young age. Am J Cardiol 101:1657–62 . doi: 10.1016/j.amjcard.2008.01.050

98. Pushparajah K, Wong J, Hussain T, et al Pulmonary vasodilatation does not improve exercise hemodynamics in children with Fontan circulation. Prelim Rep

99. Wong J, Pushparajah K, De Vecchi A, et al (2014) Myocardial contractile response to dobutamine in hypoplastic left heart syndrome post-Fontan. J Cardiovasc Magn Reson 16:O104 . doi: 10.1186/1532-429X-16-S1-O104

100. Tanaka N, Nozawa T, Yasumura Y, et al (1990) Heart-rate-proportional oxygen consumption for constant cardiac work in dog heart. Jpn J Physiol 40:503–521 . doi: 10.2170/jjphysiol.40.503

101. Alphonso N, Baghai M, Sundar P, et al (2005) Intermediate-term outcome following the fontan operation: a survival, functional and risk-factor analysis. Eur J Cardiothorac Surg 28:529–35 . doi: 10.1016/j.ejcts.2005.06.035

102. Khairy P, Fernandes SM, Mayer JE, et al (2008) Long-term survival, modes of death, and predictors of mortality in patients with Fontan surgery. Circulation 117:85–92 . doi: 10.1161/CIRCULATIONAHA.107.738559

103. Piran S (2002) Heart Failure and Ventricular Dysfunction in Patients With Single or Systemic Right Ventricles. Circulation 105:1189–1194 . doi: 10.1161/hc1002.105182

104. Griffiths E, Kaza A (2009) Evaluating Failing Fontans for Heart Transplantation : Predictors of Death. Ann Thorac Surg 88:558–564 . doi: 10.1016/j.athoracsur.2009.03.085

105. Simpson KE, Cibulka N, Lee CK, et al (2012) Failed Fontan heart transplant candidates with preserved vs impaired ventricular ejection: 2 distinct patient populations. J Hear Lung Transplant 31:545–547 . doi: 10.1016/J.HEALUN.2012.02.003

106. Murtuza B, Hermuzi A, Crossland DS, et al (2017) Impact of mode of failure and end-organ dysfunction on the survival of adult Fontan patients undergoing cardiac transplantation. Eur J Cardiothorac Surg 51:135–141 . doi: 10.1093/ejcts/ezw243

107. Ostrow AM, Freeze H, Rychik J (2006) Protein-losing enteropathy after Fontan operation: Investigations into possible pathophysiologic mechanisms. Ann Thorac Surg 82:695–700 . doi: 10.1016/j.athoracsur.2006.02.048

108. Itkin M, Piccoli DA, Nadolski G, et al (2017) Protein-Losing Enteropathy in Patients With Congenital Heart Disease. J Am Coll Cardiol 69:2929–2937 . doi: 10.1016/j.jacc.2017.04.023

109. Miller JR, Simpson KE, Epstein DJ, et al (2016) Improved survival after heart transplant for failed Fontan patients with preserved ventricular function. J Hear Lung Transplant 35:877–883 . doi: 10.1016/j.healun.2016.02.005

110. Anderson PAW, Breitbart RE, McCrindle BW, et al (2010) The Fontan patient: inconsistencies in medication therapy across seven pediatric heart network centers. Pediatr Cardiol 31:1219–28 . doi: 10.1007/s00246-010-9807-5

111. Wilson TG, Iyengar AJ, Winlaw DS, et al (2016) Use of ACE inhibitors in Fontan: Rational or irrational? Int J Cardiol 210:95–99 . doi: 10.1016/J.IJCARD.2016.02.089

112. Shabanian R, Shahbaznejad L, Razaghian A, et al (2013) Sildenafil and Ventriculo-Arterial Coupling in Fontan-Palliated Patients: A Noninvasive Echocardiographic Assessment. Pediatr Cardiol 34:129–134 . doi: 10.1007/s00246-012-0400-y

113. Latus H, Gerstner B, Kerst G, et al (2016) Effect of inhaled nitric oxide on blood flow dynamics in patients after the Fontan procedure using cardiovascular magnetic resonance flow measurements. Pediatr Cardiol 37:504–511 . doi: 10.1007/s00246-015-1307-1

114. Goldberg DJ, French B, McBride MG, et al (2011) Impact of oral sildenafil on exercise performance in children and young adults after the fontan operation: a randomized, double-blind, placebo-controlled, crossover trial. Circulation 123:1185–93 . doi: 10.1161/CIRCULATIONAHA.110.981746

115. Hebert A, Mikkelsen UR, Thilen U, et al (2014) Bosentan improves exercise capacity in adolescents and adults after Fontan operation: The TEMPO study. Circulation 130:2021–30 . doi: 10.1161/CIRCULATIONAHA.113.008441

116. Derk G, Houser L, Miner P, et al (2015) Efficacy of endothelin blockade in adults with Fontan physiology. Congenit Heart Dis 10:E11–E16 . doi: 10.1111/chd.12189

117. Schuuring MJ, Vis JC, van Dijk APJ, et al (2013) Impact of bosentan on exercise capacity in adults after the Fontan procedure: a randomized controlled trial. Eur J Heart Fail 15:690–8 . doi: 10.1093/eurjhf/hft017

118. Gatehouse PD, Keegan J, Crowe L a., et al (2005) Applications of phase-contrast flow and velocity imaging in cardiovascular MRI. Eur Radiol 15:2172–2184 . doi: 10.1007/s00330-005-2829-3

119. Wigström L, Sjöqvist L, Wranne B (1996) Temporally resolved 3D phase-contrast imaging. Magn Reson Med 36:800–3

120. Pelc NJ, Bernstein MA, Shimakawa A, Glover GH (1991) Encoding strategies for three-direction phase-contrast MR imaging of flow. J Magn Reson Imaging 1:405–413 . doi: 10.1002/jmri.1880010404

121. Sengupta PP, Pedrizzetti G, Kilner PJ, et al (2012) Emerging trends in CV flow visualization. JACC Cardiovasc Imaging 5:305–316 . doi: 10.1016/j.jcmg.2012.01.003

122. Stankovic Z, Allen BD, Garcia J, et al (2014) 4D flow imaging with MRI. Cardiovasc Diagn Ther 4:173–192 . doi: 10.3978/j.issn.2223-3652.2014.01.02

123. Tsao J, Boesiger P, Pruessmann KP (2003) k-t BLAST and k-t SENSE: dynamic MRI with high frame rate exploiting spatiotemporal correlations. Magn Reson Med 50:1031–42 . doi: 10.1002/mrm.10611

124. Giese D, Schaeffter T, Kozerke S (2013) Highly undersampled phase-contrast flow measurements using compartment-based k-t principal component analysis. Magn Reson Med 69:434–43 . doi: 10.1002/mrm.24273

125. Uribe S, Beerbaum P, Sørensen TS, et al (2009) Four-dimensional (4D) flow of the whole heart and great vessels using real-time respiratory self-gating. Magn Reson Med 62:984–992 . doi: 10.1002/mrm.22090

126. La Gerche A, Gewillig M (2010) What Limits Cardiac Performance during Exercise in Normal Subjects and in Healthy Fontan Patients? Int J Pediatr 2010: . doi: 10.1155/2010/791291

127. Arena R, Myers J, Williams M a, et al (2007) Assessment of functional capacity in clinical and research settings: a scientific statement from the American Heart Association Committee on Exercise, Rehabilitation, and Prevention of the Council on Clinical Cardiology and the Council on Cardiovascular N. Circulation 116:329–43 . doi: 10.1161/CIRCULATIONAHA.106.184461

128. Bellenger NG, Davies LC, Francis JM, et al (2000) Reduction in sample size for studies of remodeling in heart failure by the use of cardiovascular magnetic resonance. J Cardiovasc Magn Reson 2:271–8

129. Valsangiacomo Buechel ER, Mertens LL (2012) Imaging the right heart: The use of integrated multimodality imaging. Eur Heart J 33:949–60 . doi: 10.1093/eurheartj/ehr490

130. Schmitt B, Steendijk P, Lunze K, et al (2009) Integrated assessment of diastolic and systolic ventricular function using diagnostic cardiac magnetic resonance

catheterization: validation in pigs and application in a clinical pilot study. JACC Cardiovasc Imaging 2:1271–81 . doi: 10.1016/j.jcmg.2009.09.007

131. Lehtonen LA, Antila S, Pentikäinen PJ (2004) Pharmacokinetics and pharmacodynamics of intravenous inotropic agents. Clin Pharmacokinet 43:187–203 . doi: 10.2165/00003088-200443030-00003

132. Binkley PF, Murray KD, Watson KM, et al (1991) Dobutamine increases cardiac output of the total artificial heart. Implications for vascular contribution of inotropic agents to augmented ventricular function. Circulation 84:1210–5

133. Asrress KN, Schuster A, Ali NF, et al (2013) Myocardial haemodynamic responses to dobutamine stress compared to physiological exercise during cardiac magnetic resonance imaging. J Cardiovasc Magn Reson 15:P16 . doi: 10.1186/1532-429X-15-S1-P16

134. Sugimoto T, Bandera F, Generati G, et al (2017) Left atrial function dynamics during exercise in heart failure. JACC Cardiovasc Imaging 10:1253–64 . doi: 10.1016/j.jcmg.2016.09.021

135. Roest AA, Kunz P, Lamb HJ, et al (2001) Biventricular response to supine physical exercise in young adults assessed with ultrafast magnetic resonance imaging. Am J Cardiol 87:601–5 . doi: 10.1016/S0002-9149(00)01438-7

136. Pieles GE, Szantho G, Rodrigues JCL, et al (2014) Adaptations of aortic and pulmonary artery flow parameters measured by phase-contrast magnetic resonance angiography during supine aerobic exercise. Eur J Appl Physiol 114:1013–1023 . doi: 10.1007/s00421-014-2833-x

137. Heiberg J, Asschenfeldt B, Maagaard M, Ringgaard S (2017) Dynamic bicycle exercise to assess cardiac output at multiple exercise levels during magnetic resonance imaging. Clin Imaging 46:102–107 . doi: 10.1016/J.CLINIMAG.2017.07.010

138. Weber TF, von Tengg-Kobligk H, Kopp-Schneider A, et al (2011) High-resolution phase-contrast MRI of aortic and pulmonary blood flow during rest and physical exercise using a MRI compatible bicycle ergometer. Eur J Radiol 80:103–108 . doi: 10.1016/J.EJRAD.2010.06.045

139. Lurz P, Muthurangu V, Schievano S, et al (2009) Feasibility and reproducibility of biventricular volumetric assessment of cardiac function during exercise using real-time radial k-t SENSE magnetic resonance imaging. J Magn Reson Imaging 29:1062–70 . doi: 10.1002/jmri.21762

140. Bovens AM, van Baak MA, Vrencken JG, et al (1993) Maximal aerobic power in cycle ergometry in middle-aged men and women, active in sports, in relation to age and physical activity. Int J Sports Med 14:66–71 . doi: 10.1055/s-2007-1021148

141. Walsh-Riddle M, Blumenthal JA (1989) Cardiovascular responses during upright and semi-recumbent cycle ergometry testing. Med Sci Sports Exerc 21:581–5

142. Basha TA, Roujol S, Kissinger K V., et al (2014) Free-breathing cardiac MR stress perfusion with real-time slice tracking. Magn Reson Med 72:689–698 . doi: 10.1002/mrm.24977

143. Gusso S, Salvador C, Hofman P, et al (2012) Design and testing of an MRI-compatible cycle ergometer for non-invasive cardiac assessments during exercise. Biomed Eng

Online 11:13 . doi: 10.1186/1475-925X-11-13

144. Chen CH, Fetics B, Nevo E, et al (2001) Noninvasive single-beat determination of left ventricular end-systolic elastance in humans. J Am Coll Cardiol 38:2028–34

145. Agnoletti D, Millasseau S, Topouchian J, et al (2014) Comparison of central blood pressure devices on the basis of a modified protocol of the European Society of Hypertension. Blood Press Monit 19:103–108 . doi: 10.1097/MBP.0000000000000028

146. Mariscal Harana J, van Engelen A, Schneider T, et al (2017) Non-invasive, MRI-based estimation of patient-specific aortic blood pressure using one-dimensional blood flow modelling. Artery Res 20:54–55 . doi: 10.1016/J.ARTRES.2017.10.036

147. Wesseling KH (1990) Finapres, continuous noninvasive finger arterial pressure based on the method of Peñáz. In: Blood Pressure Measurements. Steinkopff, Heidelberg, pp 161–172

148. Silke B, Spiers JP, Boyd S, et al (1994) Evaluation of non-invasive blood pressure measurement by the Finapres method at rest and during dynamic exercise in subjects with cardiovascular insufficiency. Clin Auton Res 4:49–56 . doi: 10.1007/BF01828838

149. Sagiv M, Ben-Sira D, Goldhammer E (1999) Direct vs. indirect blood pressure measurement at peak anaerobic exercise. Int J Sports Med 20:275–278 . doi: 10.1055/s-2007-971130

150. Usman M, Ruijsink B, Nazir MS, et al (2017) Free breathing whole-heart 3D CINE MRI with self-gated Cartesian trajectory. Magn Reson Imaging 38:129–137 . doi: 10.1016/J.MRI.2016.12.021

151. Usman M, Atkinson D, Kolbitsch C, et al (2015) Manifold learning based ECG-free free-breathing cardiac CINE MRI. J Magn Reson Imaging 41:1521–1527 . doi: 10.1002/jmri.24731

152. Ruijsink B, Puyol-Antón E, Usman M, et al (2017) Semi-automatic Cardiac and Respiratory Gated MRI for Cardiac Assessment During Exercise. Springer, Cham, pp 86–95

153. Peters DC, Nezafat R, Eggers H, et al (2008) 2D free-breathing dual navigator-gated cardiac function validated against the 2D breath-hold acquisition. J Magn Reson Imaging 28:773–777

154. Larson AC, White RD, Laub G, et al (2004) Self-gated cardiac cine MRI. Magn Reson Med 51:93–102

155. Liu C, Bammer R, Kim D-H, Moseley ME (2004) Self-navigated interleaved spiral (SNAILS): application to high-resolution diffusion tensor imaging. Magn Reson Med 52:1388–1396

156. Paul J, Divkovic E, Wundrak S, et al (2015) High-resolution respiratory self-gated golden angle cardiac MRI: comparison of self-gating methods in combination with k-t SPARSE SENSE. Magn Reson Med 73:292–298

157. Crowe ME, Larson AC, Zhang Q, et al (2004) Automated rectilinear self-gated cardiac cine imaging. Magn Reson Med 52:782–788

158. Feng L, Axel L, Chandarana H, et al (2016) XD-GRASP: Golden-angle radial MRI with reconstruction of extra motion-state dimensions using compressed sensing. Magn Reson Med 75:775–788

159. Kim WS, Mun CW, Kim DJ, Cho ZH (1990) Extraction of cardiac and respiratory

motion cycles by use of projection data and its applications to NMR imaging. Magn Reson Med 13:25–37

160. Yoon H, Kim KS, Kim D, et al (2014) Motion adaptive patch-based low-rank approach for compressed sensing cardiac cine MRI. IEEE Trans Med Imaging 33:2069–2085

161. Hansen MS, Sørensen TS, Arai AE, Kellman P (2012) Retrospective reconstruction of high temporal resolution cine images from real-time MRI using iterative motion correction. Magn Reson Med 68:741–750

162. van Amerom JFP, Lloyd DFA, Price AN, et al (2018) Fetal cardiac cine imaging using highly accelerated dynamic MRI with retrospective motion correction and outlier rejection. Magn Reson Med 79:327–338 . doi: 10.1002/mrm.26686

163. Fratz S, Chung T, Greil GF, et al (2013) Guidelines and protocols for cardiovascular magnetic resonance in children and adults with congenital heart disease: SCMR expert consensus group on congenital heart disease. J Cardiovasc Magn Reson 15:51 . doi: 10.1186/1532-429X-15-51

164. Thirion J-P (1998) Image matching as a diffusion process: an analogy with Maxwell's demons. Med Image Anal 2:243–260

165. Cahalin LP, Chase P, Arena R, et al (2013) A meta-analysis of the prognostic significance of cardiopulmonary exercise testing in patients with heart failure. Heart Fail Rev 18:79–94 . doi: 10.1007/s10741-012-9332-0

166. Han F, Zhou Z, Han E, et al (2017) Self-gated 4D multiphase, steady-state imaging with contrast enhancement (MUSIC) using rotating cartesian K-space (ROCK): Validation in children with congenital heart disease. Magn Reson Med 78:472–83

167. Puyol-Anton E, Ruijsink B, Langer H, et al Fully automated myocardial strain estimation form cine MRI using convolutional neural networks. 2018:

168. Claessen G, Claus P, Delcroix M, et al (2014) Interaction between respiration and right versus left ventricular volumes at rest and during exercise: a real-time cardiac magnetic resonance study. Am J Physiol Heart Circ Physiol 306:H816-24 . doi: 10.1152/ajpheart.00752.2013

169. Seely RD, Nerlich WE, Gregg DE (1950) A Comparison of Cardiac Output Determined by the Fick Procedure and a Direct Method Using the Rotameter. Circulation 1:1261–6

170. Claessen G, Claus P, Ghysels S, et al (2014) Right ventricular fatigue developing during endurance exercise. Med Sci Sport Exerc 46:1717–1726 . doi: 10.1249/MSS.0000000000000282

171. Borer JS, Le Heuzey J-Y (2008) Characterization of the heart rate-lowering action of ivabradine, a selective I(f) current inhibitor. Am J Ther 15:461–73 . doi: 10.1097/MJT.0b013e3181758855

172. Berdeaux A (2007) Preclinical results with If current inhibition by ivabradine. Drugs 67:25–33 . doi: 10.2165/00003495-200767002-00004

173. Asner L, Hadjicharalambous M, Chabiniok R, et al (2015) Estimation of passive and active properties in the human heart using 3D tagged MRI. Biomech Model

Mechanobiol 15:1121–39 . doi: 10.1007/s10237-015-0748-z

174. Hadjicharalambous M, Chabiniok R, Asner L, et al (2014) Analysis of passive cardiac constitutive laws for parameter estimation using 3D tagged MRI. Biomech Model Mechanobiol. doi: 10.1007/s10237-014-0638-9

175. Klotz S, Dickstein ML, Burkhoff D (2007) A computational method of prediction of the end-diastolic pressure-volume relationship by single beat. Nat Protoc 2:2152–8 . doi: 10.1038/nprot.2007.270

176. Sommer G, Haspinger DC, Andrä M, et al (2015) Quantification of shear deformations and corresponding stresses in the biaxially tested human myocardium. Ann Biomed Eng 43:2334–2348 . doi: 10.1007/s10439-015-1281-z

177. Steding-Ehrenborg K, Boushel RC, Calbet JA, et al (2015) Left ventricular atrioventricular plane displacement is preserved with lifelong endurance training and is the main determinant of maximal cardiac output. J Physiol 5932323:5157–5166 . doi: 10.1113/JP271621

178. Guyton (1973) Circulatory physiology: Cardiac output and its regulation. Saunders

179. Dawson EA, Shave R, Whyte G, et al (2007) Preload maintenance and the left ventricular response to prolonged exercise in men. Exp Physiol 92:383–390 . doi: 10.1113/expphysiol.2006.035089

180. Stöhr EJ, McDonnell B, Thompson J, et al (2012) Left ventricular mechanics in humans with high aerobic fitness: adaptation independent of structural remodelling, arterial haemodynamics and heart rate. J Physiol 590:2107–19 . doi: 10.1113/jphysiol.2012.227850

181. Beaumont A, Hough J, Sculthorpe N, Richards J (2017) Left ventricular twist mechanics during incremental cycling and knee extension exercise in healthy men. Eur J Appl Physiol 117:139–150 . doi: 10.1007/s00421-016-3506-8

182. Scharf M, Brem MH, Wilhelm M, et al (2010) Atrial and ventricular functional and structural adaptations of the heart in elite triathletes assessed with cardiac MR imaging. Radiology 257:71–9 . doi: 10.1148/radiol.10092377

183. van Everdingen WM, Walmsley J, Cramer MJ, et al (2017) Echocardiographic prediction of cardiac resynchronization therapy response requires analysis of both mechanical dyssynchrony and right ventricular function: A combined analysis of patient data and computer simulations. J Am Soc Echocardiogr 30:1012–20 . doi: 10.1016/j.echo.2017.06.004

184. O'Byrne ML, Desai S, Lane M, et al (2017) Relationship between habitual exercise and performance on cardiopulmonary exercise testing differs between children with single and biventricular circulations. Pediatr Cardiol 38:472–483 . doi: 10.1007/s00246-016-1537-x

185. Anderson MB, Goldstein J, Milano C, et al (2015) Benefits of a novel percutaneous ventricular assist device for right heart failure: The prospective RECOVER RIGHT study of the Impella RP device. J Hear Lung Transplant 34:1549–1560 . doi: 10.1016/j.healun.2015.08.018

186. Janoušek J, Kovanda J, Ložek M, et al (2017) Pulmonary right ventricular resynchronization in congenital heart disease: Acute improvement in right ventricular mechanics and contraction efficiency. Circ Cardiovasc Imaging 10:e006424 . doi: 10.1161/CIRCIMAGING.117.006424

187. Giridharan GA, Koenig SC, Kennington J, et al (2013) Performance evaluation of a

pediatric viscous impeller pump for Fontan cavopulmonary assist. J Thorac Cardiovasc Surg 145:249–257 . doi: 10.1016/j.jtcvs.2012.01.082

188. Sinha P, Deutsch N, Ratnayaka K, et al (2014) Effect of mechanical assistance of the systemic ventricle in single ventricle circulation with cavopulmonary connection. J Thorac Cardiovasc Surg 147:1271–5 . doi: 10.1016/j.jtcvs.2013.12.018

189. Naeije R, Chesler N, Naeije R, Chesler N (2012) Pulmonary Circulation at exercise. In: Comprehensive Physiology. John Wiley & Sons, Inc., Hoboken, NJ, USA

190. Hebert A, Jensen AS, Mikkelsen UR, et al (2014) Hemodynamic causes of exercise intolerance in Fontan patients. Int J Cardiol 175:478–483 . doi: 10.1016/j.ijcard.2014.06.015

191. Wong J, Pushparajah K, de Vecchi A, et al (2017) Pressure-volume loop-derived cardiac indices during dobutamine stress: a step towards understanding limitations in cardiac output in children with hypoplastic left heart syndrome. Int J Cardiol 230:439–446 . doi: 10.1016/j.ijcard.2016.12.087

192. Inai K, Saita Y, Takeda S, et al (2004) Skeletal muscle hemodynamics and endothelial function in patients after Fontan operation. Am J Cardiol 93:792–7 . doi: 10.1016/j.amjcard.2003.11.062

193. Harmer J, Pushparajah K, Toussaint N, et al (2013) In vivo myofibre architecture in the systemic right ventricle. Eur Heart J 34:3640–3640 . doi: 10.1093/eurheartj/eht442

194. Lauzier B, Vaillant F, Gélinas R, et al (2011) Ivabradine reduces heart rate while preserving metabolic fluxes and energy status of healthy normoxic working hearts. Am J Physiol Heart Circ Physiol 300:H845-52 . doi: 10.1152/ajpheart.01034.2010

195. Senzaki H, Chen C-H, Kass DA (1996) Single-beat estimation of end-systolic pressure-volume relation in humans: A new method with the potential for noninvasive application. Circulation 94:2497–2506 . doi: 10.1161/01.CIR.94.10.2497

196. Shishido T, Hayashi K, Shigemi K, et al (2000) Single-beat estimation of end-systolic elastance using bilinearly approximated time-varying elastance curve. Circulation 102:1983–1989 . doi: 10.1161/01.CIR.102.16.1983

197. Suga H, Hisano R, Hirata S, et al (1983) Heart rate-independent energetics and systolic pressure-volume area in dog heart. Am J Physiol Hear Circ Physiol 244:H206-214

198. Burkhoff D, Yue DT, Oikawa RY, et al (1987) Influence of ventricular contractility on non-work-related myocardial oxygen consumption. Heart Vessels 3:66–72

199. Suga H, Hisano R, Goto Y, et al (1983) Effect of positive inotropic agents on the relation between oxygen consumption and systolic pressure volume area in canine left ventricle. Circ Res 53:306–18 . doi: 10.1161/01.RES.53.3.306

200. Chantler PD, Lakatta EG, Najjar SS (2008) Arterial-ventricular coupling: mechanistic insights into cardiovascular performance at rest and during exercise. J Appl Physiol 105:1342–51 . doi: 10.1152/japplphysiol.90600.2008

201. Burkhoff D, Sagawa K (1986) Ventricular efficiency predicted by an analytical model. Am J Physiol Integr Comp Physiol 250:R1021–R1027 . doi: 10.1152/ajpregu.1986.250.6.R1021

202. Chen C-H, Fetics B, Nevo E, et al (2001) Noninvasive single-beat determination of left ventricular end-systolic elastance in humans. J Am Coll Cardiol 38:2028–2034 . doi: 10.1016/S0735-1097(01)01651-5

203. Sullivan LM (2008) Repeated measures. Circulation 117:1238–43 . doi: 10.1161/CIRCULATIONAHA.107.654350

204. Carroll JD, Hess OM, Hirzel HO, Krayenbuehl HP (1983) Dynamics of left ventricular filling at rest and during exercise. Circulation 68:59–67 . doi: 10.1161/01.CIR.68.1.59

205. Cortes RGS, Satomi G, Yoshigi M, Momma K (1994) Maximal hemodynamic response after the Fontan procedure: Doppler evaluation during the treadmill test. Pediatr Cardiol 15:170–177 . doi: 10.1007/BF00800671

206. Hebert A, Jensen AS, Mikkelsen UR, et al (2014) Hemodynamic causes of exercise intolerance in Fontan patients. Int J Cardiol 175:478–83 . doi: 10.1016/j.ijcard.2014.06.015

207. Schlangen J, Fischer G, Petko C, et al (2013) Arterial elastance and its impact on intrinsic right ventricular function in palliated hypoplastic left heart syndrome. Int J Cardiol 168:5385–9 . doi: 10.1016/j.ijcard.2013.08.052

208. Evans CL, Matsuoka Y (1915) The effect of various mechanical conditions on the gaseous metabolism and efficiency of the mammalian heart. J Physiol 49:378–405 . doi: 10.1113/jphysiol.1915.sp001716

209. Suga H, Hisano R, Hirata S, et al (1982) Mechanism of higher oxygen consumption rate: pressure-loaded vs. volume-loaded heart. Am J Physiol Circ Physiol 242:H942–H948 . doi: 10.1152/ajpheart.1982.242.6.H942

210. Suga H, Hayashi T, Shirahata M (1981) Ventricular systolic pressure-volume area as predictor of cardiac oxygen consumption. Am J Physiol 240:H39-44

211. Kouatli AA, Garcia JA, Zellers TM, et al (1997) Enalapril does not enhance exercise capacity in patients after Fontan procedure. Circulation 96:1507–1512 . doi: 10.1161/01.CIR.96.5.1507

212. Giardini A, Balducci A, Specchia S, et al (2008) Effect of sildenafil on haemodynamic response to exercise and exercise capacity in Fontan patients. Eur Heart J 29:1681–7 . doi: 10.1093/eurheartj/ehn215

213. Goldberg DJ, French B, Szwast AL, et al (2012) Impact of sildenafil on echocardiographic indices of myocardial performance after the Fontan operation. Pediatr Cardiol 33:689–96 . doi: 10.1007/s00246-012-0196-9

214. Hebert A, Jensen AS, Idorn L, et al (2013) The effect of bosentan on exercise capacity in Fontan patients; rationale and design for the TEMPO study. BMC Cardiovasc Disord 13:36 . doi: 10.1186/1471-2261-13-36

215. Swedberg K, Komajda M, Böhm M, et al (2010) Ivabradine and outcomes in chronic heart failure (SHIFT): a randomised placebo-controlled study. Lancet 376:875–85 . doi: 10.1016/S0140-6736(10)61198-1

216. Van De Bruaene A, Claessen G, La Gerche A, et al (2015) Effect of respiration on cardiac filling at rest and during exercise in Fontan patients: A clinical and computational modeling study. IJC Hear Vasc 9:100–108 . doi: 10.1016/j.ijcha.2015.08.002

217. Chantler PD, Lakatta EG, Najjar SS (2008) Arterial-ventricular coupling: mechanistic insights into cardiovascular performance at rest and during exercise. J Appl Physiol

105:1342–1351 . doi: 10.1152/japplphysiol.90600.2008

218. Spruijt OA, de Man FS, Groepenhoff H, et al (2015) The effects of exercise on right ventricular contractility and right ventricular - arterial coupling in pulmonary hypertension. Am J Respir Crit Care Med 191:1050–7 . doi: 10.1164/rccm.201412-2271OC

219. Burkhoff D (2013) Pressure-volume loops in clinical research: a contemporary view. J Am Coll Cardiol 62:1173–6 . doi: 10.1016/j.jacc.2013.05.049

220. Sermesant M, Chabiniok R, Chinchapatnam P, et al (2012) Patient-specific electromechanical models of the heart for the prediction of pacing acute effects in CRT: A preliminary clinical validation. Med Image Anal 16:201–215

221. Chapelle D, Felder A, Chabiniok R, et al (2015) Patient-specific biomechanical modeling of cardiac amyloidosis -- A case study. In: Proc. of FIMH 2015. Springer, pp 295–303

222. Pennati G, Corsini C, Hsia T-Y, Migliavacca F (2013) Computational fluid dynamics models and congenital heart diseases. Front Pediatr 1:4 . doi: 10.3389/fped.2013.00004

223. Sainte-Marie J, Chapelle D, Cimrman R, Sorine M (2006) Modeling and estimation of the cardiac electromechanical activity. Comput Struct 84:1743–1759

224. Chapelle D, Le Tallec P, Moireau P, Sorine M (2012) An energy-preserving muscle tissue model: formulation and compatible discretizations. Int J Multiscale Comput Eng 10:189–211 . doi: 10.1615/IntJMultCompEng.2011002360

225. Caruel M, Chabiniok R, Moireau P, et al (2014) Dimensional reductions of a cardiac model for effective validation and calibration. Biomech Model Mechanobiol 13:897–914 . doi: 10.1007/s10237-013-0544-6

226. Razavi R, Baker A, Qureshi, Shakeel Rosenthal E, et al (2001) Hemodynamic response to continuous infusion of dobutamine in Alagille's Syndrome. Transplantation 72:823–828

227. Holzapfel GA, Ogden RW (2009) Constitutive modelling of passive myocardium: a structurally based framework for material characterization. Philos Trans R Soc London A Math Phys Eng Sci 367:3445–3475

228. Klotz S, Hay I, Dickstein ML, et al (2006) Single-beat estimation of end-diastolic pressure-volume relationship: a novel method with potential for noninvasive application. Am J Physiol Hear Circ Physiol 291:H403--H412

229. Chapelle D, Felder A, Chabiniok R, et al (2015) Patient-Specific Biomechanical Modeling of Cardiac Amyloidosis – A Case Study. Springer, Cham, pp 295–303

230. Bazett HC (1920) An analysis of the time-relations of electrocardiograms. Heart 7:353–370

231. Caremania M, Pinzautia F, Reconditia M, et al (2016) Size and speed of the working stroke of cardiac myosin in situ. PNAS 113:3675–80

232. Szabó G, Buhmann V, Graf A, et al (2003) Ventricular energetics after the Fontan operation: Contractility-afterload mismatch. J Thorac Cardiovasc Surg 125:1061–1069 . doi: 10.1067/mtc.2003.405

233. Starr I (1940) Role of the ``Static Blood Pressure'' in abnormal increments of venous pressure, especially in heart failure. II. Clinical and experimental studies. A J M Sc 199:40

234. Maas JJ, Pinsky MR, de Wilde RB, et al (2013) Cardiac output response to norepinephrine in postoperative cardiac surgery patients: Interpretation with venous return and cardiac function curves. Crit Care Med 41:143–150

235. Kwak Y, Nam S, Akçakaya M, et al (2013) Accelerated aortic flow assessment with compressed sensing with and without use of the sparsity of the complex difference image. Magn Reson Med 70:851–8 . doi: 10.1002/mrm.24514

236. Roy CW, Seed M, van Amerom JFP, et al (2013) Dynamic imaging of the fetal heart using metric optimized gating. Magn Reson Med 70:1598–1607 . doi: 10.1002/mrm.24614